

FRACTURE ANALYSIS OF WELDED CONNECTIONS

A THESIS SUBMITTED TO
THE GRADUATE SCHOOL OF NATURAL AND APPLIED SCIENCES
OF
MIDDLE EAST TECHNICAL UNIVERSITY

BY

ALİ YETGİN

IN PARTIAL FULFILLMENT OF THE REQUIREMENTS
FOR
THE DEGREE OF MASTER OF SCIENCE
IN
MECHANICAL ENGINEERING

SEPTEMBER 2013

Approval of the Thesis:

FRACTURE ANALYSIS OF WELDED CONNECTIONS

submitted by **ALİ YETGİN** in partial fulfillment of the requirements for the degree of **Master of Science in Mechanical Engineering Department, Middle East Technical University** by,

Prof. Dr. Canan Özgen
Dean, Graduate School of **Natural and Applied Sciences**

Prof. Dr. Süha Oral
Head of Department, **Mechanical Engineering**

Prof. Dr. Suat Kadioğlu
Supervisor, **Mechanical Engineering Department, METU**

Examining Committee Members:

Prof. Dr. Metin Akkök
Mechanical Engineering Dept., METU

Prof. Dr. Suat Kadioğlu
Mechanical Engineering Dept., METU

Assoc. Prof. Dr. Serkan Dağ
Mechanical Engineering Dept., METU

Assist. Prof. Dr. Gökhan Özgen
Mechanical Engineering Dept., METU

Mr. Bülent Acar, MSc
Lead Engineer, ROKETSAN

Date: 04.09.2013

I hereby declare that all information in this document has been obtained and presented in accordance with academic rules and ethical conduct. I also declare that, as required by these rules and conduct, I have fully cited and referenced all material and results that are not original to this work.

Name, Last name : Ali Yetgin

Signature :

ABSTRACT

FRACTURE ANALYSIS OF WELDED CONNECTIONS

Yetgin, Ali

M.S., Department of Mechanical Engineering

Supervisor: Prof. Dr. Suat Kadioğlu

September 2013, 96 pages

The main objective of this thesis is to evaluate structural integrity of a multi barrel launcher system on fracture mechanics basis by using finite element method. A global finite element model that includes necessary kinematic and elastic connections is built. Dynamic firing forces are applied on global finite element model and general structural response is obtained. Sub modeling method is used in order to perform crack analysis. Since size of global model is too large to include solid crack elements which are relatively finer, separate finite element models must be created. Therefore, sub models were created and boundary conditions were imported from the global finite element model. Firing tests of the launcher system was performed and measurements were taken from tests. Strain gage and displacement sensors were used on several locations and test results were compared with the global finite element model. After the global finite element model was verified by firing tests, sub modeling and crack modeling methods were verified against literature studies. In sub models, a critical welded connection is investigated. Three different crack configurations that are likely to occur in that region are studied. Semi elliptical surface crack at weld toe, inner surface of closed section member and embedded circular crack are modeled. Stress intensity factor values were given for those configurations and compared.

Keywords: Fracture Mechanics, Crack, Welded connections, Finite Element Method, Launcher

ÖZ

KAYNAKLI BAĞLANTILARIN KIRILMA MEKANİĞİ ANALİZİ

Yetgin, Ali

Yüksek Lisans, Makina Mühendisliği Bölümü

Tez Yöneticisi: Prof. Dr. Suat Kadiođlu

Eylül 2013, 96 sayfa

Bu tezin amacı çok namlulu roketatar sistemde bulunan kaynaklı bağlantıların kırılma mekaniđi kullanılarak yapısal bütünlük açısından sonlu elemanlar yöntemi kullanılarak incelenmesidir. Gerekli kinematik ve elastik bağlantıları içeren genel bir sonlu elemanlar modeli oluşturulmuştur. Bu genel sonlu elemanlar modeline dinamik atış yükleri uygulanmış ve sistemin yapısal cevabı elde edilmiştir. Çatlak analizlerini gerçekleştirmek için alt modelleme yöntemi kullanılmıştır. Genel modelin boyutu daha yoğun oluşturulan katı çatlak elemanlarını içermeyecek şekilde büyük olmaktadır. Bu nedenle, alt modeller oluşturulmuş ve sınır koşulları genel modelden aktarılmıştır. Roketatar sisteminin atışlı testleri gerçekleştirilmiş ve çeşitli ölçümler alınmıştır. Gerinim ölçer ve deplasman sensörleri farklı noktalarda kullanılmış ve ölçüm sonuçları genel sonlu elemanlar modeli ile karşılaştırılmıştır. Genel sonlu elemanlar modeli test sonuçları ile doğrulandıktan sonra alt modelleme ve çatlak modelleme yöntemleri literatürdeki çalışmalarla doğrulanmıştır. Alt modellerde kritik bir kaynaklı bağlantı incelenmiştir. İncelenen bölgede olması muhtemel üç farklı çatlak konfigürasyonu çalışılmıştır. Kaynak dibinde ve kapalı kesit profilin iç yüzeyinde yarı eliptik yüzey çatlađı ve gömülü dairesel çatlak modellenmiştir. Bu konfigürasyonlar için gerilme şiddeti faktörleri elde edilmiş ve karşılaştırılmıştır.

Anahtar Kelimeler: Kırılma Mekaniđi, Çatlak, Kaynaklı bağlantılar, Sonlu Elemanlar Yöntemi, Roketatar

To My Family

ACKNOWLEDGEMENTS

I would like to express my deepest thanks and gratitude to Prof. Dr. Suat KADIOĞLU for his supervision, professional support and constant guidance throughout the completion of this thesis work.

I am indebted to Bülent ACAR, lead engineer at ROKETSAN, for his crucial advises, invaluable efforts for this thesis and encouragement throughout the completion of this thesis work.

I also thank my colleague, Buğra ŞİMŞEK for his technical supports during this study.

I am grateful to Necip UYGUN, Hasan SOYLU and Fatih ŞAHAN for their encouragement and patience.

I would like to thank to ROKETSAN for partially supporting this study.

Finally, my gratitude is endless for my family to whom this thesis is devoted. Without them nothing would have been possible.

TABLE OF CONTENTS

ABSTRACT.....	v
ÖZ.....	vi
ACKNOWLEDGEMENTS.....	viii
TABLE OF CONTENTS.....	ix
LIST OF TABLES.....	xi
LIST OF FIGURES.....	xii
NOMENCLATURE.....	xv
LIST OF ABBREVIATIONS.....	xvi
CHAPTERS	
1. INTRODUCTION.....	1
1.1 Background.....	1
1.2 Scope of the Thesis.....	4
1.3 Purpose of the Thesis.....	4
1.4 Outline of the Thesis.....	6
2. LITERATURE SURVEY.....	7
3. THEORETICAL BACKGROUND OF FRACTURE MECHANICS.....	13
3.1 Stress Concentration Factor.....	13
3.2 Stress Intensity Factor.....	14
3.3 Fracture Toughness.....	18
3.4 Energy Release Rate.....	19
4. MATERIAL CHARACTERIZATION.....	21
4.1 Fracture Toughness Test Methods.....	21
4.2 Fracture Toughness Test of Welds.....	23
5. VERIFICATION OF FINITE ELEMENT APPROACH TO FRACTURE MECHANICS ANALYSIS.....	27
5.1 Verification of Global Finite Element Model.....	27
5.2 Verification of Sub Modeling.....	29
5.3 Verification of Crack Modeling.....	31
5.3.1 Embedded Circular Crack.....	32

5.3.2 Semi-elliptical Surface Crack.....	34
5.3.3 Through Thickness Surface Crack With Residual Stress.....	38
6. FINITE ELEMENT MODELING OF WELDED CONNECTIONS ON FRACTURE MECHANICS BASIS.....	45
6.1 Problem Definition	45
6.2 Finite Element Modeling Methodology	46
6.2.1 Global and Sub Model	46
6.2.2 Elements Overview	53
6.2.2.1 Quadrilateral Shell Element S4R.....	53
6.2.2.2 Hexahedral Solid Element C3D8.....	53
6.2.2.3 Collapsed Solid Element C3D20	54
6.2.3 Stress Intensity Factor Calculation.....	55
6.2.4 Boundary Conditions	56
6.2.5 Crack Modeling.....	58
6.2.6 Residual Stress	59
6.2.7 Material Properties	62
6.3 Results of Finite Element Analysis of Cracks in Welded Connections.....	63
6.3.1 Semi Elliptical Surface Crack at Weld Toe	67
6.3.2 Semi Elliptical Surface Crack at Inner Surface.....	72
6.3.3 Embedded circular Crack at Weld Inner Surface.....	76
6.3.4 Conclusion	79
7. TEST STUDIES	81
7.1 Firing Test of Multi Barrel Launcher	82
7.1.1 Strain Measurement	83
7.1.2 Displacement Measurement	86
7.2 Fracture Toughness Tests	87
8. SUMMARY AND CONCLUSIONS	91
8.1 Summary	91
8.2 General Conclusions.....	92
8.3 Recommendations for Future Work	93
REFERENCES	94

LIST OF TABLES

TABLES

Table 1. Stress intensity factor results for embedded circular crack.....	32
Table 2. Stress intensity factor results for semi elliptical surface crack	37
Table 3. Stress intensity factor solutions for through thickness crack under three point bending.....	44
Table 4. Properties of St52.....	62

LIST OF FIGURES

FIGURES

Figure 1. Photograph of a multi barrel launcher (courtesy of ROKETSAN)	1
Figure 2. Traditional and fracture mechanics design approaches [2]	2
Figure 3. Load versus stress for uncracked and cracked body.....	3
Figure 4. Flowchart of thesis work	5
Figure 5. Mode I loading	14
Figure 6. Mode II loading	15
Figure 7. Mode III loading.....	15
Figure 8. Components of stress field near a crack tip and coordinate system	16
Figure 9. Coordinates at crack tip.....	18
Figure 10. Thickness dependence of fracture toughness	19
Figure 11. Different sizes of compact specimens and a broken sample [23].....	21
Figure 12. Bend specimen according to ASTM E399	22
Figure 13. Typical load histories [24].....	23
Figure 14. Cracked welded specimens [25].....	24
Figure 15. Example notch locations [26].....	24
Figure 16. Crack plane orientations [26]	25
Figure 17. Normalized test and FEM strains at different strain gage locations.....	28
Figure 18. Normalized test and FEM displacements	28
Figure 19. Global shell model used for verification	29
Figure 20. Sub models created using shell and solid elements.....	30
Figure 21. Global model von Mises stress plot.....	30
Figure 22. Comparison of von Mises stress between global model and sub models.....	31
Figure 23. Embedded circular crack geometry	32
Figure 24. Finite element model of embedded circular crack.....	33
Figure 25. Stress field perpendicular to crack plane.....	33
Figure 26. Crack face of embedded circular crack	34
Figure 27. Semi elliptical surface crack geometry.....	35
Figure 28. Mode I stress intensity factor along crack front	36
Figure 29. Finite element model of semi elliptical surface crack	37
Figure 30. Crack face of semi elliptical surface crack	38
Figure 31. Geometry used in residual stress crack analysis.....	39
Figure 32. Bar dimensions	39
Figure 33. Finite element model of residual stress model	40
Figure 34. Crack zone of finite element model.....	40
Figure 35. Results of large axial deformation step	41
Figure 36. Results after activating contact between wedge and frame	42

Figure 37. Residual stress (left) imported on cracked finite element model (right)	43
Figure 38. Mode I stress intensity factor variation along crack front	43
Figure 39. Launcher system model (side view)	47
Figure 40. Launcher system model (top view).....	47
Figure 41. Launcher system model (front view).....	48
Figure 42. Cradle finite element model	49
Figure 43. Slewing ring balls detail	50
Figure 44. Spring elements representing slewing ring balls	50
Figure 45. Nonlinear spring constant for balls.....	51
Figure 46. Location of slewing ring on launcher system.....	52
Figure 47. Shell element notation [30].....	53
Figure 48. Hexahedral element notation [30]	54
Figure 49. Degenerate element notation [30].....	54
Figure 50. Schematic of boundary conditions.....	57
Figure 51. Total reaction forces and moments at fix boundary location.....	57
Figure 52. Coarse and fine crack models	58
Figure 53. Stress intensity factor for coarse and fine models	59
Figure 54. Residual stress distribution curve	60
Figure 55. Finite element models built in ANSYS (left) and ABAQUS (right).....	61
Figure 56. Loadings; residual compressive(left) at first step and bending(right) at second step	61
Figure 57. Finite element solution in ABAQUS and ANSYS with and without residual stress.....	62
Figure 58. Maximum principal stress distribution in cradle model	64
Figure 59. Stress history of a point in dynamic solution.....	64
Figure 60. Critical location interested in this study	65
Figure 61. A propagated crack initiating at weld toe[34]	66
Figure 62. Undercut occurring at weld toe after welding process[35]	66
Figure 63. Sub model of semi elliptical surface crack at weld toe	67
Figure 64. Dimensions of solid section of sub model.....	67
Figure 65. Sub model crack detail	68
Figure 66. Equivalent forces and moments at boundaries	68
Figure 67. Crack dimensions and angle definition	69
Figure 68. Variation of normalized stress intensity factors for angle phi with $a/c=0.5$	70
Figure 69. Variation of normalized stress intensity factors for different contours used for J integral	70
Figure 70. Variation stress intensity factor for crack size with $a/c=0.5$	71
Figure 71. Variation of normalized stress intensity factor for different “a” values	72
Figure 72. Sub model of semi elliptical surface crack at inside.....	73
Figure 73. Dimensions of solid section of sub model.....	73
Figure 74. Sub model crack detail	74
Figure 75. Crack dimensions and angle definition	74
Figure 76. Variation of normalized mode I stress intensity factor for angle phi with $a/c=0.5$	75

Figure 77. Variation of normalized mode I stress intensity factor for crack size with $a/c=0.5$	75
Figure 78. Sub model of embedded circular crack at weld.....	76
Figure 79. Dimensions of solid section of sub model.....	77
Figure 80. Sub model crack detail	77
Figure 81. Crack dimensions and angle definition	78
Figure 82. Variation of normalized mode I stress intensity factor for angle ϕ	78
Figure 83. Variation of normalized mode I stress intensity factor for crack size	79
Figure 84. Comparison of three crack configuration	80
Figure 85. Firing of rocket from launcher	82
Figure 86. Three axis and single axis metal foil strain gages [37].....	83
Figure 87. Quarter bridge strain gage circuit[37]	84
Figure 88. Sensor locations.....	85
Figure 89. Linear potentiometric transducer circuit [39].....	86
Figure 90. Sensor locations.....	87
Figure 91. Broken face of a test specimen.....	88
Figure 92. Load versus crack opening displacement curve for a test specimen	88

NOMENCLATURE

A	Crack area
B	Pre logarithmic energy factor matrix
E	Elastic Modulus
G	Shear Modulus
ν	Poisson's Ratio
k_C	Stress concentration factor
J	J integral
$K_{I,II,III}$	Stress intensity factor in Mode I,II,III
K_{IC}	Mode I critical stress intensity factor
K_C	Critical stress intensity factor
G	Energy release rate
$G_{I,II,III}$	Energy release rate in Mode I,II,III
Γ	Strain energy
$\sigma_{x,y,z}$	Normal stress in x, y, z direction
τ_{xy}	Shear stress in crack plane
u,v,w	Displacement in x, y, z direction
θ	Angle measured from crack plane
r	Distance from crack tip

LIST OF ABBREVIATIONS

ASTM	American Society for Testing and Materials
ASME	American Society of Mechanical Engineering
BSI	British Standards Institution
BVPC	Boiler and Pressure Vessel Code
CTOD	Crack Tip Opening Displacement
DIC	Digital Image Correlation
EPFM	Elastic Plastic Fracture Mechanics
FAC	Failure Assessment Curve
FEA	Finite Element Analysis
FEM	Finite Element Method
HAZ	Heat Affected Zone
LEFM	Linear Elastic Fracture Mechanics
SIF	Stress Intensity Factor

CHAPTER 1

INTRODUCTION

1.1 Background

Multi barrel rocket launchers contain multiple rockets and are used for artillery support in the army. They are usually agile and need little preparation time for firing. The launchers can be used with guided and unguided munitions. Rocket launcher systems which are unguided are used to cover a certain region by heavy artillery fire instead of single accurate shots. The launchers have different properties according to their purpose of usage. Some of them are used with small caliber munitions. In this case the system is required to carry relatively large amount of munitions. Since the amount of munitions increased, loading and unloading time must be kept at minimum in order to be ready for operational conditions within a reasonable amount of time. The movement speed is another parameter required for such a system. The launcher must position the munitions in a little time and fire. In some cases, launcher can be used with very large diameter rockets or missiles. The launcher system may be large in dimensions and may carry only one rocket or missile.



Figure 1. Photograph of a multi barrel launcher (courtesy of ROKETSAN)

Launcher system consists of a vehicle, munitions canisters and a cradle. During operations, launcher systems are usually accompanied by other vehicles. A loader vehicle is necessary to load munitions to the launcher system. Though, some launcher systems may be equipped with a loader crane onboard. Another vehicle used in field is munitions vehicle. This vehicle travels with the launcher and loader vehicle and carries spare rockets to be fired. Since operation field may be far away from storage of munitions, it would be infeasible to go on field with few rockets that can be carried by launcher system. In some cases, launcher systems may not be designed to transfer rockets with it into the firing site. The rockets are transferred separately if this is the case. Rockets are loaded in canisters that rest on cradle. Cradle positions rockets to be fired in azimuth and elevation angles. Since rockets do not have guidance, it is very important to have initial positioning as accurate as possible in order to hit the target successfully.

The launcher systems are needed to be used many times in the field. Thus the system is subjected to repetitive loading. It is crucial to determine the loads on the system very accurately and evaluate the structural integrity precisely. It would be catastrophic if any malfunction of the system occurs during field operations. It puts personnel and mission at great risk.

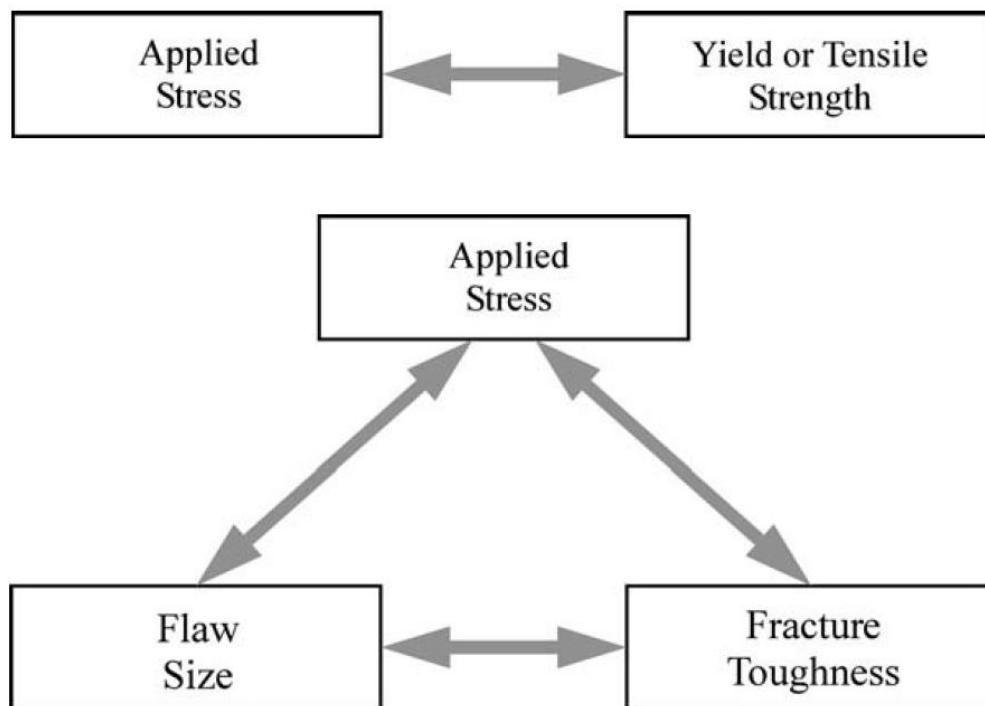


Figure 2. Traditional and fracture mechanics design approaches [2]

Structural integrity evaluation of the system is vital in such military applications. Components must be checked for every possible failure mode in order to ensure mission success. It is nearly impossible to build a structure without any kind of imperfection. Therefore it is important to have a design that endures imperfections up to some level. At this point fracture mechanics comes in picture. With fracture mechanics, new damage tolerant designs have become available [1]. Structure's integrity is now dependent on applied stress, flaw size and fracture toughness of the material. (Figure 2) Evolution of fracture mechanics is built on many tragic accidents. Many ships during World War II, aircrafts and bridges suffered failure due to fracture. Geometric discontinuities in the body cause increased stress field around them. This situation causes local stresses to reach material's strength limit even in modest nominal loadings [1]. (Figure 3) Fracture limit of the structure can be lower than plastic limit of the material. It is important to include fracture mechanics analysis in design cycle.

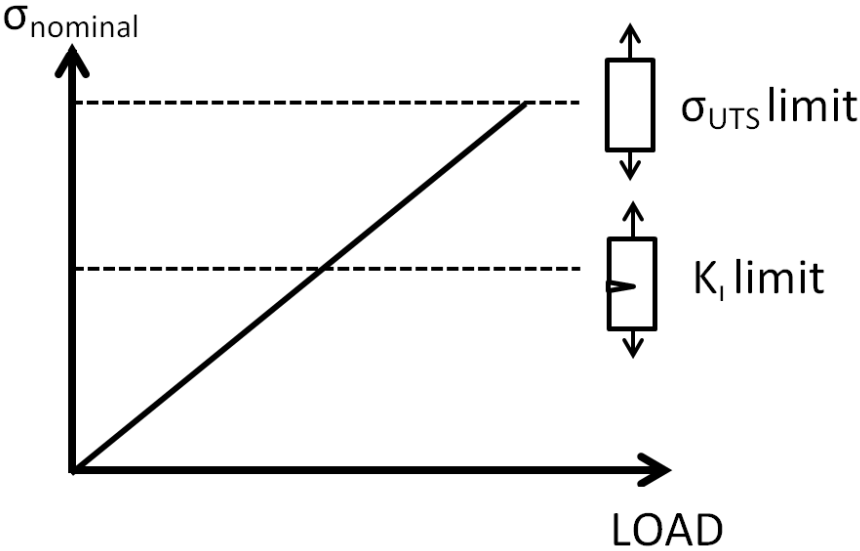


Figure 3. Load versus stress for uncracked and cracked body

Critical stress intensity factor for a material is known as fracture toughness of it. In plane strain condition, fracture toughness value is lowest and very little yielding takes place. Therefore structures are designed against plane strain fracture toughness limit in order to be on the safe side.

Critical systems like rocket launchers require safe life design approach. In safe life design, for certain operational life the system is ensured to function well and no failure will occur. The system is then replaced or repaired after expected service period. The life of the system is determined through accurate analysis and testing. In safe life design philosophy since the system is designed not to fail during service period, accurate analysis and thorough testing

is essential. Fatigue and fracture mechanics are key analysis methods in safe life design approach. The cost of failure of a rocket launcher system during mission may be loss of personnel or an unaccomplished mission. Chosen design approach must be applied well and the design must allow proper inspection of the system for any indication of failure. Although systems have determined operational life with some safety factor, system should be checked against for any indication of failure.

The study presented in this thesis work is a part of safe life design approach that is used in design of a multi barrel rocket launcher. Fracture mechanics along with fatigue are major analyses in a safe life design.

1.2 Scope of the Thesis

In this thesis, structural integrity of welded connections in a multi barrel launcher system is investigated on a fracture mechanics basis. Material characterization for welded and base materials was performed in order to obtain mechanical properties. Finite element model of the launcher system is built on a global scale on commercial finite element software package. Global model includes all necessary elements such as kinematic and elastic connections, in order to simulate structural and dynamic response of the launcher. Weld details are investigated on separate local models. Local models, namely sub models, include finer finite element mesh and global model results were used as boundary conditions for local models. The launcher prototype is manufactured and tested on the field. Certain measurements were made and these measurements were compared with finite element model. With validated methodology structural integrity assessment of the structure is done against operational loads and defects on the welds.

1.3 Purpose of the Thesis

The objective of this thesis is to accurately assess the structural integrity of a multi barrel launcher system against possible defects on welded connections that make up the structure. The structure is loaded under operational loads which are over elastic limits of the material at certain locations. It is crucial to correctly determine the limiting size and locations of the defects against failure during mission. Material characterization of the base and welded material is performed in order to use in modeling and assessment procedures. The modeling and assessment methodology of the structure against failure on a fracture mechanics basis is used. The flow of this thesis work is given in Figure 4. It is believed that this study will increase the analysis capabilities of the System Design Department of ROKETSAN Missile Industries Inc.

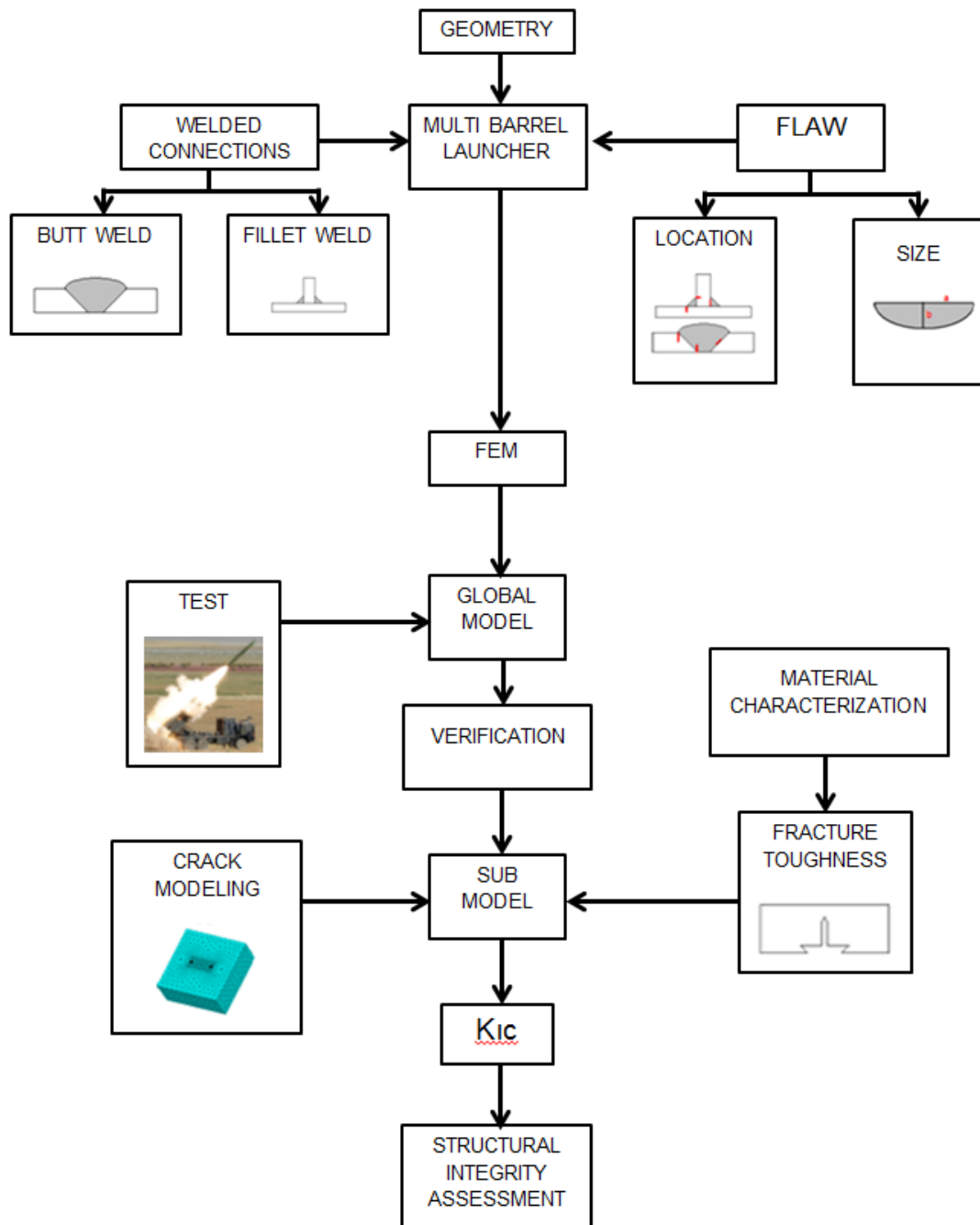


Figure 4. Flowchart of thesis work

1.4 Outline of the Thesis

The chapters are organized as follows. In Chapter 2, literature survey on fracture mechanics analysis of welds, finite element modeling and assessment are introduced. In Chapter 3, theoretical background information about fracture mechanics which is the basis of this study is given. In Chapter 4, detailed information about material characterization for mechanical properties that are used in modeling and assessment of the base and welded materials is provided. In Chapter 5, verification studies and compared modeling results are given. In Chapter 6, developed methodology is introduced and applied to the real structure under dynamic operational loading. Results of crack modeling are provided. In Chapter 7, test studies and measurements are mentioned. In Chapter 8, summary and conclusions of this thesis study and recommendations for the future works are given.

CHAPTER 2

LITERATURE SURVEY

The main objective of this study is to investigate structural integrity of welded connections under operation loads against weld defects that occurs inherently due to welding process or result from repeated operational loads.

The usage of finite element method for fracture mechanics analysis is now widely accepted. It makes feasible to make calculations for complex geometries and loading. Sometimes it may not be possible to obtain analytical solution for a case or empirical relations may not cover it. In this study finite element method is used for fracture mechanics evaluation of welded connections.

Acar [3] is one of the first engineers who applied finite element method to fracture mechanics in Turkey. In his work, he investigated the stress intensity factors in discrete functionally graded materials (FGM). The model consists of two coaxially located cylindrical parts with different elastic mechanical properties. The cracks were placed at inner radius, outer radius and interface of two parts. Subsequently, he calculated stress intensity factors for various crack geometry and loading conditions. Other than that, he also located cracks at various geometries such as pressure vessels, and examined stress intensity factors accordingly.

Gordon and McDowell [4] used finite element method for cracks located in interface of two different metals. Time dependent material properties were used for two materials. They presented numerical results for compact tension specimens using variable material properties from crack face to interface distance and homogenous properties. They compared results to homogenous material cases. Results showed that calculated fracture parameters are affected by transition layer properties and transition layer causes less stress concentration.

Negre et al [5] investigated fracture of aluminum laser weld both numerically and experimentally. They have used Al 6000 laser weld with crack initiation introduced at heat affected zone (HAZ). The authors studied crack in HAZ due to changing microstructure. They experimented compact tension specimen and determined deviation from straight path of crack using 3D topography. They used Gurson-Tvergaard-Needleman damage model

and cohesive zone model for fracture resistance simulations. Results showed that extension of cracks in aluminum can be dealt with both continuum damage and cohesive models.

Lie et al. [6] proposed a modeling approach for cracks in rectangular hollow section members. The proposed method can be used to create mesh for cracks at any location, dimension and configuration at joint of members. The control over element dimensions, transition properties and crack dimensions make the method flexible and efficient. They also verified their method against numerical and experimental works. They modeled a cracked T shaped joint and obtained numerical and experimental results. The results were in agreement with experiments.

Diamantoudis and Labeas [7] studied the stress intensity factor (SIF) calculation for the cracks existing in the pressure vessels. They obtained SIF solutions for different surface crack dimension and locations under various pressure loads. Pursuing this aim they implemented Finite Element Analysis (FEA) technique using ANSYS. First global model without cracks are solved for different configurations and then they used sub-models containing the cracks for SIF calculations. This method is proven to be efficient instead of modeling the whole model containing cracks. Displacement results obtained from the global model are imposed on the boundary of sub-model. Thus they connected the two models. They compared the findings of their method with American Society of Mechanical Engineering (ASME) Boiler and Pressure Vessel Code (BPVC) solutions and obtained good agreement. For validation of sub-model technique they also solved the same problem for different sizes of sub-model boundaries; after which a size of $b \times b$ square region where b is three times of crack length is found to be enough.

Giglio and Manes [8] investigated crack growth on helicopter panel on an experimental and FEA basis. In the experiment phase, full scale tests were conducted on aluminum panel with initial crack under fatigue loads. During the test crack growth and strain measurements are taken on various positions on the panel. In FEA phase, global model of the panel and sub-model containing crack region were created. SIFs are calculated using FEA models and analytical methods. Then the findings are compared with each other. The crack propagation prediction made by FEA model and experimental results are also compared with each other. The results yielded good agreement.

Shi et al. [9] studied the effect of weld and geometry parameters on the relation between J integral and crack tip opening displacement (CTOD). They used FEA method by ABAQUS with elastic-plastic material behavior. Several models were created and investigated in order to relate the effect of weld strength mismatch, crack size, weld width. As a result they found that weld strength mismatch exerts less influence than crack size on the relation. Weld width have greater influence under greater loads.

Meneghetti [10] in his paper extended the usage of peak stress method which is validated only for mode I stress singularity to mode II stress singularity and proposed an equivalent peak stress. In finite element method peak stress method makes it possible to determine notch stress intensity factor at weld toe using linear elastic peak stress, for certain element size conditions. This method is confirmed against connections with fillet welds where only

mode I stresses are considered to be important. The author calibrated mode I relation to mode II loading using finite element models by varying parameters such as geometry, mesh size and related this calibration method to strain energy density.

Négre et al [11] studied laser welded aluminum sheets. The extensions of cracks which are located initially at the different places in the welded plate are investigated by numerical analyses. They implemented FEA technique using ABAQUS with Gurson-Tvergaard-Needleman model as a user subroutine. Material characterization test are carried out in order to determine fusion zone (FZ), heat affected zone (HAZ) and base material (BM) boundaries using micro-flat-tension specimens. The fracture toughness tests were conducted using compact specimens with initial crack at different zones – BM, FZ, HAZ. They modeled the crack growth for these three different configurations and compared with the experimental results. A good agreement between modeling and experiments was obtained.

Manjgo et al. [12] studied welded plates with a surface notch subjected to tensile loading. They built finite element models to investigate behavior of the plate accounting for heat affected zone (HAZ). They applied 3 different modeling strategies for HAZ modeling which are equating properties of HAZ to weld material, to base material and assigning two different regions in HAZ using base and weld material properties. The mechanical properties obtained from material characterization are fed into finite element models. They also conducted an experiment program for specimens with surface notches in different zones that are studied numerically. They concluded that notches in weld material are better approximated than those in HAZ using their modeling strategies. They also stated that better determination of the properties of different regions using micro specimens will improve material modeling.

Paonelli et al. [13] in their work proposed a new aspect of determining fracture toughness property of materials. In current standards calculations are based on in plane displacement and load history of the specimen. Since digital image correlation (DIC) technique made it possible to make 3D displacement measurement, the authors used this technique's potential to investigate 3D effects on fracture toughness of materials. In DIC surface photos are taken using left and right cameras and movements of surface points is tracked. 3D displacements of these points are determined using two cameras' images and used to compute crack tip opening displacement of the tested specimens. They made experiments in order to determine fracture toughness of a steel material using US and British standards and also their proposed method. The results of their method showed good agreement with standards. In addition by measuring out of plane displacement they developed a new approach to fracture toughness measurement of ductile materials.

Atzori et al. [14] applied local stress field approach which is used to determine fatigue life of notched components to welded aluminum joints and proposed a new simple method to estimate fatigue strength of welded joint. While applying local stress field approach, stress field around a welded connection is divided into a structural component due to geometry and a local component due to weld parameters. The authors showed that stress field around

a fillet weld toe can be approximated by finding stress field around a lateral V notch subjected to remote loading of maximum principal stress found in geometrical model. With the help of new proposed equivalent stress field method, they can predict the fatigue strength of welded aluminum connection.

Kai et al [15] used symmetric Galerkin boundary element method (SGBEM) for fracture assessment of non load carrying fillet welds. They have obtained stress intensity factor solutions from this method for fracture mechanics evaluation. In their work they calculated magnification factors for weld geometric parameter and plate thickness. The calculated results from SGBEM were compared against values from finite element method and published in earlier works. They have presented that using relatively less elements, quite accurate solutions can be obtained.

Lin et al. [16] studied mis-match effects on strength of weld joints in their paper. They used finite element method in order to simulate crack growth in single edged specimen. The crack was located at midsection of weld material. They used cohesive zone model for fracture modeling. They studied effects of different yield strengths between materials and thickness of weld material. In results they indicated that both strength mis-match and thickness have significant effects on mechanical performance of weld joints.

Guo et al. [17] studied pipeline weldments in order to extract data for fracture evaluation. They produced data of pipeline girth weld for different configurations and J-R curves that are used for Engineering Critical Assessment (ECA). They tested single edge notch tensile specimen for fracture toughness determination. They machined notched specimen and fatigue precracked it in order to obtain sharp crack tip. Crack opening displacement and load were recorded while testing specimen. After tests, critical flaw sizes and locations were determined. Results showed that correlation between fracture toughness, ECA and validation studies exist for large strained pipe.

Residual stresses occur in structures due to manufacturing processes involving hot and cold mechanical operations. They have to be taken into account while evaluating structure for failure. They may extend or shorten life depending on whether they are compressive or tensile, or location. In literature, residual stresses on welded connections are studied widely. Different methods for determining residual stresses by welding simulations or applying these on finite element models exist. In this study, a predetermined residual stress distribution is applied as a first step prior to loadings.

Lee et al [18] studied residual stresses on components considering linear elastic fracture mechanics (LEFM) analysis. Several components were investigated for residual stress distributions and a generic distribution with some uncertainty is adopted. After reviewing large amount of residual stresses on various parts after different welding and measurement methods, they considered a linearly varying residual stress distribution. For a stress distribution consisting of membrane and bending components SIF is calculated using an equation that contains membrane and bending stress components, geometry factors and crack size. The authors also obtained geometry factors by FEA method using ABAQUS.

For this, they applied unit membrane and bending stress. They conducted a sensitivity study on the dependency of SIF values on geometry factors and stress components.

Liljedahl et al. [19] studied the formation of residual stress field on a welded aluminum component under cyclic loading. Experimental studies are performed on welded specimens and residual stress and strain measurements were made. The specimen was initially cracked with a known geometry using electrical discharge machining. Elastic and elasto-plastic finite element model of the specimen was created by using ABAQUS and FEM results are compared with the experimental results. The authors predicted the formation of residual stresses well using elastic model and including initial residual stress distribution.

Barsoum and Barsoum [20] studied effect of residual stress on welded structures for fatigue life. They studied the welding process in order to estimate residual stress forming after welding is done. Temperature distribution on welded component is predicted first by applying a heat source representing weld torch. Material modeling at high temperatures becomes important for welding simulation. Then they built a finite element subroutine in order to perform linear elastic fracture mechanics calculations for stress intensity factor and crack propagation. They used another subroutine for accounting for the residual stresses in stress intensity calculations. Effective stress intensity was defined by superposing stress intensity due to residual stress for life calculations. Residual stresses are mapped to mechanical analysis model via use of a subroutine. For validation purposes, they compared the results with experiment and literature values.

Bao et al. [21] propose a finite element method in order to calculate residual stress on welded samples. They studied applications of finite element method and weight function, and compared these methods for some given cases. Residual stress distributions are obtained from measurements and applied in finite element model in first step. They have used displacement extrapolation methods using finite element package ANSYS for stress intensity factor calculations.

After reviewing literature, it can be concluded that fracture mechanics calculation with finite element method first started at mid 90s. Its usage to calculate stress intensity factor increased rapidly especially after 2000s, by developing high end computer technology. In 60s only simple crack configurations and geometries could be analyzed. After introduction of computers to engineering environment in mid 80s, it could be possible to study different geometries for stress distribution. It was a burden to calculate SIFs for complex geometries using analytical methods. It is a good practice of using finite element method for fracture mechanics analysis.

CHAPTER 3

THEORETICAL BACKGROUND OF FRACTURE MECHANICS

3.1 Stress Concentration Factor

When a structure is loaded, applied external force is distributed through cross section of the structure. If the geometry of the cross section changes in the structure, distribution of load varies at different regions of the structure. Holes, cross section transition regions, fillets are common discontinuities occurring on most structures which cause stress elevation compared to nominal distribution due to external load. In other words, these features on the structure cause the stresses to concentrate on certain regions. This concentration is related to nominal distribution of the stress through a concentration factor k_c . [22]

$$\sigma_{\text{concentrated}} = k_c \sigma_{\text{nominal}} \quad (3.1)$$

Stress concentration value, k_c can be usually determined using elasticity relations for properly defined shapes such as circular or elliptical holes, fillets and smooth thickness transitions. In case of a plate with an elliptical hole subjected to remote tensile loading, stress concentration factor is given as follows:

$$k_c = \left(1 + 2 \frac{a}{b}\right) \quad (3.2)$$

where a and b are major and minor radii respectively. Radius at the major axis can be approximated by

$$\rho = \frac{b^2}{a} \quad (3.3)$$

When equation (3.2) is rearranged

$$k_c = 1 + 2 \sqrt{\frac{a}{\rho}} \quad (3.4)$$

In case of a sharp crack tip, radius, ρ , approaches to zero and k_C goes to infinity. Therefore, determination of the stress concentration around a sharp radius cannot be possible using stress concentration concept and a different approach, namely stress intensity factor is proposed.

3.2 Stress Intensity Factor

In fracture mechanics stress and strain field near an imperfection with a sharp crack tip is defined using a parameter named stress intensity factor. This parameter is a measure of the magnitude of stress intensity. In a structural member with a crack, stress field near the crack tip is a function of both remote loading on the member and crack geometry. Thus stress intensity factor is dependent on applied loading as well as crack size. Three main loading directions are defined for a crack tip in a structural member. In Mode I loading as can be seen in Figure 5, crack is loaded in tensile direction which causes the crack faces to open. Displacements near the crack tip are symmetric with respect to x-y and x-z planes. In Figure 6, crack is loaded in Mode II, which is in plane direction so there is in plane shear on the crack faces. In this loading mode, displacements are symmetric with respect to x-y plane and anti-symmetric with respect to x-z plane. In Figure 7, crack is loaded in Mode III. In this mode crack faces move in direction of crack front. Displacements are anti-symmetric with respect to both x-y and x-z planes [22].

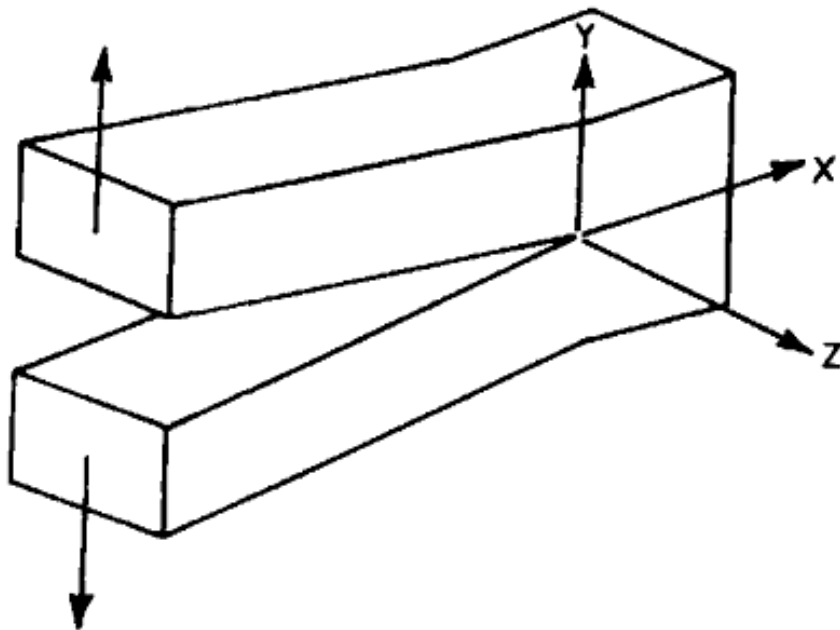


Figure 5. Mode I loading

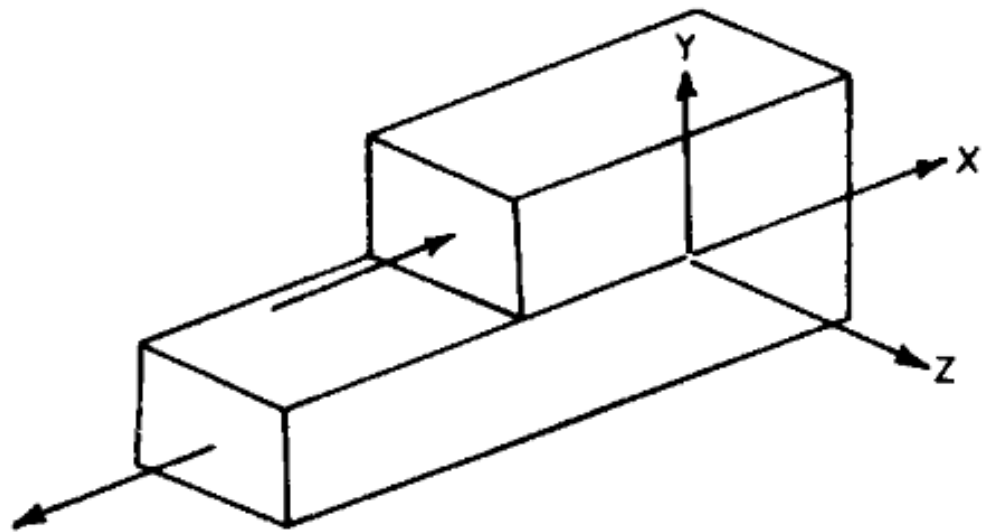


Figure 6. Mode II loading

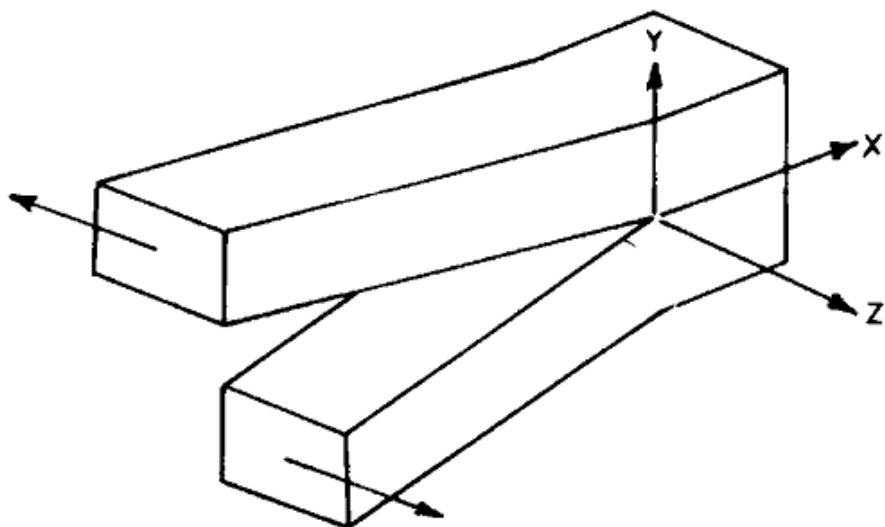


Figure 7. Mode III loading

Mode I, II and III are the basic types of loadings that a crack in a structural member can be loaded. A crack can be loaded in any of these modes or combination of these modes which is named mixed-mode loading. Among these basic modes, Mode I is the most critical

loading mode. Most of the failures occur due to Mode I loading and many of engineering calculations are made by considering Mode I loading [22].

Stress field near a crack tip is given for different loading modes as follows:

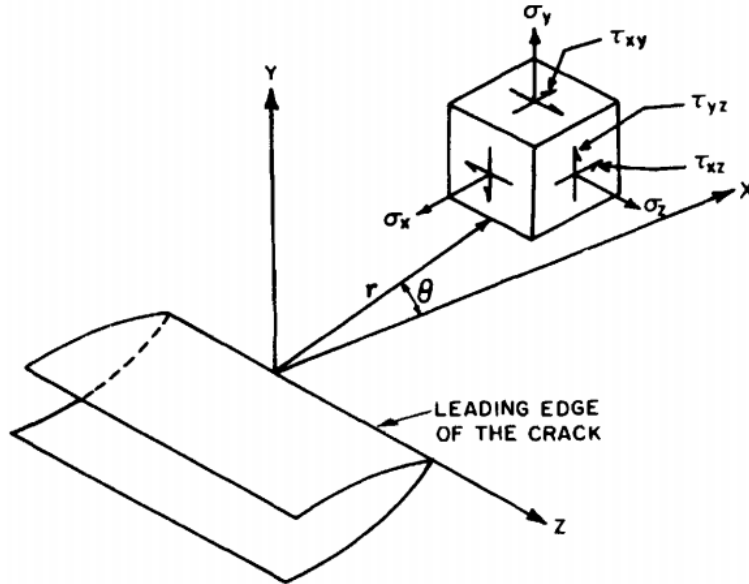


Figure 8. Components of stress field near a crack tip and coordinate system

Mode I:

$$\sigma_x = \frac{K_I}{(2\pi r)^{1/2}} \cos \frac{\theta}{2} \left[1 - \sin \frac{\theta}{2} \sin \frac{3\theta}{2} \right] \quad (3.5)$$

$$\sigma_y = \frac{K_I}{(2\pi r)^{1/2}} \cos \frac{\theta}{2} \left[1 + \sin \frac{\theta}{2} \sin \frac{3\theta}{2} \right] \quad (3.6)$$

$$\tau_{xy} = \frac{K_I}{(2\pi r)^{1/2}} \sin \frac{\theta}{2} \cos \frac{\theta}{2} \cos \frac{3\theta}{2} \quad (3.7)$$

$$\sigma_z = \nu(\sigma_x + \sigma_y) \quad (3.8)$$

$$u = \frac{K_I}{G} \left[\frac{r}{2\pi} \right]^{1/2} \cos \frac{\theta}{2} \left[1 - 2\nu + \sin^2 \frac{\theta}{2} \right] \quad (3.9)$$

$$v = \frac{K_I}{G} \left[\frac{r}{2\pi} \right]^{1/2} \sin \frac{\theta}{2} \left[1 - 2\nu - \cos^2 \frac{\theta}{2} \right] \quad (3.10)$$

$$w = 0 \quad (3.11)$$

Mode II:

$$\sigma_x = -\frac{K_{II}}{(2\pi r)^{1/2}} \sin \frac{\theta}{2} \left[2 + \cos \frac{\theta}{2} \cos \frac{3\theta}{2} \right] \quad (3.12)$$

$$\sigma_y = \frac{K_{II}}{(2\pi r)^{1/2}} \sin \frac{\theta}{2} \cos \frac{\theta}{2} \cos \frac{3\theta}{2} \quad (3.13)$$

$$\tau_{xy} = \frac{K_{II}}{(2\pi r)^{1/2}} \sin \frac{\theta}{2} \left[1 - \sin \frac{\theta}{2} \sin \frac{3\theta}{2} \right] \quad (3.14)$$

$$\sigma_z = \nu(\sigma_x + \sigma_y) \quad (3.15)$$

$$u = \frac{K_{II}}{G} \left[\frac{r}{2\pi} \right]^{1/2} \sin \frac{\theta}{2} \left[2 - 2\nu + \cos^2 \frac{\theta}{2} \right] \quad (3.16)$$

$$v = \frac{K_{II}}{G} \left[\frac{r}{2\pi} \right]^{1/2} \cos \frac{\theta}{2} \left[-1 + 2\nu - \sin^2 \frac{\theta}{2} \right] \quad (3.17)$$

$$w = 0 \quad (3.18)$$

Mode III:

$$\tau_{xz} = -\frac{K_{III}}{(2\pi r)^{1/2}} \sin \frac{\theta}{2} \quad (3.19)$$

$$\tau_{yz} = -\frac{K_{III}}{(2\pi r)^{1/2}} \cos \frac{\theta}{2} \quad (3.20)$$

$$\sigma_x = \sigma_y = \sigma_z = \tau_{xy} = 0 \quad (3.21)$$

$$w = \frac{K_{III}}{G} \left[2 \frac{r}{\pi} \right]^{1/2} \sin \frac{\theta}{2} \quad (3.22)$$

$$u = v = 0 \quad (3.23)$$

Stress intensity factor definitions for different types of loadings are given as follows:

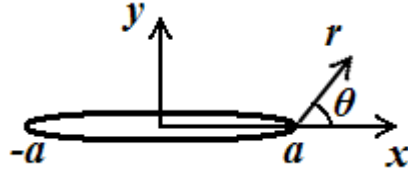


Figure 9. Coordinates at crack tip

Mode I:

$$K_I(a) = \lim_{x \rightarrow a^+} \sqrt{2\pi(x-a)} \sigma_y(x, 0) \quad (3.24)$$

$$K_I(-a) = \lim_{x \rightarrow a^-} \sqrt{2\pi(-x-a)} \sigma_y(x, 0) \quad (3.25)$$

Mode II:

$$K_{II}(a) = \lim_{x \rightarrow a^+} \sqrt{2\pi(x-a)} \tau_{xy}(x, 0) \quad (3.26)$$

$$K_{II}(-a) = \lim_{x \rightarrow a^-} \sqrt{2\pi(-x-a)} \tau_{xy}(x, 0) \quad (3.27)$$

Mode III:

$$K_{III}(a) = \lim_{x \rightarrow a^+} \sqrt{2\pi(x-a)} \tau_{yz}(x, 0) \quad (3.28)$$

$$K_{III}(-a) = \lim_{x \rightarrow a^-} \sqrt{2\pi(-x-a)} \tau_{yz}(x, 0) \quad (3.29)$$

3.3 Fracture Toughness

A crack can be loaded up to some limiting value until total fracture in the structural member occurs. This limiting value is named critical stress intensity factor, K_c . Fracture toughness is resistance of a crack to grow in a structural member under loading. It can be thought analogous to yield stress which is the limiting value of stress at a section at which

yielding occurs (under uniaxial loading). Fracture toughness of a material is dependent on temperature, loading rate and size of the specimen. As the thickness of the specimen increases, crack is loaded in plane strain conditions and fracture occurs in a brittle manner. However, when the specimen is in plane stress conditions where the thickness is less, yielding can take place instead of brittle fracture. The dependence of fracture toughness of a material to thickness is shown in Figure 10 [2].

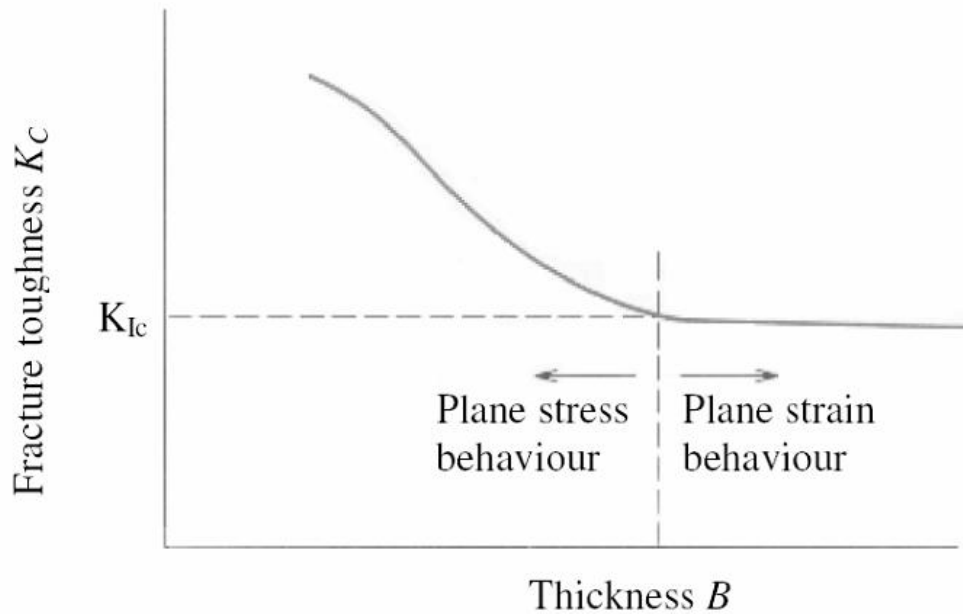


Figure 10. Thickness dependence of fracture toughness

Plane strain fracture toughness of a material, denoted as K_{Ic} , has the lowest value and hence it is more critical. Most of the fracture mechanics designs are made against plane strain fracture toughness.

3.4 Energy Release Rate

In a structural member with a crack in it, for crack size to grow, strain energy released during an increase in crack size must be equal to or greater than energy needed to form new crack faces. In other words, energy release rate in a crack must exceed a certain critical value in order to increase the crack size.

$$G \geq G_c \quad (3.30)$$

Critical energy release rate is a material property and determined experimentally. Energy release rate, G , is change of strain energy, Γ , per crack area, A .

$$G = -\frac{d\Gamma}{dA} \quad (3.31)$$

For plain strain conditions, energy release rate is related to stress intensity factor as follows:

$$G = G_I + G_{II} + G_{III} = \frac{1 - \nu^2}{E} (K_I^2 + K_{II}^2) + \frac{1 + \nu}{E} K_{III}^2 \quad (3.32)$$

In case of plain stress equation (1.32) becomes:

$$G = G_I + G_{II} + G_{III} = \frac{1}{E} (K_I^2 + K_{II}^2 + (1 + \nu)K_{III}^2) \quad (3.33)$$

CHAPTER 4

MATERIAL CHARACTERIZATION

Evaluation of structural members on a fracture mechanics basis requires certain material properties to be determined. As mentioned before, in order to determine criticality of crack against fracture, fracture toughness of the material must be known. Unlike conventional tensile or compression test methods, fracture toughness test requires certain conditions to be met in order to obtain proper results. Certain organizations around the world have published test methods regarding fracture toughness determination of metallic materials in order to standardize testing.

4.1 Fracture Toughness Test Methods

American Society for Testing and Materials (ASTM) has several standards for fracture toughness testing of materials. These standards include aspects to be considered before and after testing. Specimens must be prepared accordingly regarding material and loading conditions. ASTM E399 standard defines test method to determine materials plane strain fracture toughness. Test is conducted in an increasing force trend applied as tensile or three point bending loading. In order to obtain a linear elastic case and negligible plastic zone around the crack tip, specimen to be tested has to match certain proportional dimensions. Thickness of the specimen is determined by material's fracture toughness to yield strength ratio.



Figure 11. Different sizes of compact specimens and a broken sample [23]

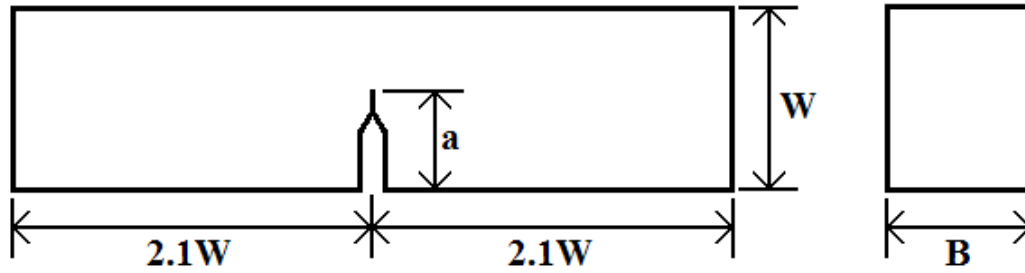


Figure 12. Bend specimen according to ASTM E399

$$B, (W - a) > 2.5 \left(\frac{K_{IC}}{\sigma_{yield}} \right)^2 \quad (4.1)$$

K_{IC} is fracture toughness, σ_{yield} is yield strength, $(W-a)$ is the ligament size and B is the thickness of the specimen.

The specimen is cut into proper dimensions and a notch is machined in the middle of it. Then the specimen is subjected to fatigue pre-cracking where crack on the notch is grown so that a natural sharp crack tip is obtained. In this process specimen is loaded cyclically up to a stress intensity level proportional to material's expected fracture toughness.

During test, the specimen is loaded until fracture and load-displacement history is recorded. When test is completed, there are other certain checks to be made in order to obtain a valid fracture toughness of the material. Typical load history curves that can be seen during a fracture toughness test can be seen on Figure 13.

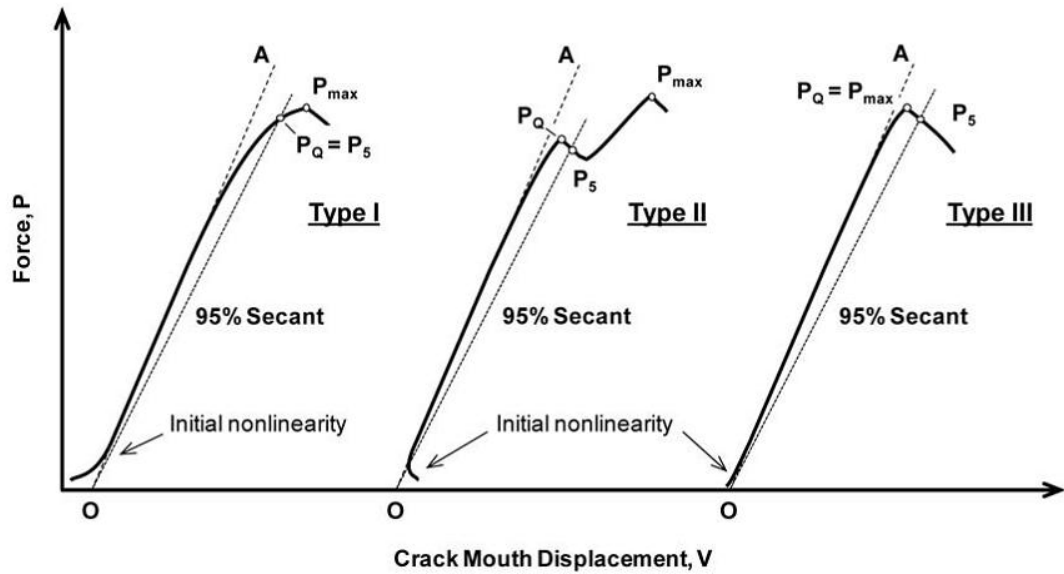


Figure 13. Typical load histories [24]

In Figure 13 typical load histories of fracture toughness tests are shown. After specimen is loaded until fracture, validity of the test must be checked as follows:

$$\frac{P_{\max}}{P_Q} < 1.1 \quad (4.2)$$

P_{\max} is maximum value in load curve, P_5 is intersection point of load curve and 95% secant curve and P_Q is conditional load value.

After all requirements of fracture toughness test are satisfied, a valid fracture toughness value can be obtained for the material. These checks ensure critical stress intensity factor in plane strain conditions for the material is obtained.

4.2 Fracture Toughness Test of Welds

British Standards Institution (BSI) has standard for determination of fracture toughness of welds in metallic materials besides standards for metallic materials without welds. In this standard, special considerations for determining fracture toughness of welds are defined in addition to metallic test standard without welds. In this testing method, the notched may be positioned in the weld section, or in heat affected zone (HAZ). In Figure 14, broken samples of welded fracture toughness test specimens are shown [25].

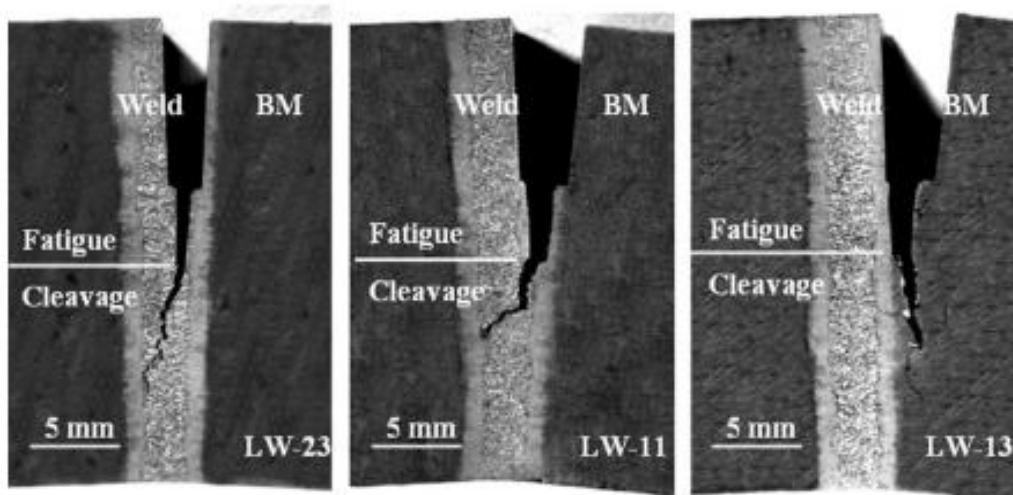


Figure 14. Cracked welded specimens [25]

In Figure 15, notches placed in the middle of weld section and heat affected zone are given as an example.

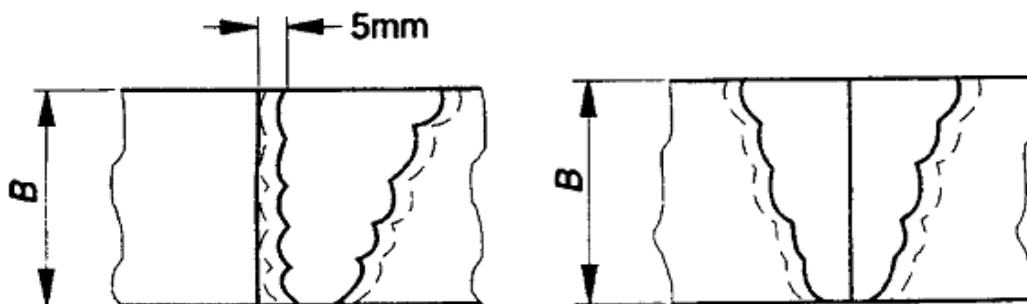


Figure 15. Example notch locations [26]

In Figure 16, crack plane that can be placed in a welded fracture toughness specimen is given. In this figure;

- N is normal to weld direction
- P is parallel to weld direction
- Q is weld thickness direction

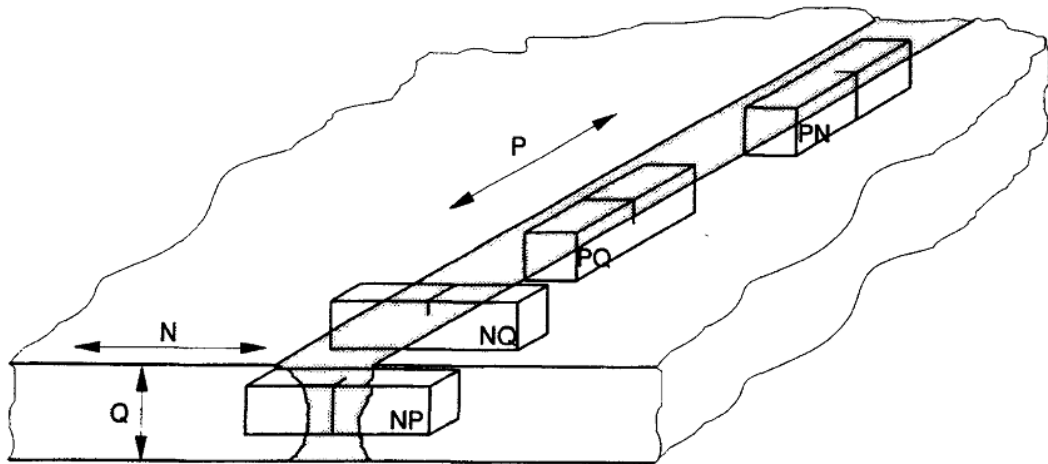


Figure 16. Crack plane orientations [26]

After the specimen is machined into dimensions defined by the standard and notch is positioned into desired position, it is subjected to fatigue pre cracking process as in ASTM standard case. In case of welded specimens, some exceptions to this process apply. These exceptions include calculation of maximum fatigue loading and crack plane straightness.

CHAPTER 5

VERIFICATION OF FINITE ELEMENT APPROACH TO FRACTURE MECHANICS ANALYSIS

Global and sub models of the launcher system were built and analyzed in the scope of this thesis work. Finite element method was used to evaluate the launcher for structural integrity under operational loads. In order to make accurate evaluations, finite element models and methodology must be sufficient to simulate real conditions. Global models were used to create boundary conditions for sub models. Therefore it is crucial for global finite element model to capture dynamic response of the launcher. Sub modeling methodology proposed in this work must also be accurate enough in reflecting stress distribution from global model in order to evaluate cracks in the model. Therefore finite element approach proposed in this work was verified against test results and cases with known solutions.

5.1 Verification of Global Finite Element Model

The global finite element model of the multi barrel rocket launcher, which is given in Figure 39, was tested under real operating conditions. The model must reflect the response of the structure in order to accurately evaluate the structure. Dynamic response of the structure was compared under operational loads to the finite element solution using displacement measurements at different locations which are also shown in Figure 90. In addition to that, strain gages were placed at several locations which are given in Figure 88 and overall stress distribution of the finite element solution was verified.

Results of strain gage measurements at the locations shown in Figure 88 and finite element model are given in Figure 17. Magnitudes are normalized against maximum value obtained among strain gage locations. Results of displacement measurements and finite element model are given in Figure 18. Detailed information about measurement is given in Chapter 7.

When results are compared, it is concluded that global model is quite satisfactory to capture the response of the structure. Stress and displacement field of the finite element model is very close to the values obtained at test measurement locations.

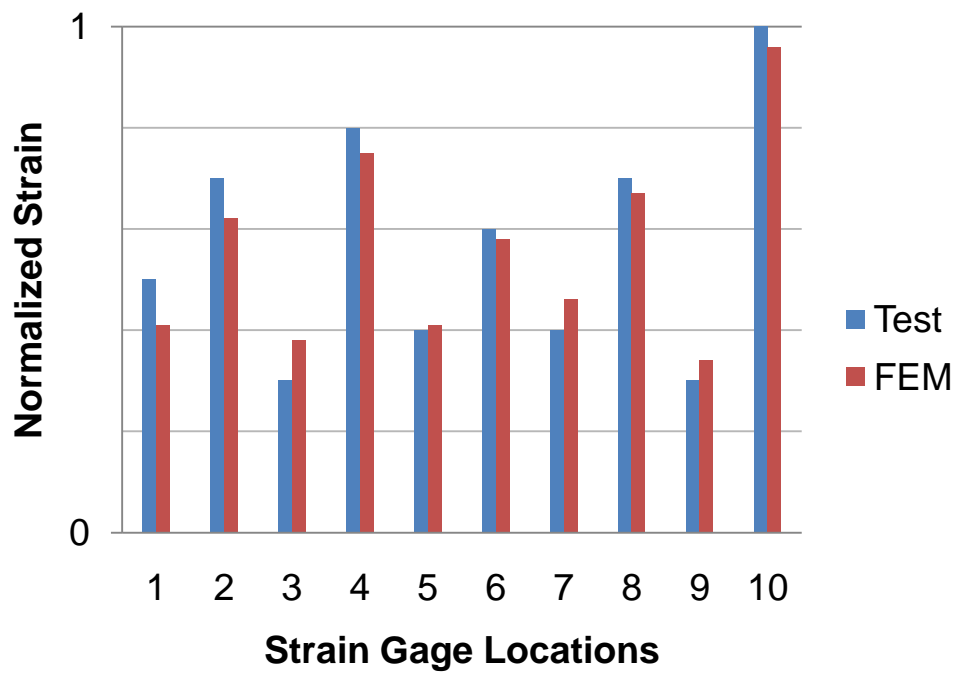


Figure 17. Normalized test and FEM strains at different strain gage locations

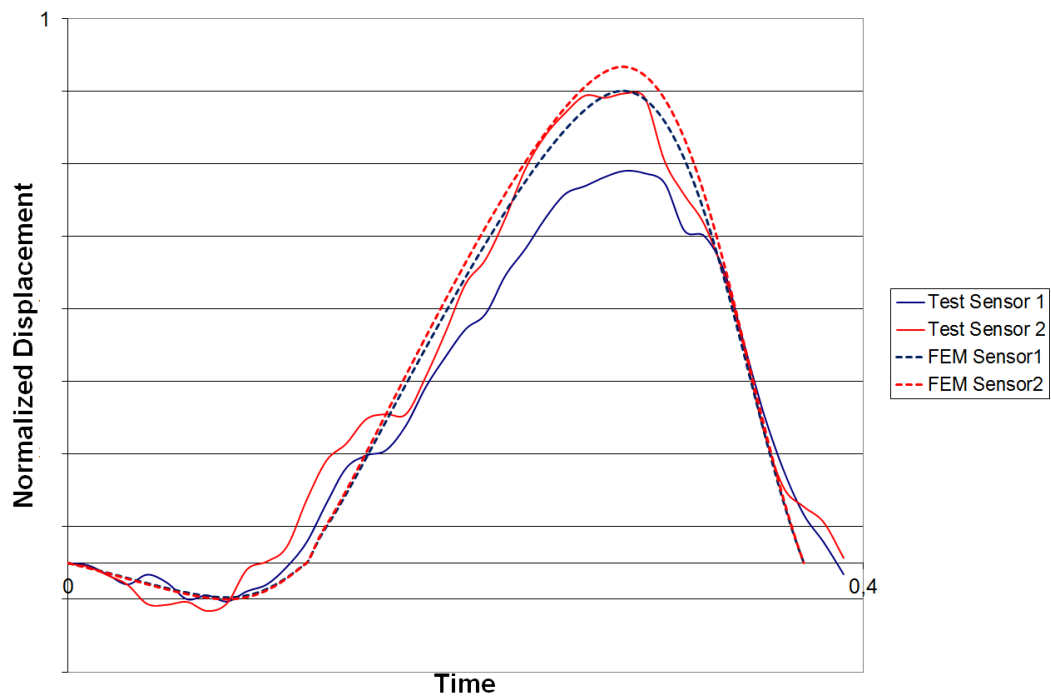


Figure 18. Normalized test and FEM displacements

5.2 Verification of Sub Modeling

The global model was constructed using usually shell elements and boundary conditions were applied on it. The result of the global model is required in order to solve sub models. The sub model boundary conditions are taken from global model result. In order to verify sub modeling approach a test model of a frame has been constructed and subjected to certain test loads. This model has low number of such elements that it would permit an accurate global analysis. After finding the critical points sub models are taken around these points and analyzed again. The frame model is fixed at bottom end and applied concentrated force at other end that causes bending. The global model consists of all shell elements. (Figure 19) Sub models were created using both shell and solid elements. (Figure 20)

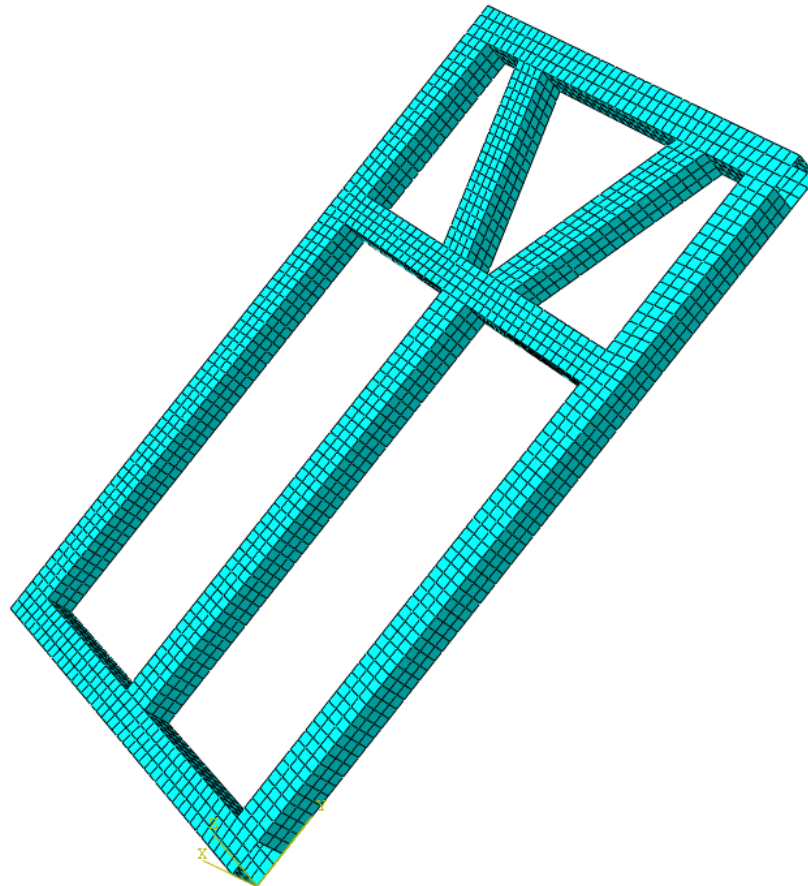


Figure 19. Global shell model used for verification

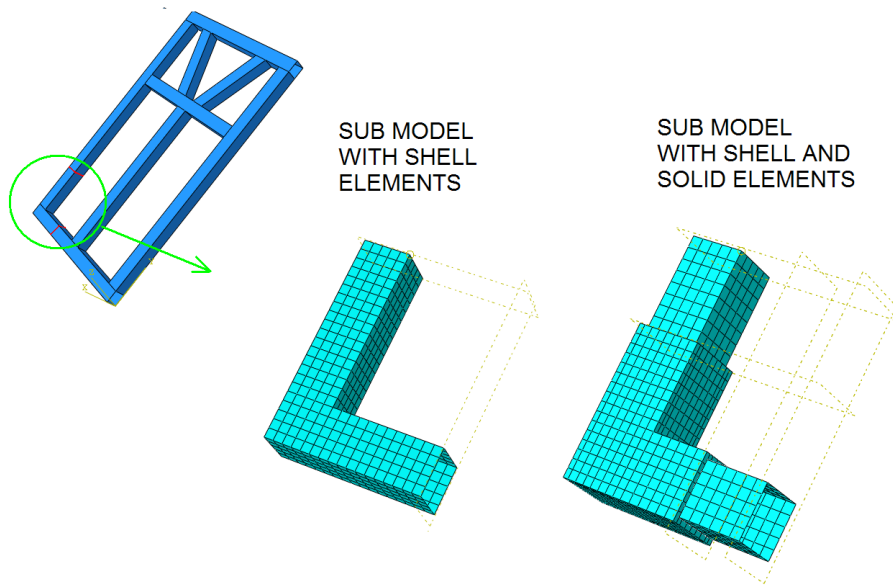


Figure 20. Sub models created using shell and solid elements

The global results are given in Figure 21 and compared between sub models in Figure 22. As seen on von Mises stress plots, sub model results are consistent when compared to global model results.

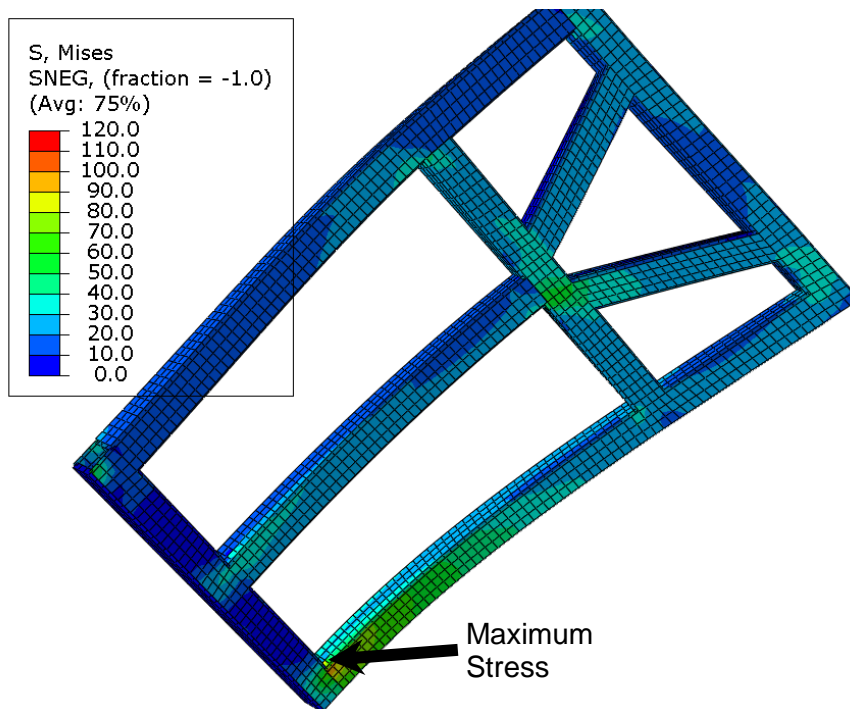


Figure 21. Global model von Mises stress plot

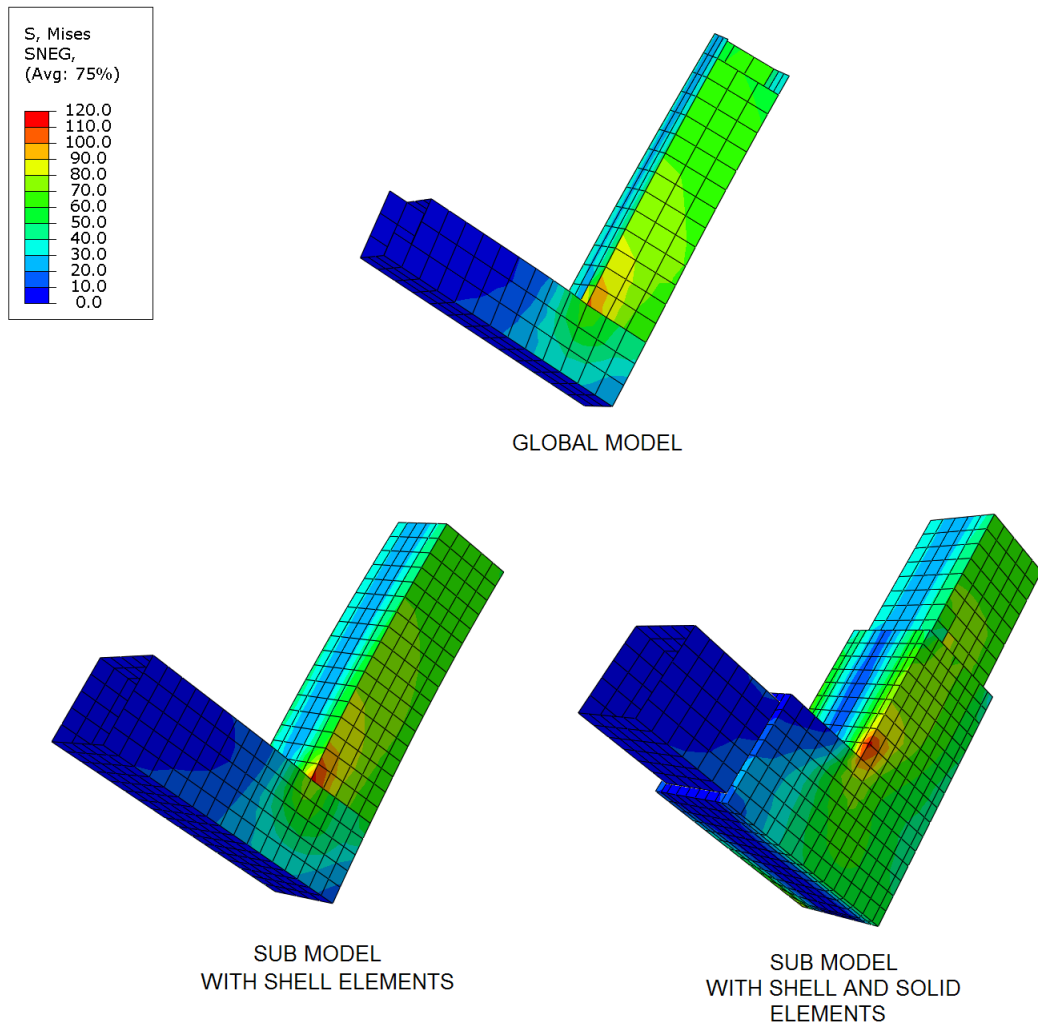


Figure 22. Comparison of von Mises stress between global model and sub models

5.3 Verification of Crack Modeling

In order to verify crack modeling, stress intensity factors obtained for different crack conditions are compared with finite element models studied in this thesis. Finite element model of an embedded circular crack was built and stress intensity factor obtained from model was compared against analytical solution that is for embedded circular crack in an infinite body under tensile loading [27]. Then, semi elliptical surface crack was modeled and compared with Newman's solution [28]. Finally a recent study was investigated for a through thickness crack [29].

5.3.1 Embedded Circular Crack

Stress intensity factor for an embedded circular crack is given as [27]:

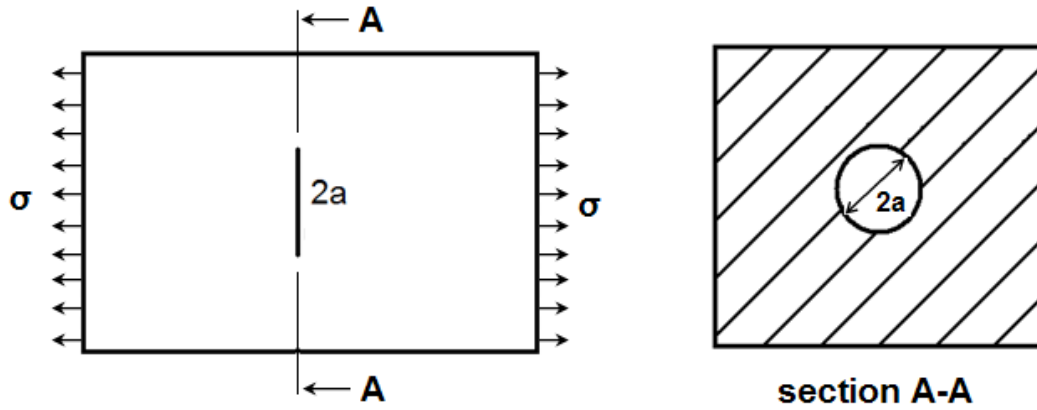


Figure 23. Embedded circular crack geometry

$$K_I = \frac{2}{\pi} \sigma \sqrt{\pi a} \quad (5.1)$$

Finite element model was created for $a=1\text{mm}$. Since formula is given for an embedded circular crack in an infinite body, dimensions of finite element model were chosen much greater than crack dimension. Crack is located in the middle of a $30 \times 30 \times 30\text{mm}$ cube in the finite element model. Stress intensity factor in Mode I was obtained under tensile loading.

When results are investigated, stress intensity factor from finite element model is very close to analytic formulation although model has finite dimensions.

Table 1. Stress intensity factor results for embedded circular crack

Elastic Modulus	Poisson's Ratio	σ	Formula	FEM	% Difference
210 GPa	0.3	1 MPa	$1.1283 \text{ MPa}\cdot\text{mm}^{0.5}$	$1.1236 \text{ MPa}\cdot\text{mm}^{0.5}$	0.42

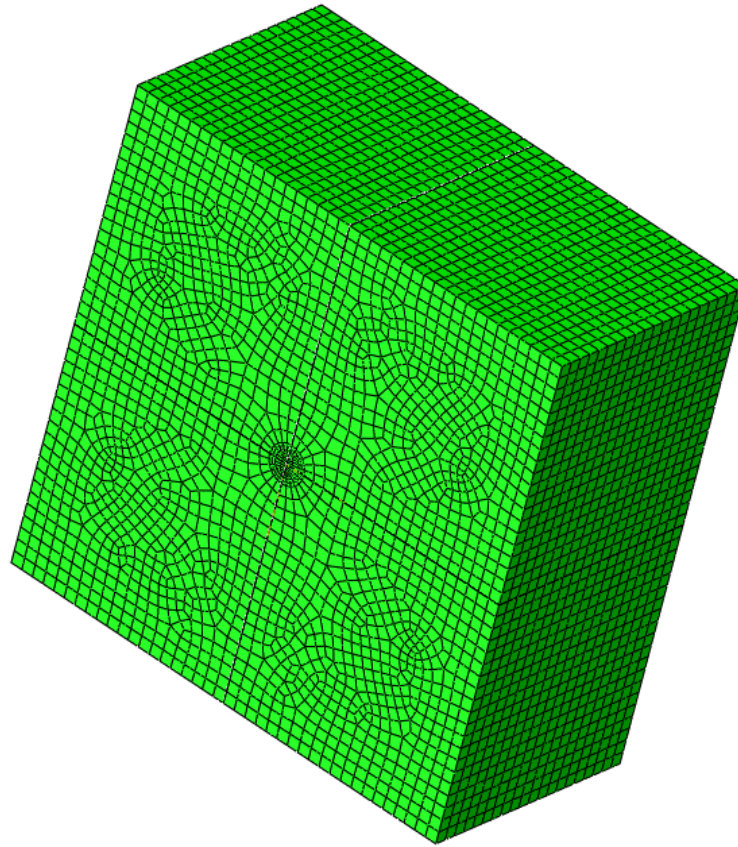


Figure 24. Finite element model of embedded circular crack

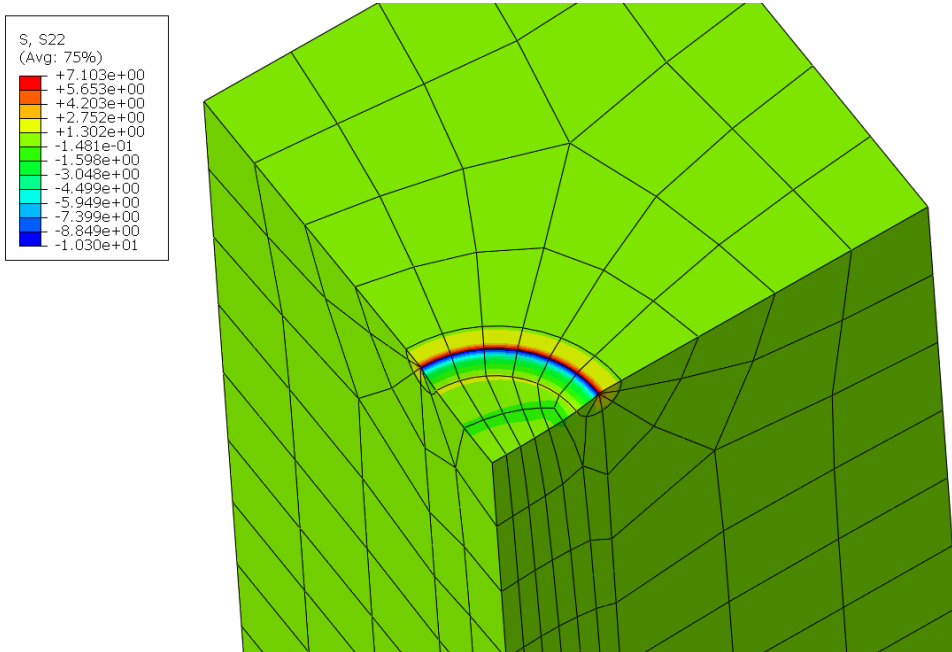


Figure 25. Stress field perpendicular to crack plane

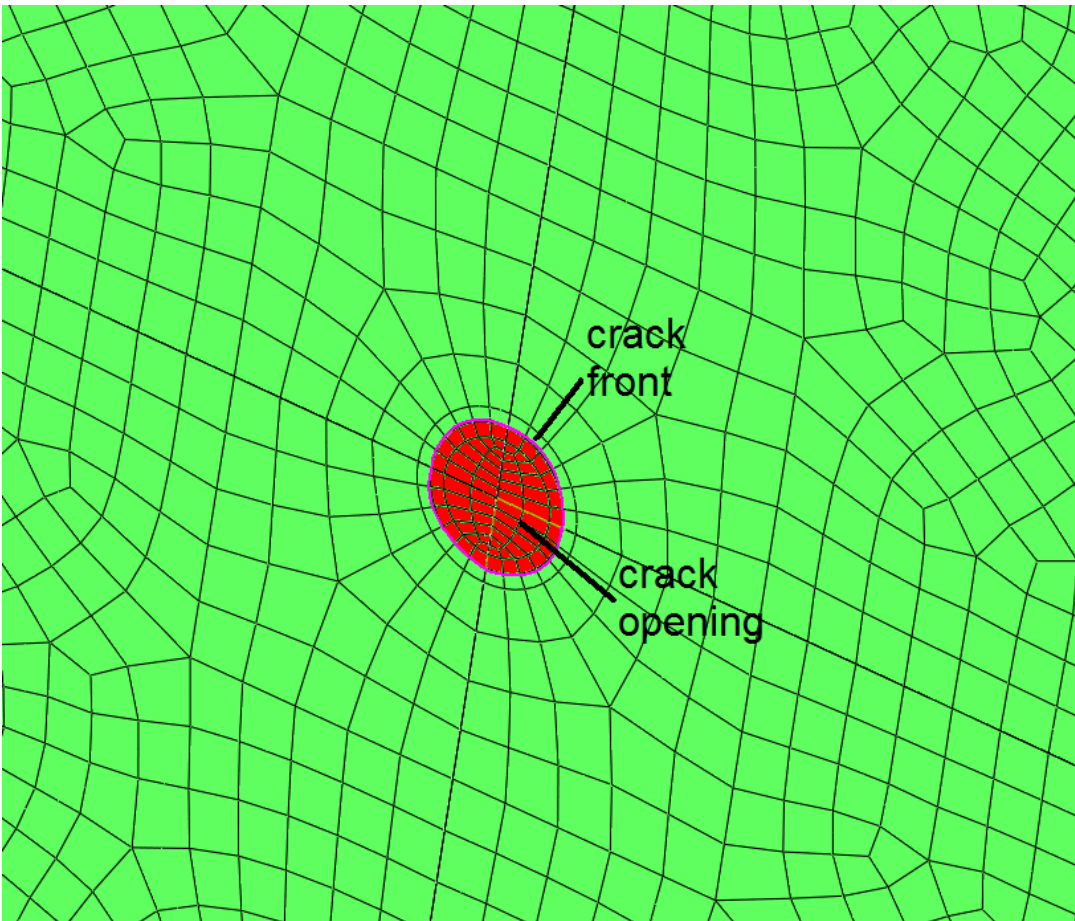


Figure 26. Crack face of embedded circular crack

5.3.2 Semi-elliptical Surface Crack

Stress intensity factor solution for a semi-elliptical surface crack in a finite volume under tensile loading is given as [28]:

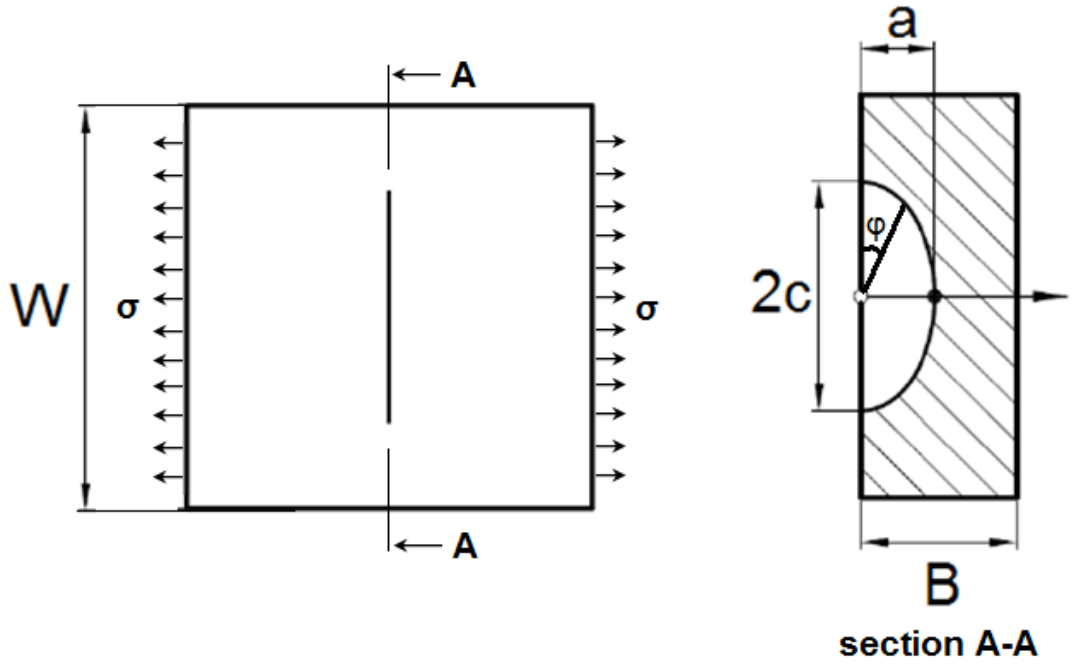


Figure 27. Semi elliptical surface crack geometry

$$K_I = \sigma \sqrt{\frac{\pi a}{Q}} M_e \quad (5.2)$$

$$Q = 1 + 1.47 \left(\frac{a}{c}\right)^{1.64}, \left(\frac{a}{c}\right) \leq 1 \quad (5.3)$$

$$M_e = \left[M_1 + M_2 \left(\frac{a}{B}\right)^2 + M_3 \left(\frac{a}{B}\right)^4 \right] f_w f_\phi g \quad (5.4)$$

$$M_1 = 1.13 - 0.1 \frac{a}{c} \quad (5.5)$$

$$M_2 = -0.54 + \frac{0.89}{0.2 + \frac{a}{c}} \quad (5.6)$$

$$M_3 = 0.5 - \frac{1}{0.65 + \frac{a}{c}} + 14 \left(1 - \frac{a}{c}\right)^{24} \quad (5.7)$$

$$f_w = \sqrt{\frac{1}{\cos\left(\frac{\pi c}{W} \sqrt{\frac{a}{B}}\right)}} \quad (5.8)$$

$$f_\varphi = \left[\left(\frac{a}{c}\right)^2 (\cos \varphi)^2 + (\sin \varphi)^2 \right]^{0.25} \quad (5.9)$$

$$g = 1 + \left(0.1 + 0.35 \left(\frac{a}{B}\right)^2\right) (1 - \sin \varphi)^2 \quad (5.10)$$

Finite element model was created for $a=1$ mm, $c=2$ mm, $W=12$ mm and $B=5$ mm. In Figure 29 and Figure 30 finite element model of semi elliptical crack can be seen. Stress intensity factor in Mode I was obtained since loading is in mode I direction. Mode I stress intensity factor along crack front obtained from FEM and formula are given in Figure 28. Angle φ is measured from free surface. When stress intensity factor at the surface along crack front is compared, it is seen that solution obtained from finite element model agrees well with the solution given above. At free surface and deepest point of the crack difference between solutions has its lowest value. In Table 2, maximum Mode I stress intensity factors and maximum difference between solutions along crack front are given.

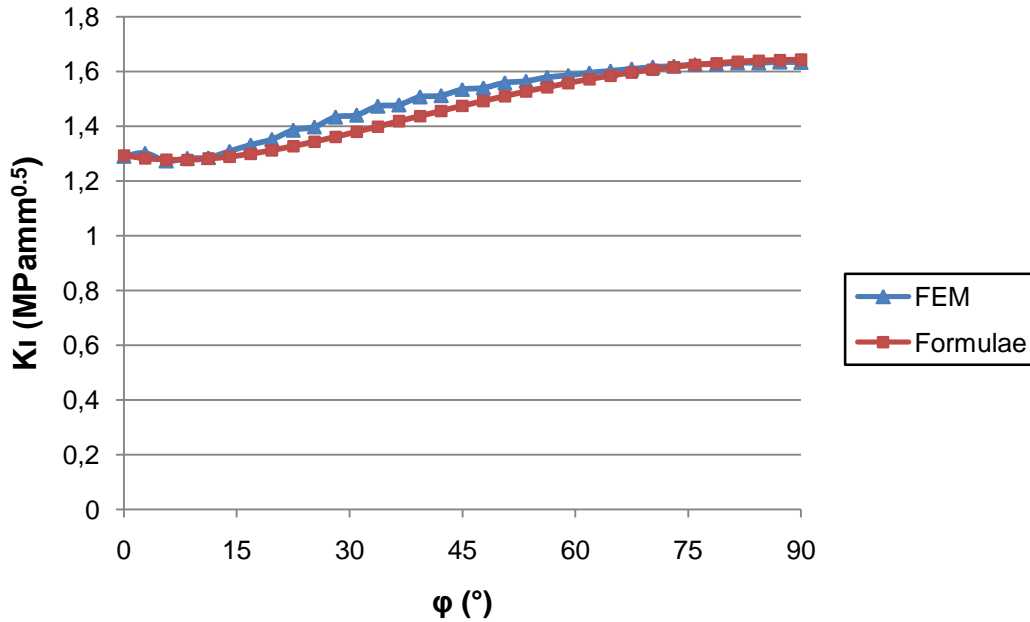


Figure 28. Mode I stress intensity factor along crack front

Table 2. Stress intensity factor results for semi elliptical surface crack

Elastic Modulus	Poisson's Ratio	σ	Formula K_I max	FEM K_I max	% Max Difference
210 GPa	0.3	1 MPa	1.6424 $\text{MPa}\cdot\text{mm}^{0.5}$	1.6331 $\text{MPa}\cdot\text{mm}^{0.5}$	5.3

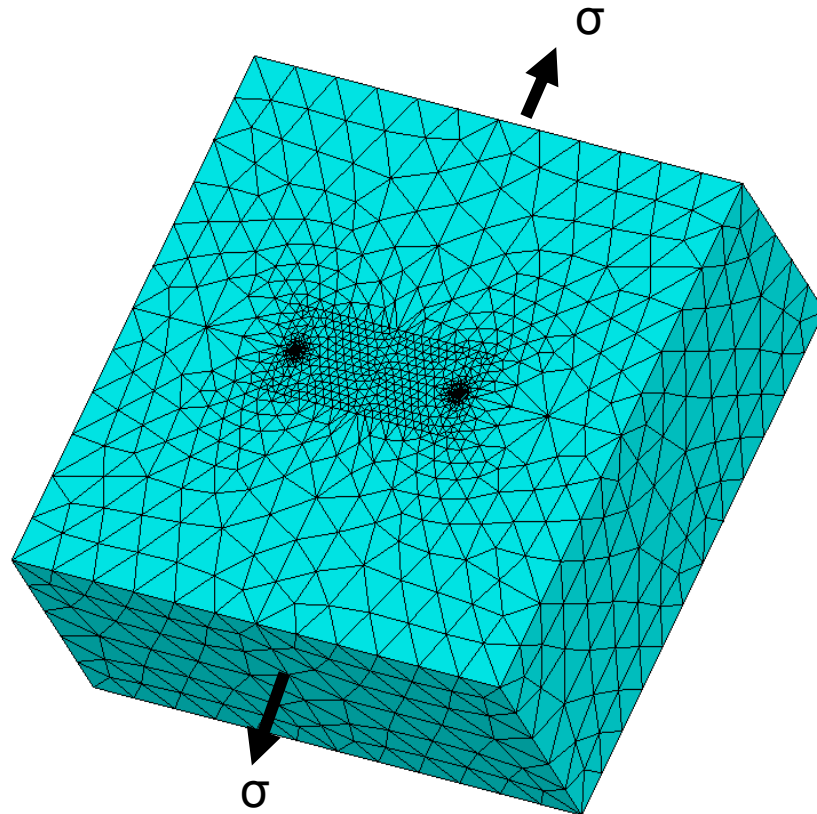


Figure 29. Finite element model of semi elliptical surface crack

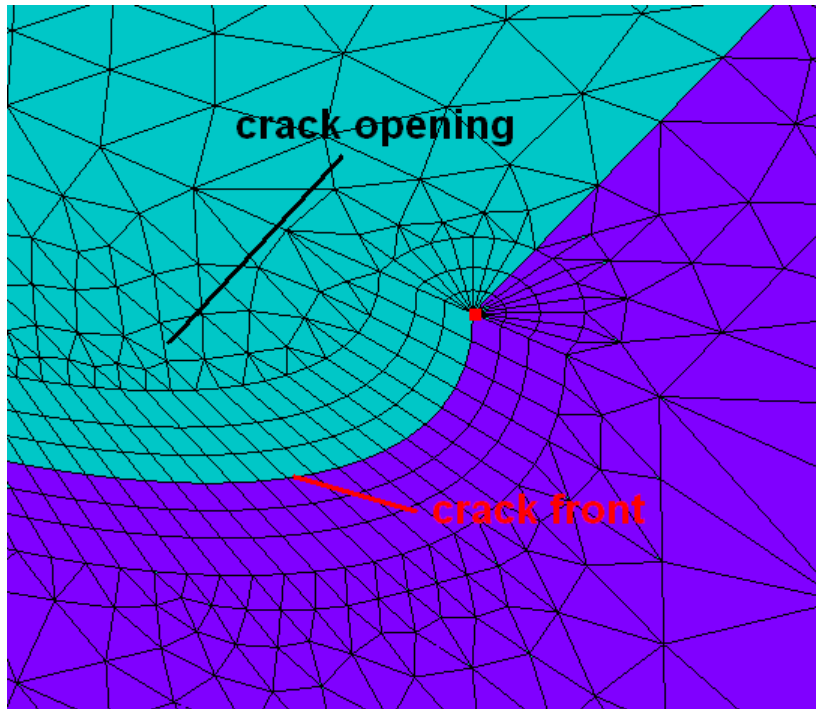


Figure 30. Crack face of semi elliptical surface crack

5.3.3 Through Thickness Surface Crack With Residual Stress

Woyak et al. [29] in their study investigated cracks on coronary stents which undergoes large strains under operational conditions. They conducted a validation study on importing residual stresses on cracked body. The model is a bar with a through thickness surface crack under three point bending. In this work, bar was first plastically deformed and released to form residual deformation. Then, bending load was applied on the body. During forming process body was treated as flawless by not allowing the crack face to separate. In another model, bar was modeled with crack face open, and stress distribution on the body was imported to the model.

The model used in their study can be seen on Figure 31 [29].

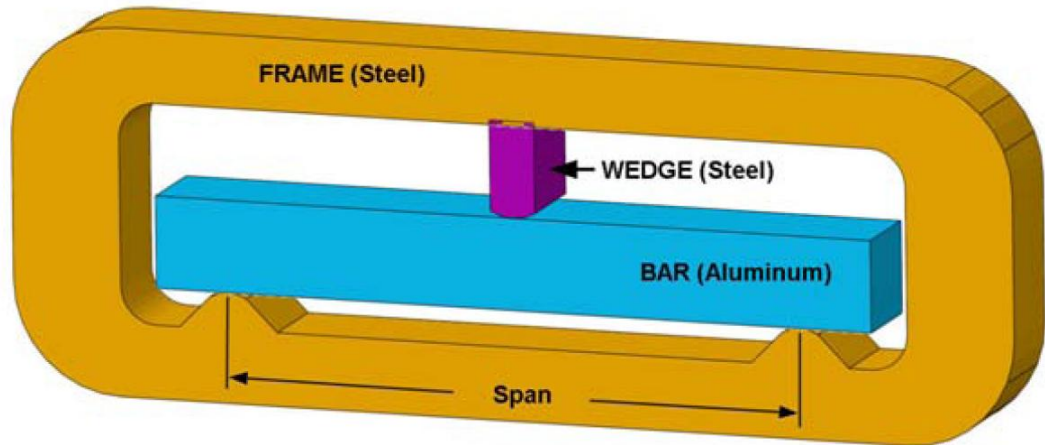


Figure 31. Geometry used in residual stress crack analysis

In this thesis work the results of [29] is attempted to be duplicated. Only half of the model was created due to symmetry. The dimensions and the material properties were taken as same in [29]. Materials and dimensions can be seen in Figure 31 Figure 32 respectively. Since not all dimensions are given in the paper, undefined dimensions are assumed based on overall geometry. Finite element model of the geometry and detailed view of crack front is given in Figure 33 and Figure 34. Plastic material property was defined for aluminum material with initial yield of 500 MPa and hardened yield of 700 MPa at 50% plastic strain.

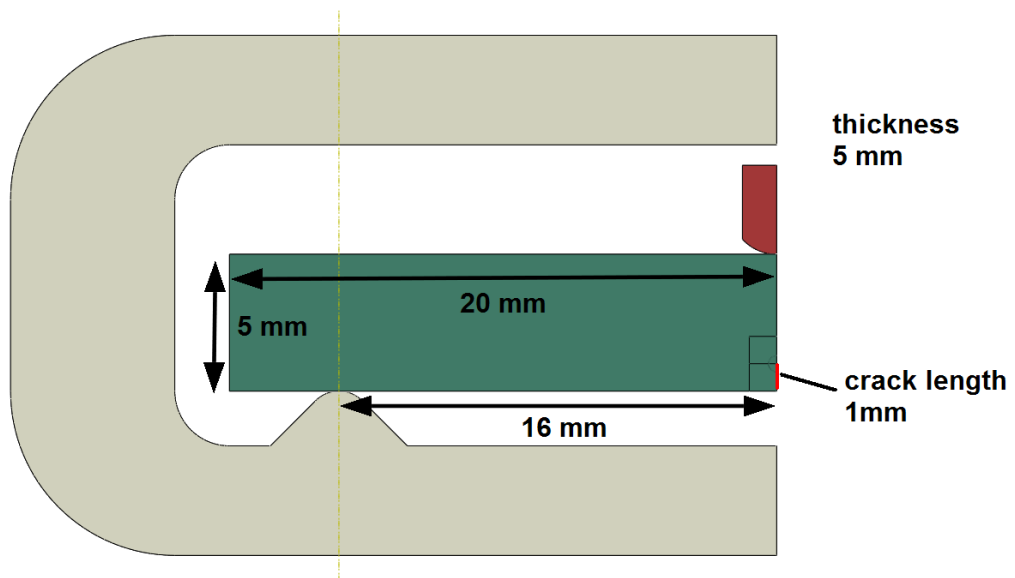


Figure 32. Bar dimensions

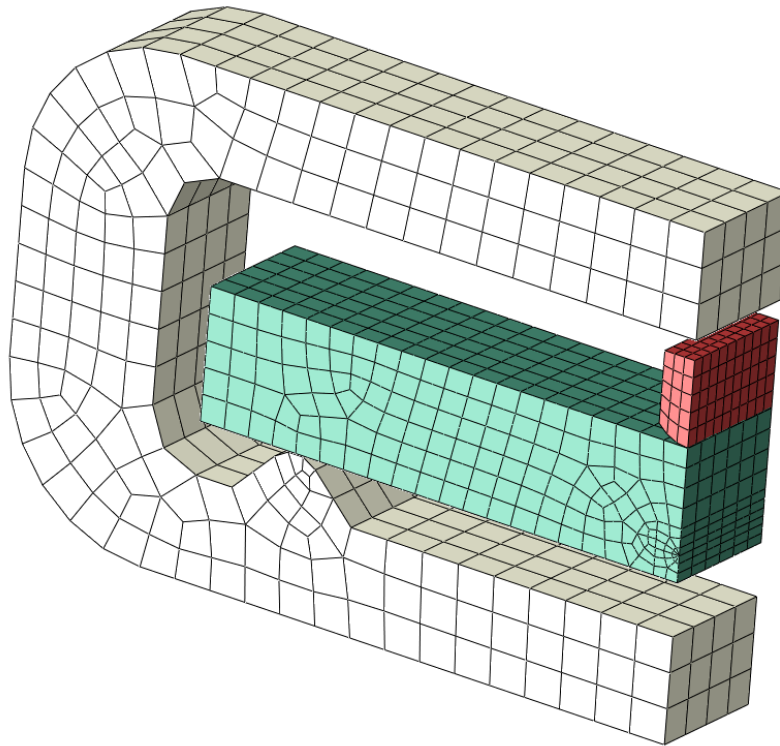


Figure 33. Finite element model of residual stress model

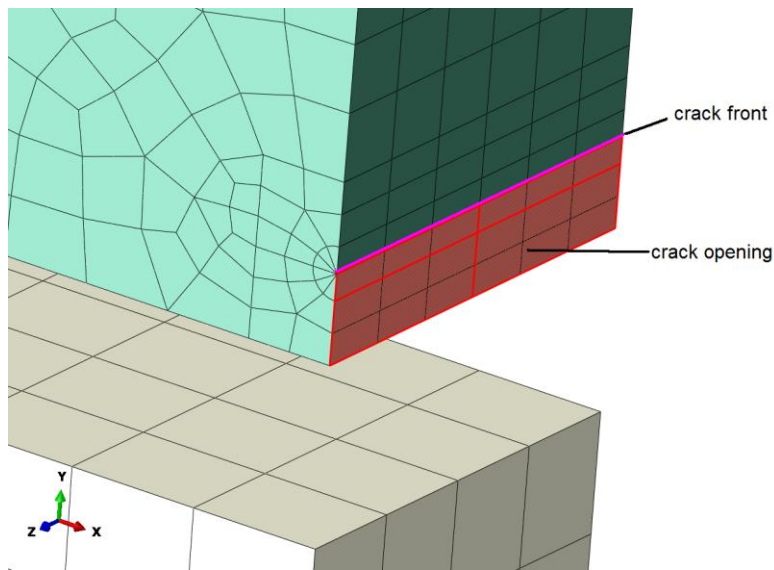


Figure 34. Crack zone of finite element model

Residual stress formation analysis contains several steps. At initial condition, aluminum bar resides on supports of steel frame and wedge has no contact with the frame. Definitions of parts were given in Figure 31. First, aluminum bar was deformed plastically in axial

direction by producing compressive forces in plane strain conditions which was imposed by proper displacement constraints. As bar axially deforms (i.e. contracts), it expands sideways simultaneously. This expansion causes wedge to interfere with steel frame. Since no contact was defined between wedge and frame at this stage, no force was exerted due to interference.

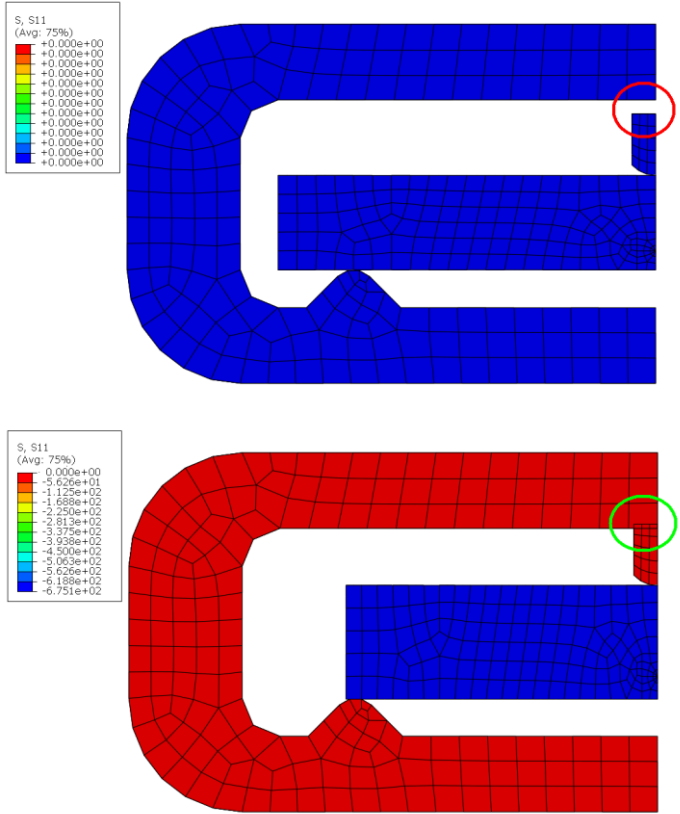


Figure 35. Results of large axial deformation step

In the following step, plane strain conditions were removed and contact between wedge and frame was activated. Also in the beginning of this step boundary conditions that caused bar to contract were removed. Upon activation, contact tries to remove overclosure between two parts. When interference was fully resolved, equal forces act on frame and wedge. In the finite element model there was no external force applied on parts. Three point bending force was applied by interference of wedge and frame due to lateral deformation of the aluminum bar in a self equilibrating manner.

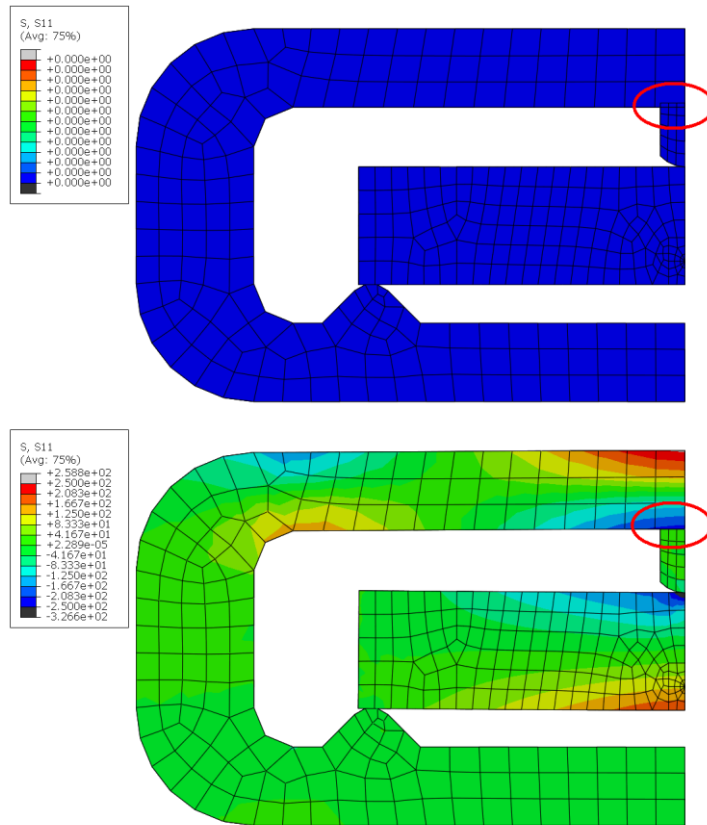


Figure 36. Results after activating contact between wedge and frame

Crack analysis was performed in two steps. In first step last configuration in the residual stress case was applied again. In the second step, crack opening was released and stress intensity factors are calculated. In the paper, stress intensity factor solution for three point bending case of these dimensions was given. Results are given in Table 3. Residual stress field imported on finite element model that contains crack and cracked finite element model solution is shown on Figure 37.

In residual stress forming steps crack faced was not allowed to separate via appropriate boundary conditions at crack face. In a separate model crack face was released and allowed to separate. Residual stress solution obtained from previous steps was applied at cracked model. Stress intensity was calculated using linear elastic material properties.

When the results are investigated, it is seen that finite element solution is in 3.2% of solution given in the paper for last step of analysis which is for open crack face configuration. In the paper not all dimensions were explicitly given, therefore some dimensions were deduced from visual context, and this may cause additional error. It can be concluded that finite element model is in acceptable range for such a solution. Also as indicated in [29] import capability of ABAQUS was used for stress intensity factor calculation of a cracked body under a residual tensile load.

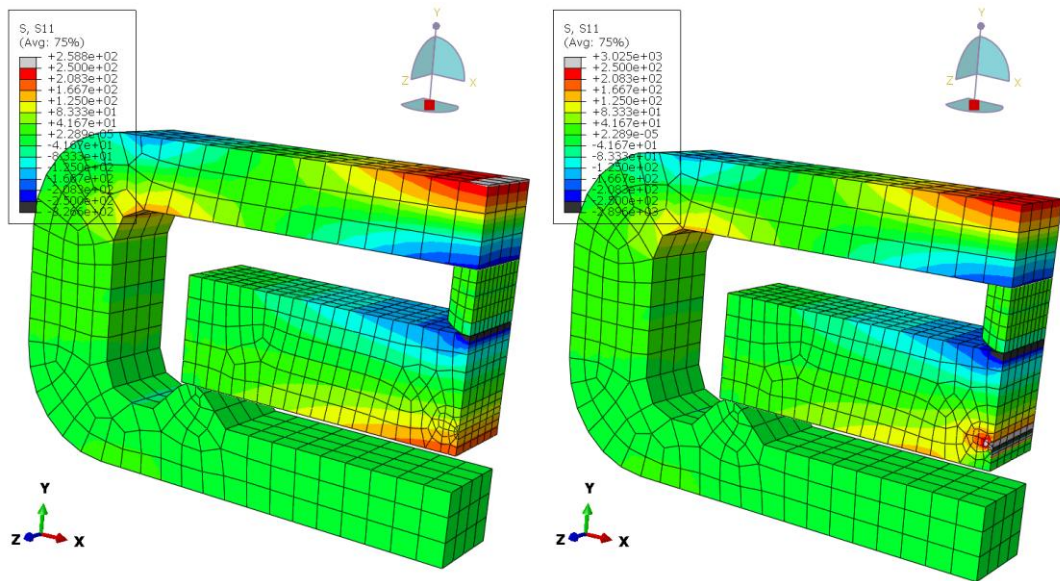


Figure 37. Residual stress (left) imported on cracked finite element model (right)

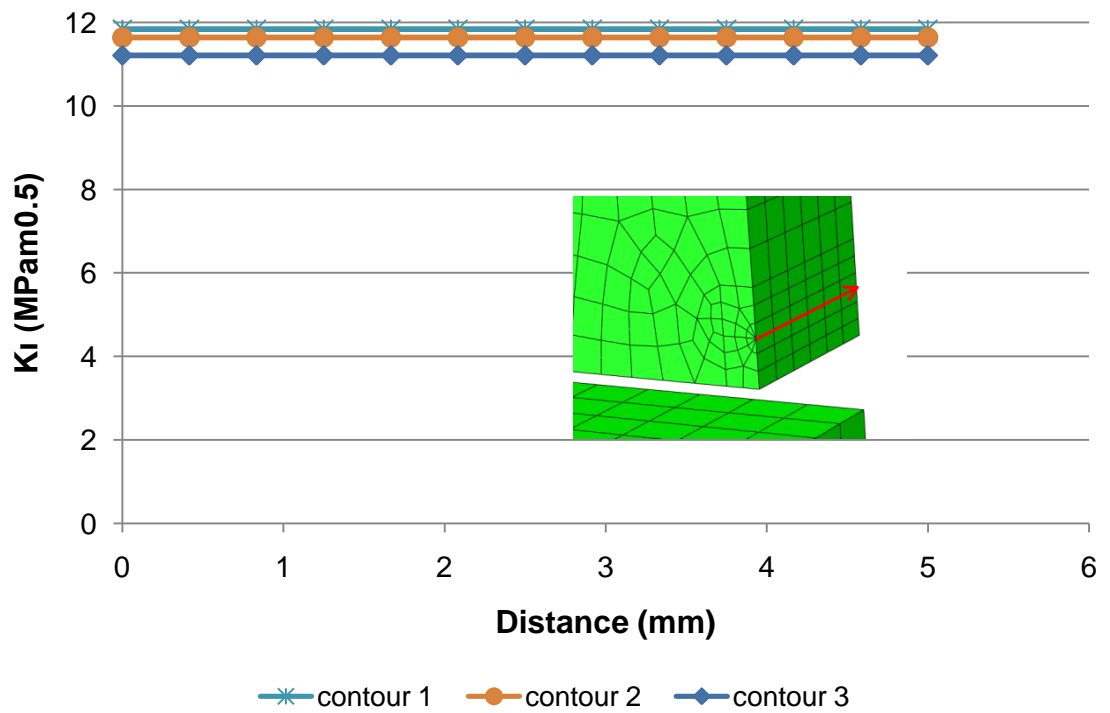


Figure 38. Mode I stress intensity factor variation along crack front

Table 3. Stress intensity factor solutions for through thickness crack under three point bending

	[29] Solution	FEM solution	% Difference
Contour 1	12.23 MPa.m ^{0.5}	11.84 MPa.m ^{0.5}	3.2
Contour 2	11.87 MPa.m ^{0.5}	11.64 MPa.m ^{0.5}	1.9
Contour 3	11.46 MPa.m ^{0.5}	11.21 MPa.m ^{0.5}	2.2

CHAPTER 6

FINITE ELEMENT MODELING OF WELDED CONNECTIONS ON FRACTURE MECHANICS BASIS

6.1 Problem Definition

Finite element analysis of structures is divided into pre and post processing sections. In pre processing, model to be analyzed is divided into elements and nodes. These elements and nodes constitute the finite element mesh of the structure. After the mesh is generated, proper loading and boundary conditions are defined on the finite element mesh. In pre processing, it is vital to choose correct element type and formulation appropriate for the problem at hand. When finite element model is completely defined, a solution is obtained. In post processing, the solution is investigated and elemental and nodal results are listed or plotted.

Real life applications include complex structures and loadings. While analyzing structures, simplifications and assumptions must be made in order to obtain feasible models. User must have a good understanding on the problem to determine level of detail to be included in the model. In many cases, models at different levels of details are prepared. Such applications are called global and local modeling. In global modeling overall displacement and stress field of the structure are obtained. Sub models import displacements on the boundaries from global model solution and they include finer mesh densities than global model in order to obtain more accurate solutions at the investigated region. Using finer model for the global model at the beginning may cost unnecessary effort during modeling and solution phase.

After finite element solutions are obtained, results must be investigated with great care. Evaluating results should be beyond listing and plotting displacement or stress field solutions. The user must first check the result if they fit to expectations and level of mesh detail is enough for the evaluation of the structure under given loading. If the structure's overall deformation is needed, a global model with moderate level of detail may be enough. However if a failed connection is to be investigated, details at that connection such as fillets, welds, holes must be included in the model.

In this thesis work, critical weld locations of a multi barrel launcher system is investigated on a fracture mechanics basis. An example of such a system can be seen on Figure 1.A global finite element model of the launcher system is constructed and critical locations are

determined. Then sub models of determined critical sections are prepared. These sub models make it possible to introduce details that are enough to include cracks on welded connections. Finally the structure is evaluated for structural integrity under operational loads.

6.2 Finite Element Modeling Methodology

6.2.1 Global and Sub Model

In order to obtain overall response of the structure under operational loads, first a global model is created. This model includes all elements that affect the response of the structure. Global models become relatively large since they include many parts and connections. Therefore, level of detail to be modeled in the mesh of the structure is reduced. However, these details do not affect the general deformation and stress field on the structure. Generally local details such as fillets, small holes, rivets or fasteners are omitted. Including all details in global model makes the finite element model too large to handle and increases computing time greatly. Therefore it is reasonable to work with global and sub models.

In sub models, all necessary details that are omitted in the global model are included. Sub models only cover a limited portion of the whole structure. The boundary conditions in the sub models are obtained from global model run. In sub models a finer mesh is applied around the details which would not be practical to include in global model. Unlimited sub models can be created and analyzed without having to run the whole model again under the same boundary conditions. This allows designer to investigate different designs and find solutions in a comparatively less time.

Finite element model of the launcher system is constructed and analyzed. The system roughly consists of three main parts namely launching vehicle, auxiliary chassis and cradle. The launching vehicle carries cradle and rockets, transports them to launching site. The auxiliary chassis provides additional mounting interfaces for cradle and peripherals, positions the launcher system in to ground in a solid manner and additional strength at needed locations. The cradle carries rockets to be fired and accurately positions them prior to firing. The launcher system is designed and constructed in steps. The cradle and auxiliary chassis is built and tested separately. Then whole components are mounted together and tested. Detailed finite element models of each component is built and analyzed as a part of design study. In this study cradle model is investigated. Launcher system models can be seen on Figures Figure 39, Figure 40 and Figure 41.

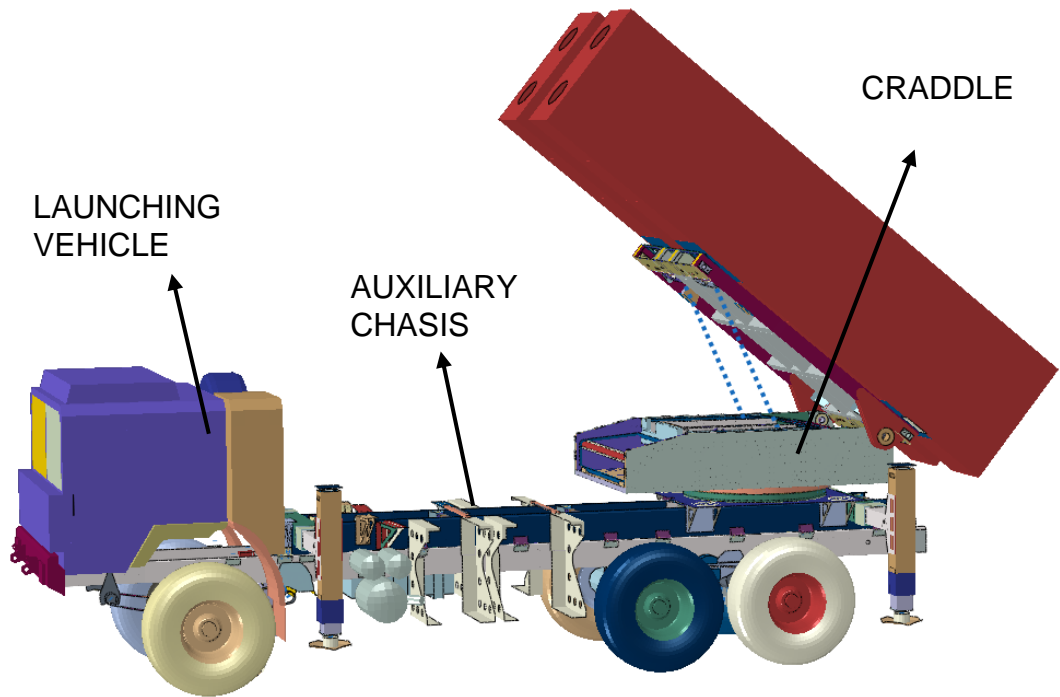


Figure 39. Launcher system model (side view)

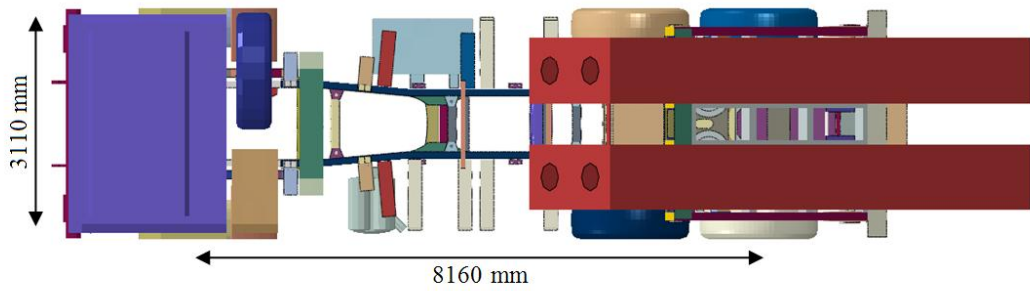


Figure 40. Launcher system model (top view)

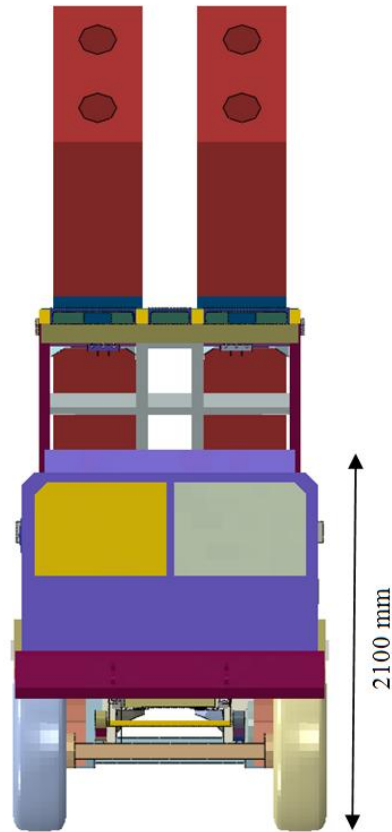


Figure 41. Launcher system model (front view)

In this study commercial software package ABAQUS is used for finite element analysis. All global and sub models are created in ABAQUS environment. A global model includes structural parts, kinematic connections, elastic springs and weld connections. The majority of the model is constructed using shell elements. (Figure 42) Hydraulic pistons are modeled using beam connections. Hinge connections are modeled using appropriate connectors. Multi barrel cradle includes a slewing ring that allows it to turn in azimuth angles (Figure 43). The slewing ring is at the connection of cradle to launching vehicle. It must withstand transportation and firing loads and allow rotation of cradle with minimum effort. The location of slewing ring on the launcher system is given in Figure 46. The slewing ring in the global model is created with a special modeling method. Every ball in the slewing ring is represented by a couple of elastic springs. These springs carry load in compression direction as it should be. (Figure 44) The slewing ring is a major component of cradle finite element model that affects dynamic response. Global finite element model includes all kinds of non linearity such as material, geometry and contact. Including necessary elements in the global model, dynamic and structural response of the structure under operational loads are captured well. This allows designers to evaluate their designs more accurately prior to testing. Realistic simulations are obtained in computer environment and hence

overall cost and time of a design cycle is reduced. An accurate model also gives opportunity to notice unexpected response of the structure if there is any.

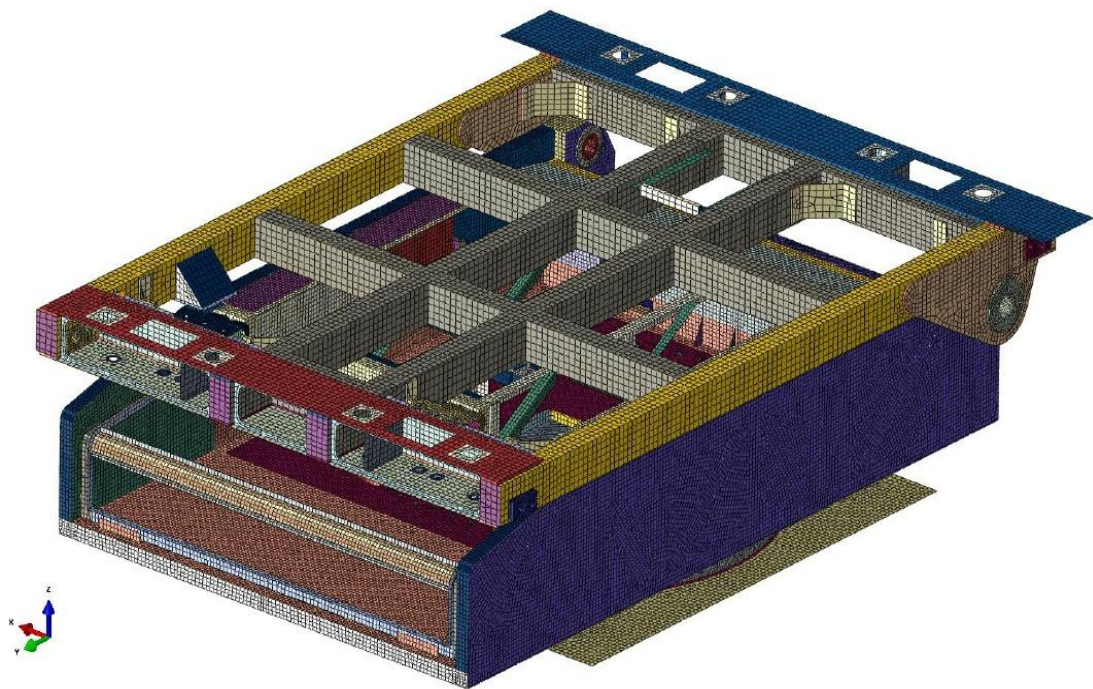


Figure 42.Craddle finite element model

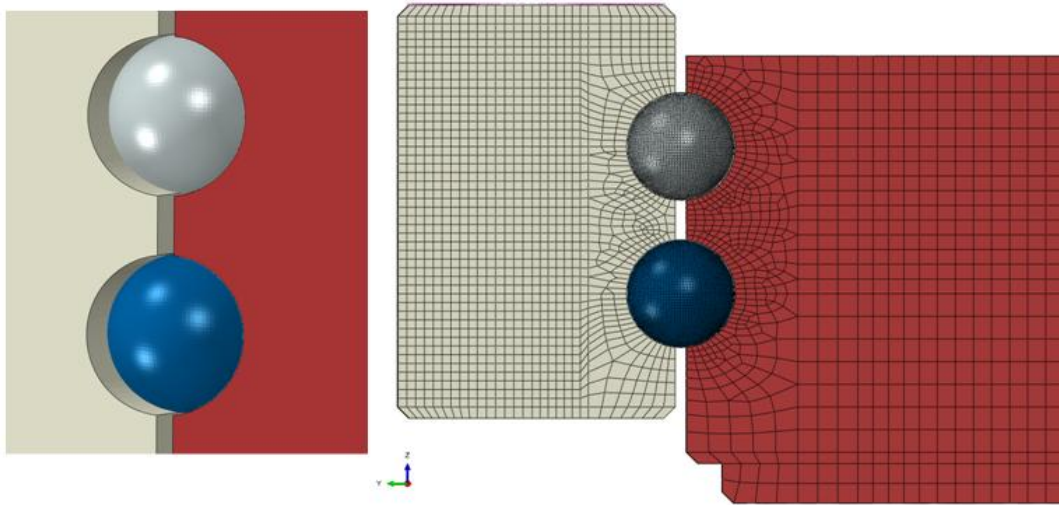


Figure 43. Slewing ring balls detail

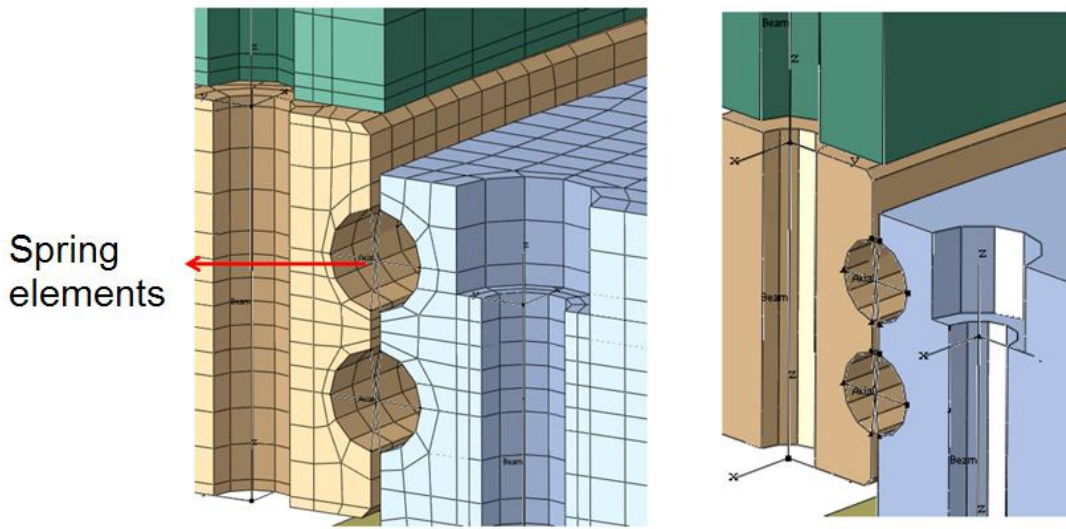


Figure 44. Spring elements representing slewing ring balls

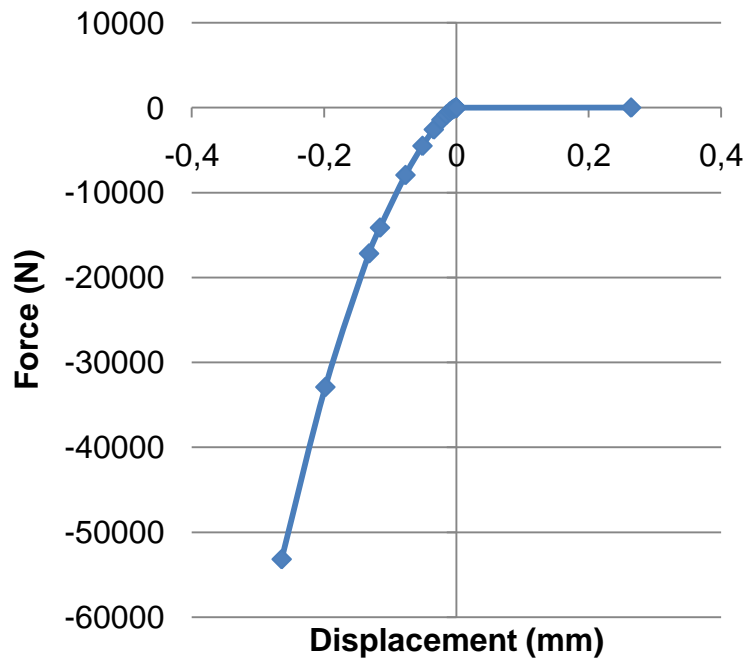


Figure 45. Nonlinear spring constant for balls

Spring constants for every ball in the slewing ring are defined by a nonlinear curve. For every ball in the ring same nonlinear spring constant is used. This definition allows balls to carry load in compression direction only as they should be. As it is seen in Figure 45, spring exerts force in compression displacement while no force under tensile displacement. This is proper behavior for a ball in raceway of slewing ring. A loaded ball will contact raceway in two points.



Figure 46. Location of slewing ring on launcher system

Sub models are created at locations where the details of the structure need to be investigated. The details investigated in this study is welded connections and crack modeling. In order to model cracks, a solid model should be created. Since global model is created using shell elements, while using sub models shell to solid conversion of boundary conditions must be performed.

The method used in this study is described as follows:

1. Local region of interest is determined
2. Local region is selected by adding some region on the boundaries.
3. Additionally selected regions are left to be modeled with shell elements.
4. Region of interest is modeled using solid elements.
5. Shell to solid coupling is defined between solid and shell parts.
6. Boundary conditions are imported from global shell model to shell boundary elements.

By using this method degree of freedoms of nodes on both global and sub models are equal on the model boundaries. Sub model now can be used for detailed investigation and crack modeling.

6.2.2 Elements Overview

In this part general information about element types used in finite element models is provided.

6.2.2.1 Quadrilateral Shell Element S4R

When geometry to be modeled has its thickness significantly smaller than other two dimensions, shell elements are used to model the geometry. Shell elements are placed at reference surface representing geometry. Thickness of geometry is defined in section property of shell elements. Conventional shell elements have six degrees of freedom at nodal points. Shell elements have top and bottom surface definitions. Positive normal direction indicates top surface whereas negative indicates bottom surface. These definitions are used when specifying offsets, defining contacts or viewing results [30].

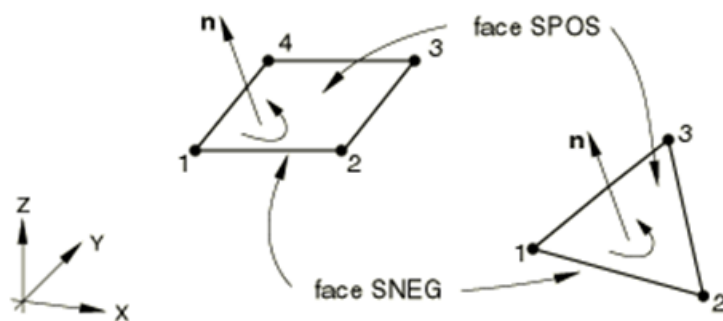


Figure 47. Shell element notation [30]

S4R element notation defines four noded conventional shell elements with reduced integration formulation. In three dimensions, reduced integral generally gives accurate results and decreases computational cost. However, when reduced integral is used with linear elements model must be check against hour glass. It can be prevented by using finer elements if any hour glass occurs.

6.2.2.2 Hexahedral Solid Element C3D8

Solid elements are used for three dimensional modeling of components. Volume of the component is filled with continuum solid elements. Solid elements can have brick,

tetrahedral or wedge shapes. However solid element mentioned here has brick form. It has eight nodes at each corner representing brick element. Solid elements have three displacement degrees of freedom at nodal points [30].

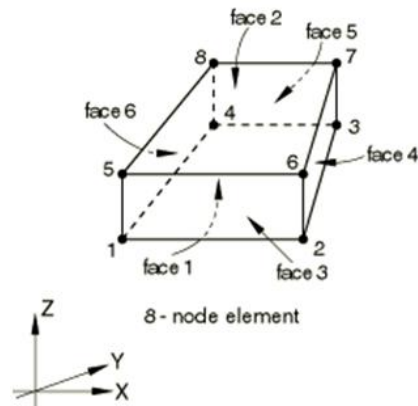


Figure 48. Hexahedral element notation [30]

C3D8 defines an eight noded linear solid element. Results of solid elements are generally given in global coordinate system of finite element model. However elemental coordinate systems can be defined if desired. These elemental coordinate systems are especially used for anisotropic material properties.

6.2.2.3 Collapsed Solid Element C3D20

Collapsed elements are degenerate forms in wedge shape of solid brick elements. Second order wedge elements are generally used for modeling singularities in the model. They provide crack tip singularity by shifting middle nodes to one quarter or element side [30].

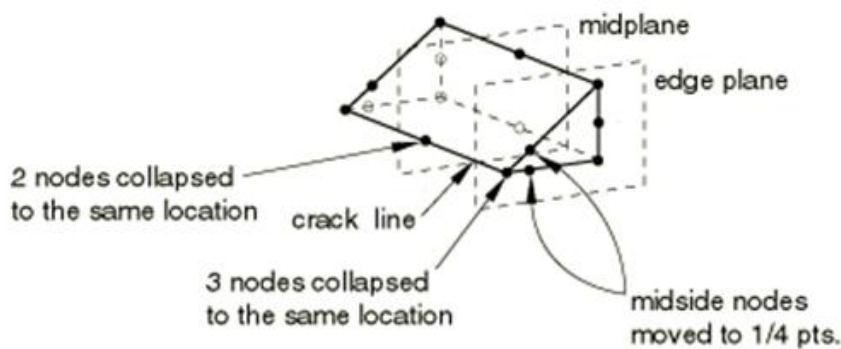


Figure 49. Degenerate element notation [30]

6.2.3 Stress Intensity Factor Calculation

ABAQUS offers different types of contour integrals for onset of cracking in fracture mechanics analysis. It uses J integral calculation if not any other type is requested by the user. If material is defined as linear, stress intensity factors can be related to J integral.

J integral for a linear elastic material can be related to stress intensity factor through equation (6.1) in which \mathbf{B} is defined as pre logarithmic energy factor matrix [30].

$$J = \frac{1}{8\pi} \mathbf{K}^T \mathbf{B}^{-1} \mathbf{K} \quad (6.1)$$

$$\mathbf{K} = [K_I, K_{II}, K_{III}]^T \quad (6.2)$$

Generally J integral can be written as:

$$J = \frac{1}{8\pi} [K_I B_{11}^{-1} K_I + 2K_I B_{12}^{-1} K_{II} + 2K_I B_{13}^{-1} K_{III} + (\text{terms not involving } K_I)] \quad (6.3)$$

I, II, III refers to 1, 2, 3 when components of B is indicated. J integral for an auxiliary shear Mode I crack tip field with k_1 as stress intensity factor can be defined as:

$$J_{\text{aux}}^I = \frac{1}{8\pi} k_1 B_{11}^{-1} K_1 \quad (6.4)$$

When auxiliary field is added to actual field:

$$J_{\text{tot}}^I = \frac{1}{8\pi} [(K_I + k_1) B_{11}^{-1} (K_I + k_1) + 2(K_I + k_1) B_{12}^{-1} K_{II} + 2(K_I + k_1) B_{13}^{-1} K_{III} + (\text{terms not involving } K_I \text{ or } k_1)] \quad (6.5)$$

Since terms not involving K_I or k_1 are equal in total field and actual field, interaction integral can be defined as:

$$\begin{aligned} J_{\text{int}}^I &= J_{\text{tot}}^I - J - J_{\text{aux}}^I \\ &= \frac{k_1}{4\pi} [B_{11}^{-1} K_I + B_{12}^{-1} K_{II} + B_{13}^{-1} K_{III}] \end{aligned} \quad (6.6)$$

When the calculations are also done for Mode II and III, an interaction integral can be given as (6.7).

$$J_{\text{int}}^{\alpha} = \frac{k_{\alpha}}{4\pi} B_{\alpha\beta}^{-1} K_{\beta} \quad (6.7)$$

Above equation can be given below form by assigning unit values to k_{α} .

$$\mathbf{K} = 4\pi\mathbf{B}\mathbf{J}_{\text{int}} \quad (6.8)$$

$$\mathbf{J}_{\text{int}} = [J_{\text{int}}^{\text{I}}, J_{\text{int}}^{\text{II}}, J_{\text{int}}^{\text{III}}]^{\text{T}} \quad (6.9)$$

The software uses an interaction integral method in order to compute stress intensity factors in mixed mode for a calculated J integral value. [30] This extraction method can be used for isotropic and anisotropic linear materials. Details of calculation method can be found in [30].

6.2.4 Boundary Conditions

Main loading on a multi barrel cradle is rocket gas flow that hits the structure. Model is first analyzed against its own weight under gravity. Another critical loading occurs on the structure while positioning the canisters. After cradle positioned, loading due to rocket gas flow is applied on the cradle which can reach total force values of 300kN (Figure 50). Reactions at fixed boundary location due to dynamic loading are given in Figure 51. Plum load is multiplied with a safety factor value in order to account for loading variations and numerical errors in finite element models.

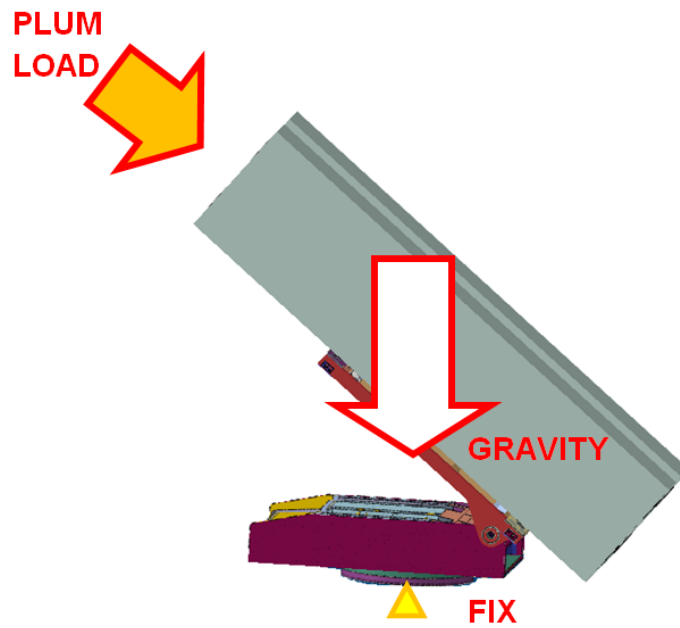


Figure 50. Schematic of boundary conditions

Global model is first solved in a static step under gravity loading. Positioning steps and different elevation angles are investigated. After static solutions are obtained, global model are solved in a dynamic implicit step under rocket gas loading. Hence, static and dynamic loading on the cradle is obtained. It should be noted that firing a rocket is a highly dynamic event. Therefore it is important to model the structure dynamically accurate in order to obtained displacement and stress field on the structure as close as to reality.

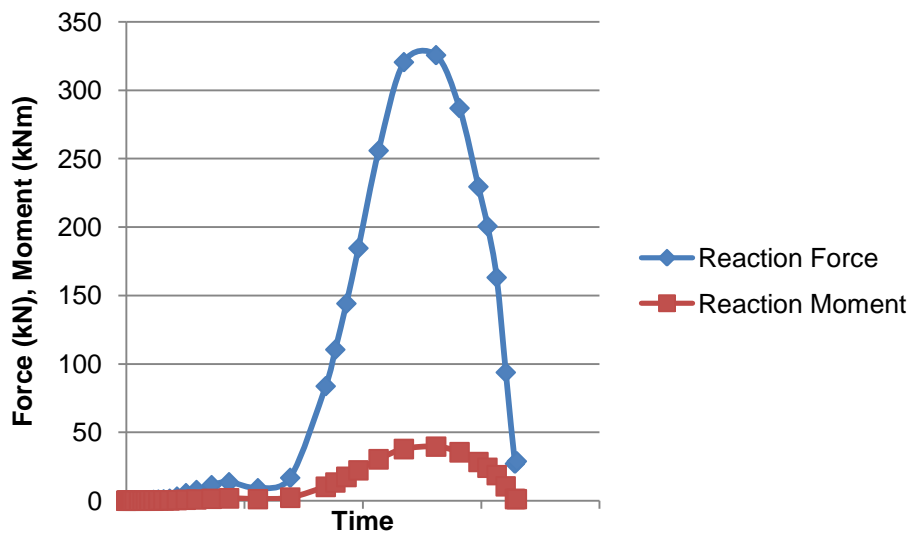


Figure 51. Total reaction forces and moments at fix boundary location

The author performed dynamic analyses of global finite element model and tuning under firing loads, crack modeling, test measurements during firing tests and data processing,

material characterization coordination. Dynamic firing load and updating studies were obtained through [40]

6.2.5 Crack Modeling

In real life, structures are likely to have semi elliptical surface or circular cracks around welds. Cracks can be positioned at different locations on weld geometry and at different angles at a location. Cracks may exist inherently due to welding process in the structure. In addition to that, cracks may occur due to operational loading on the structure. Under repeated loading these cracks grow and eventually cause total failure. In this study, maximum allowable crack size is investigated at critical stress locations and possible crack zones.

Cracks in the structure are modeled using solid elements. Therefore sub models are converted to three dimensional elements in the crack vicinity. Semi elliptical surface cracks are investigated in this study. Along crack front, special elements are created for stress intensity calculations. Collapsed wedge like quadratic elements with middle nodes positioned at quarter point from element vertex are used in order to capture square root crack tip singularity.

Crack models with different mesh densities are created and results are compared. In Figure 52 only crack zone of sub models in different mesh densities can be seen. The elements shown in Figure 52 are part of sub model that is described in section 6.3.1 and boundary conditions are the same as of that sub model. Element density is found in which stress intensity factor does not change significantly over crack front (Figure 53). In fine model overall element size of 0.14 mm with 24 elements in crack front and 8 elements in circumferential direction, in coarse model overall element size of 0.25 mm with 46 elements in crack front and 16 elements in circumferential direction were used. Angle Φ is measured from free surface of crack front.

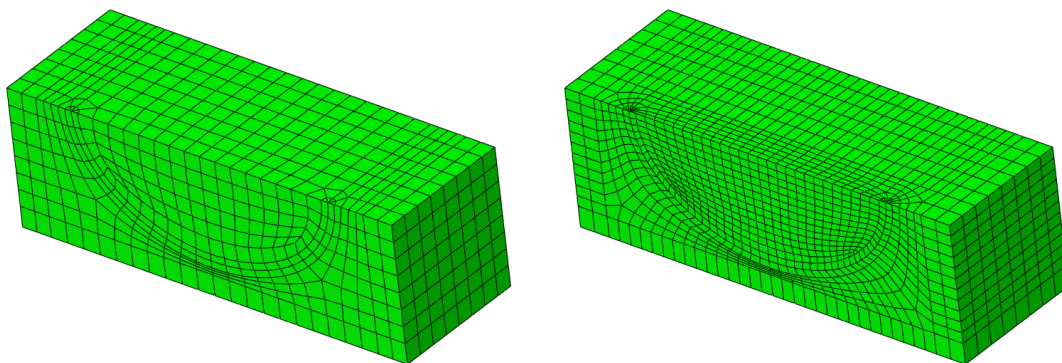


Figure 52. Coarse and fine crack models

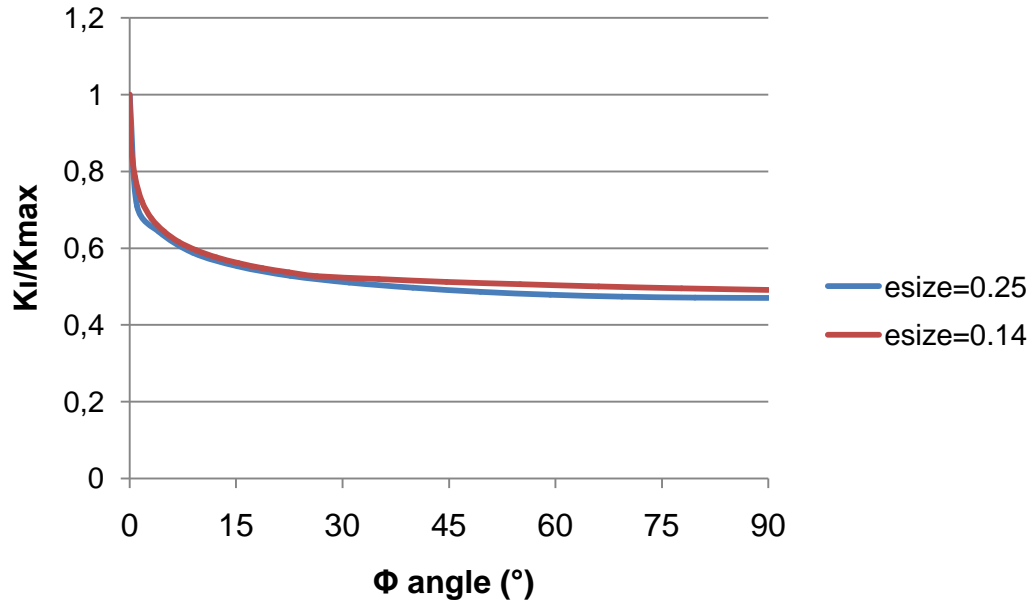


Figure 53. Stress intensity factor for coarse and fine models

6.2.6 Residual Stress

Residual stress occurs on the structure after welding process. They are inner forces and self equilibrating. In finite element modeling residual stresses are included as importing stress distribution at first step in analysis of the structure. In this study residual stress distribution is applied at crack models. In this study distribution given in Figure 54 is used. It is obtained by previous experiences of Roketsan. This stress distribution is first applied to crack finite element model and results are obtained. The results are then imported to finite element model in first step. This load distribution is applied as tensile load symmetrically to weld axis by keeping it in the middle of distribution.

In the ABAQUS manual [30] after providing the standard expression for the J integral it is stated that; “When the residual stresses are significant, the standard definition of the J-integral as described above may lead to a path-dependent value. To ensure its path independence, the J-integral evaluation must include an additional term that accounts for the residual stress field.” Having recognized this fact, ABAQUS software actually provides the appropriately modified expression which is capable of calculating J integral in the presence of residual stresses. In ABAQUS, residual stress can be defined in the model either by applying a known residual loading and operational loadings in analysis steps or importing an initial stress state defining residual stress state of the model. In this thesis, for the analysis of cracks in the welds, residual loadings were applied as an analysis step prior to operational loading. They add up with stress distribution that occurs due to applied boundary conditions. On the other hand, in the verification study given in section 5.3.3,

residual loading was applied by importing stress state due to prior loading. Detailed information about incorporating residual stresses in J integral calculations can be found in [30].

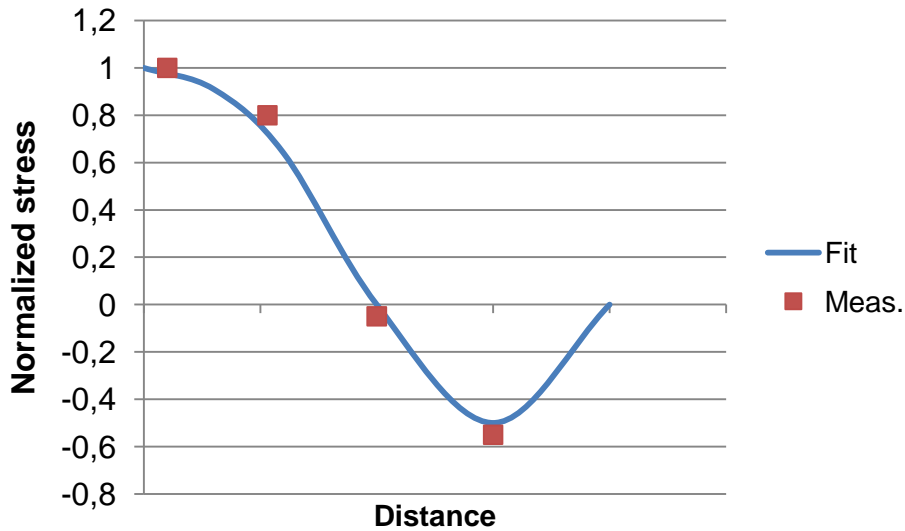


Figure 54. Residual stress distribution curve

Application of residual stresses on cracked model is demonstrated on a finite element model of semi elliptical surface crack. Finite element mesh contains quarter of the whole model. In the first step a tensile residual loading applied at one end. In subsequent step, bending loading is applied on model from tensile loaded condition. Stress intensity factors that are obtained from ABAQUS which uses J integral and an extraction method which is explained in Section 6.2.2 for stress intensity factors. Also same model was constructed in ANSYS which uses displacement extrapolation method for stress intensity factor calculations [30],[32].

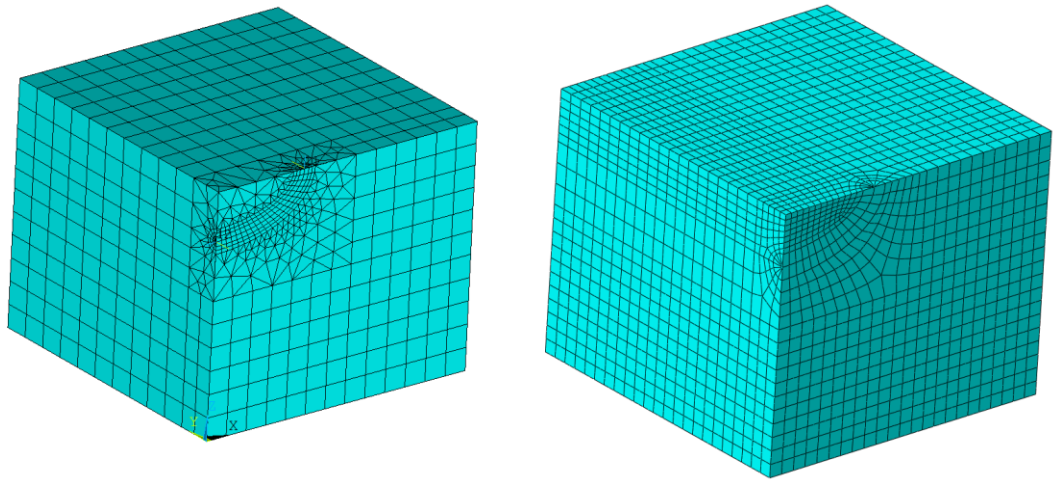


Figure 55. Finite element models built in ANSYS (left) and ABAQUS (right)

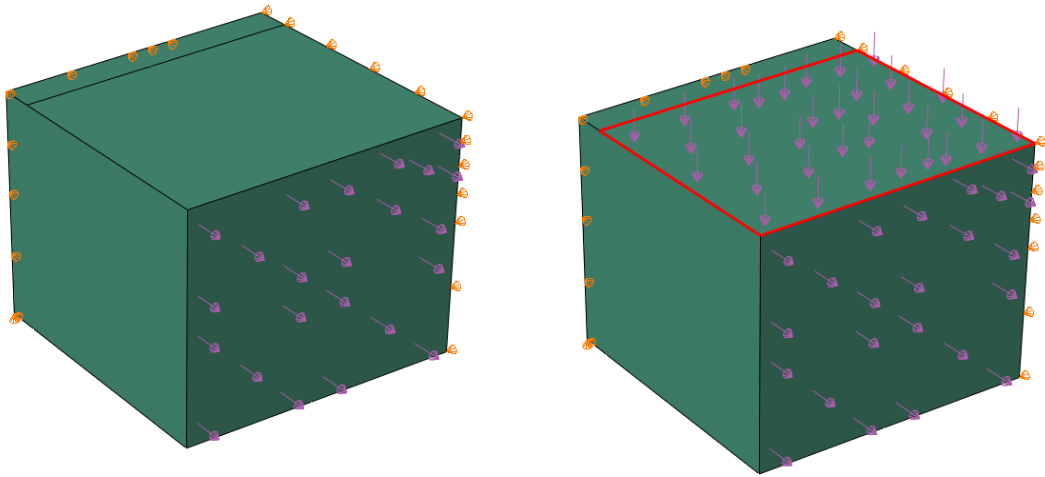


Figure 56. Loadings; residual compressive(left) at first step and bending(right) at second step

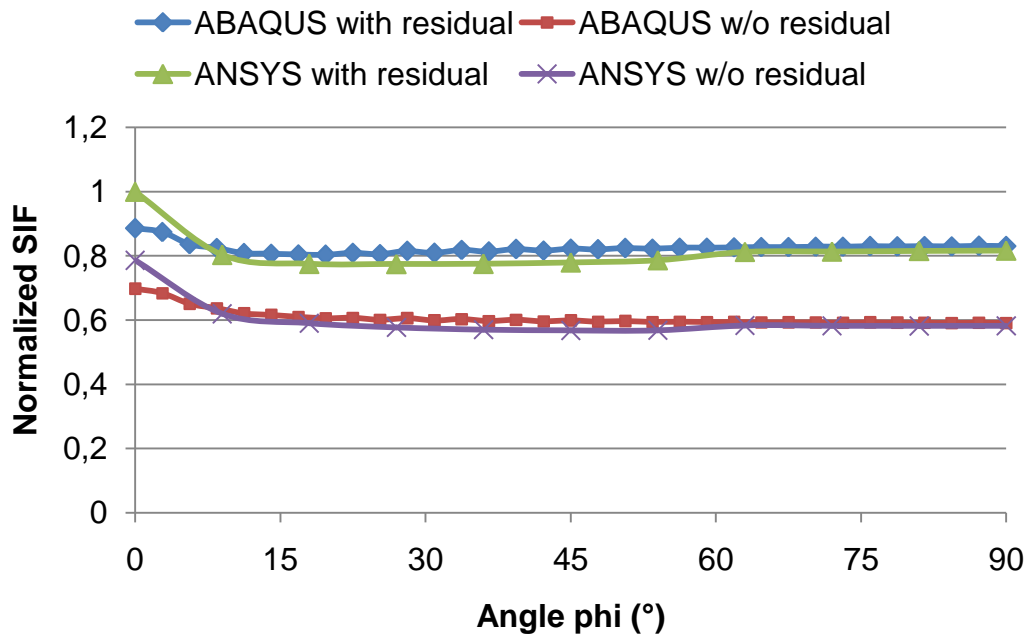


Figure 57. Finite element solution in ABAQUS and ANSYS with and without residual stress

In Figure 57 mode I stress intensity factor variation along crack front is given for with and without residual stress solutions. Angle phi is measured from free surface. Results are normalized against maximum value obtained among them. Stress intensity factor calculated from J integral and displacement extrapolation show good agreement.

6.2.7 Material Properties

Structure is built from St52 grade steel. In the analysis properties of St52 is used. Properties of steel are given in Table 4. Since elastic material properties do not change significantly over weld and base metal region, elastic properties are used for all regions in sub models containing crack.

Table 4. Properties of St52

Yield Strength	Ultimate Tensile Strength	Elongation at Break	Elastic Modulus	Poisson's Ratio	Density
358 MPa	510 MPa	20 %	210 GPa	0.3	7850 kg/m ³

6.3 Results of Finite Element Analysis of Cracks in Welded Connections

Global finite element model solution is obtained under firing load and the results are examined. Critical welded connection locations are determined and sub models are created for those locations. Possible crack geometries are modeled and results are obtained. Sub model boundaries are imported from global finite element model. Steps of importing boundary conditions from global to sub model and verification studies were given in Section 5.

Finite element model of cradle is solved in a dynamic implicit step under firing loads. Transient results are obtained for a period time. Since solution is obtained over a certain time period, results must be investigated considering all time points. At critical locations, results are plotted against time and critical time point is determined (Figure 59). It should also be noted that critical time point can be different for all locations.

Steps involved in analyzing cracks can be outlined as below:

1. Global finite element model is solved under boundary conditions given in 6.2.4 Boundary Conditions
2. Results are investigated over time and critical locations and time points are found (Figure 58, Figure 59). In cradle finite element model over 30 locations were determined and sub model is created for one of the locations (Figure 60).
3. Sub models are created and cracks at different locations and sizes are investigated.

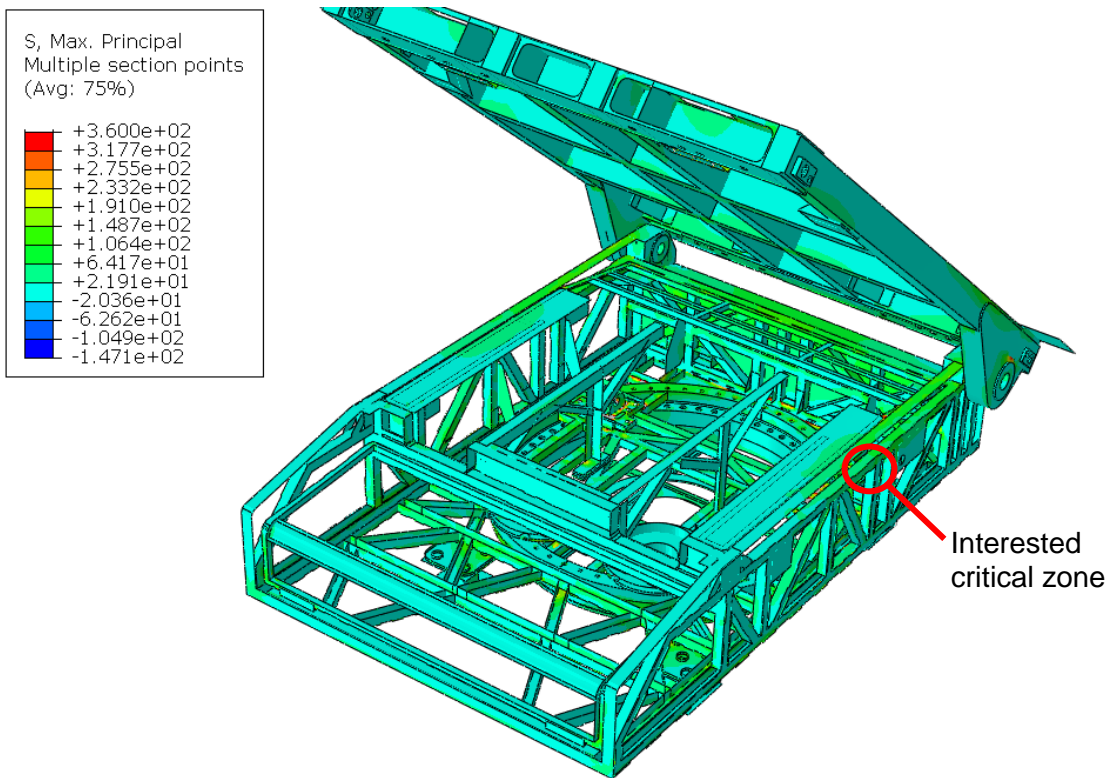


Figure 58. Maximum principal stress distribution in cradle model

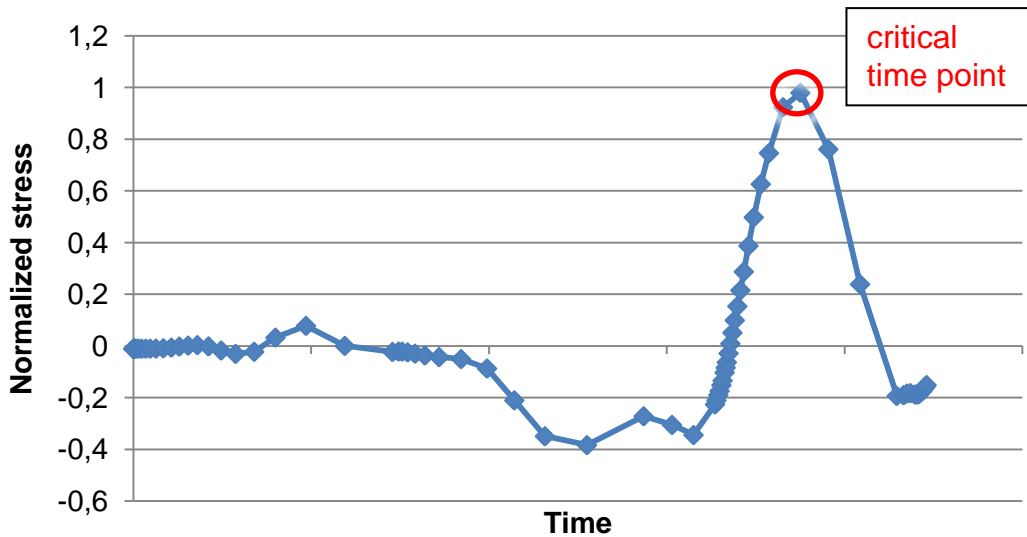


Figure 59. Stress history of a point in dynamic solution

Critical locations are determined according to maximum principal stress distribution around connections (Figure 58). In a finite element model of complicated system such as cradle, there are different critical locations for different aspects. It is not practical to evaluate such

a system over one critical location. Some locations may be critical for plastic deformation while other may be critical for fracture. In this study, one of the critical locations is studied on fracture mechanics basis (Figure 60). These locations are also checked for any plastic deformation. If there is no plastic deformation is present linear elastic fracture mechanics can be used. Region interested in this study does not include any plastic deformation, hence same linear elastic material properties are used for whole crack model.

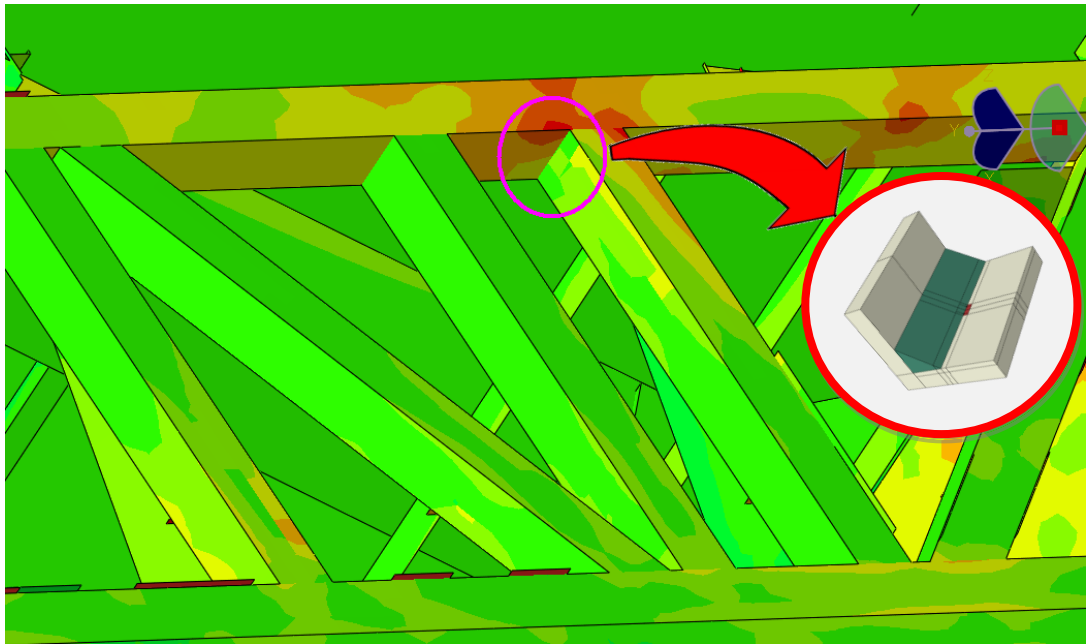


Figure 60. Critical location interested in this study

Cracks are modeled in three different locations. These locations were determined by previous design experiences. Connections were examined and positions that flaws are most likely to occur determined and used in further design studies. Cracks at weld toe are commonly seen flaws at welded structures. These cracks initiate from flaws left behind welding process. Such a flaw can be seen in Figure 62. In Figure 61 a propagated crack at weld toe can be seen.

In this study, semi elliptical surface cracks at weld toe outer and inner surfaces, and also embedded circular crack models are implemented. Stress intensity factor in three modes are plotted. Also different semi elliptical crack aspect ratios are modeled and results are plotted. Variation of these parameters is only given for semi elliptical surface crack at weld toe. For other two configurations, results are given for a single aspect ratio.

For semi elliptical surface cracks, Köşker [33] mentioned free surface effect occurring at first crack tip element in his study. Although he studied inclined surface cracks, free surface affected the stress intensity factor calculations at first crack tip element. Another problem that caused miscalculation was that it was not possible to define coordinate system perpendicular to crack front at first point since crack plane rests inclined relative to

bounding surface of body. In this thesis work, cracks are placed perpendicular to bounding surface of the body. In addition, there is not a significant variation in verification models along crack front.

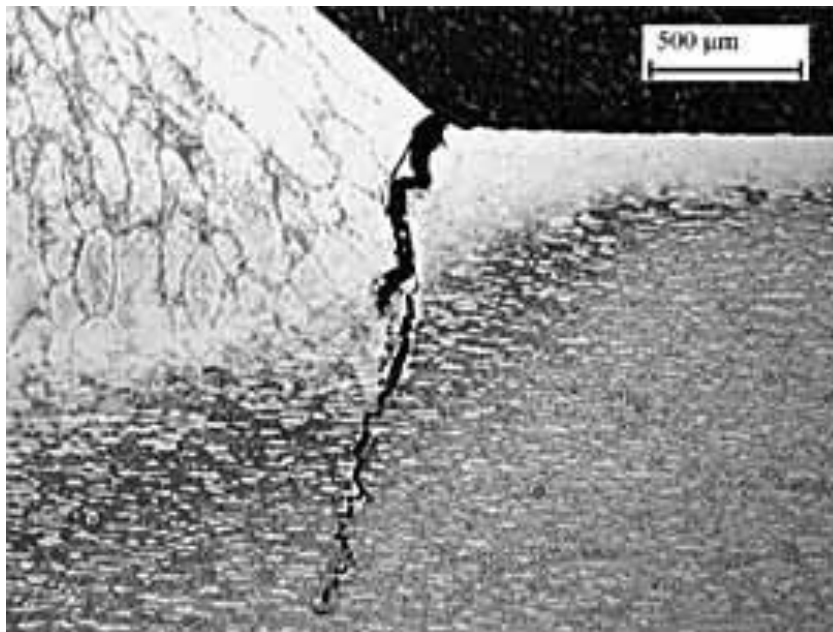


Figure 61. A propagated crack initiating at weld toe[34]

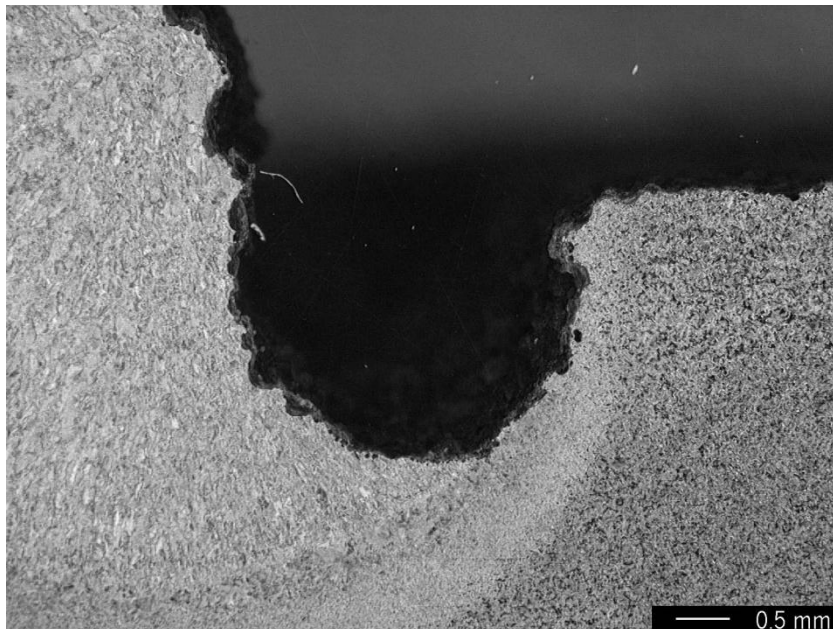


Figure 62. Undercut occurring at weld toe after welding process[35]

6.3.1 Semi Elliptical Surface Crack at Weld Toe

In this model, a semi elliptical surface crack is located at weld toe. In Figure 63, only solid section of sub model is shown. Overall dimensions are given in Figure 64. Crack detail is shown in Figure 65. Quadratic wedge elements with modified mid nodes are located around crack front and hexahedral elements around crack are connected with the rest of the model using tie constraints. Boundary conditions are imported from global finite element model results as displacements. Section forces at the boundaries in three dimensions are shown in Figure 66. Crack is located at red region in Figure 63 and can also be seen in Figure 64.

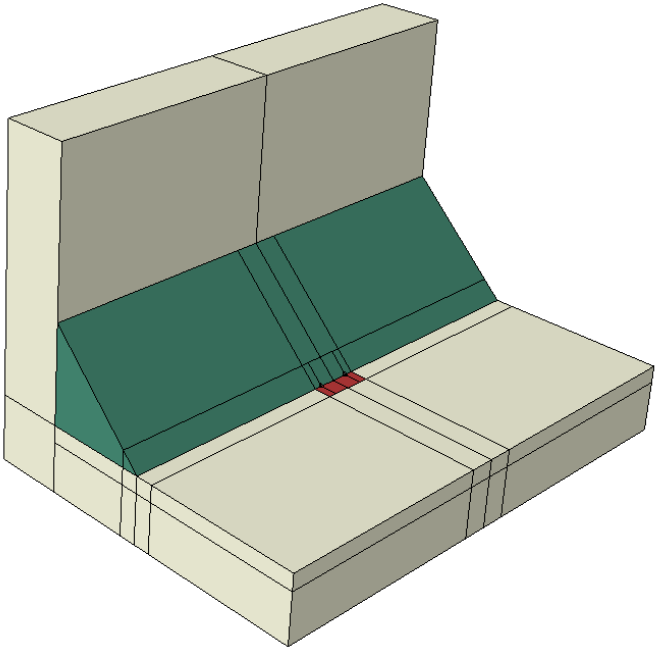


Figure 63. Sub model of semi elliptical surface crack at weld toe

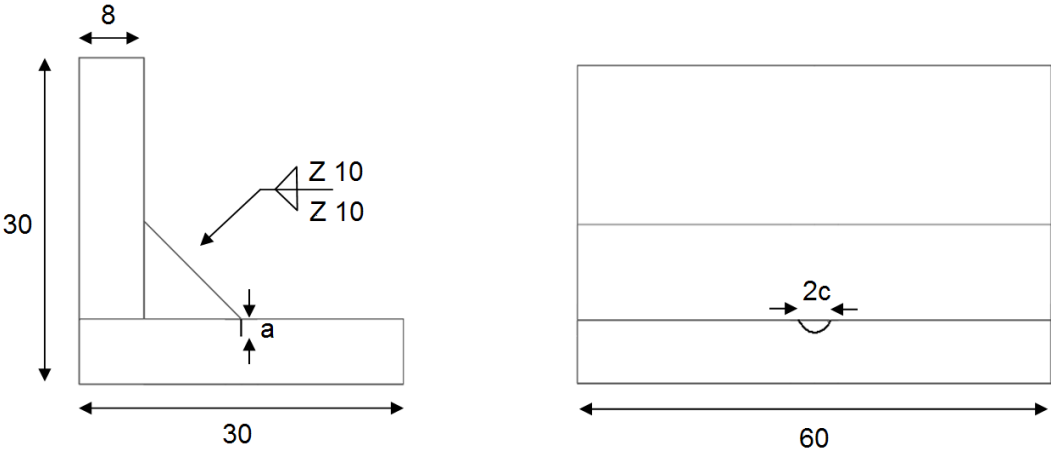


Figure 64. Dimensions of solid section of sub model

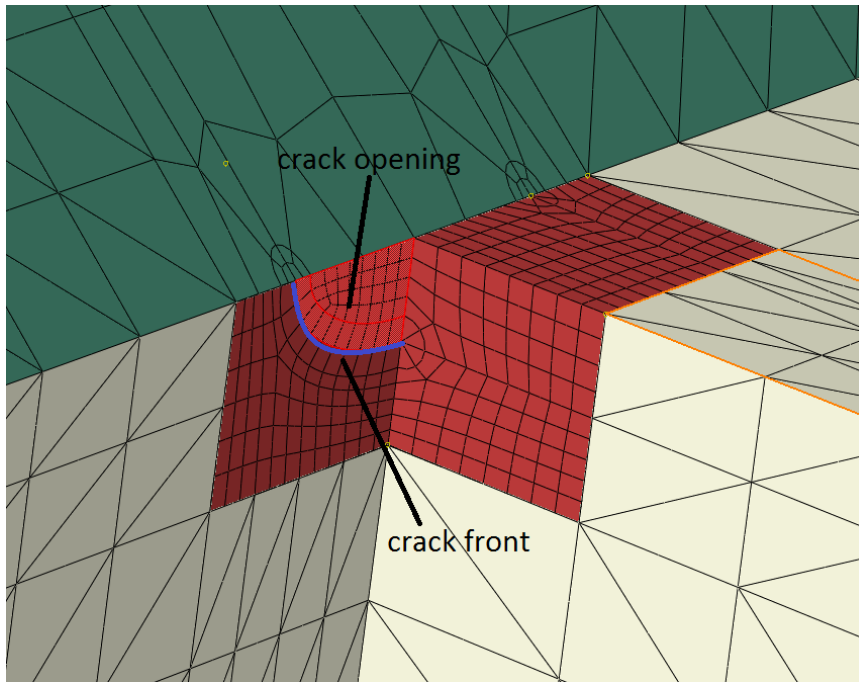


Figure 65. Sub model crack detail

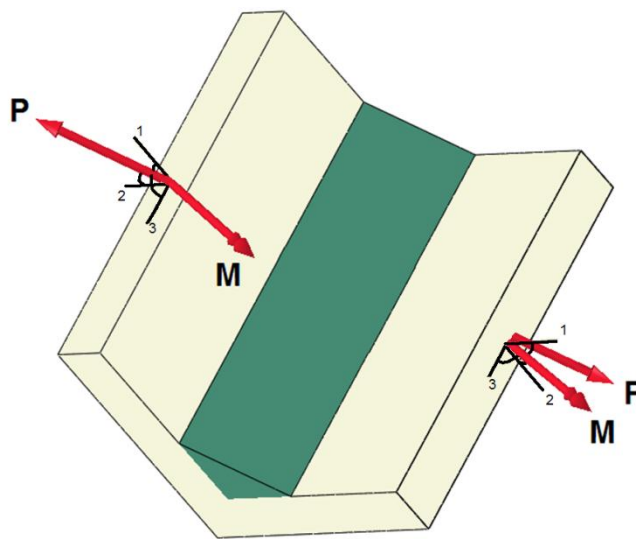


Figure 66. Equivalent forces and moments at boundaries

Since global finite element model is solved in a dynamic solution step, loads change over time. At investigated time point, loading on the boundaries can be given as $P=23\text{kN}$ and $M=1.2\text{kNm}$. The angle between axis 1, 2, 3 for force loading are respectively 9° , 32° and 41° , and for moment loading are respectively 12° , 36° and 57° .

Boundary conditions are imported from the global finite element model. Stress intensity factors are determined around crack front. Mode I, II and III stress intensity factor

variations along crack front are given in Figure 68. The values in the figure were normalized against maximum stress intensity value obtained among three of them. Along with these K^* values are calculated and plotted [36]. It is seen that combined loading causes stress intensity factors in three modes. However, contribution of stress intensities from mode II and III are small compared to mode I. It can be concluded that for this geometry and loading, mode I is the critical loading direction. Although, K_I and K^* are very close to each other, fracture toughness of material is compared to maximum K^* along crack front for critical crack size. These calculations were performed for $a/c=0.5$. Critical crack size was found by changing crack dimension a , and keeping $a/c=0.5$.

$$K^{*2} = K_I^2 + K_{II}^2 + \frac{1}{1-\nu} K_{III}^2 \quad (6.10)$$

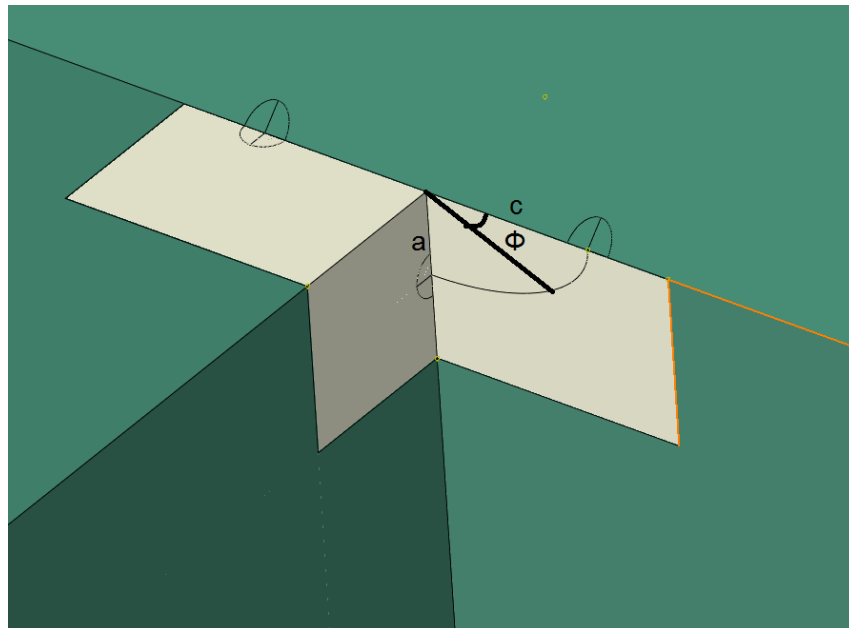


Figure 67. Crack dimensions and angle definition

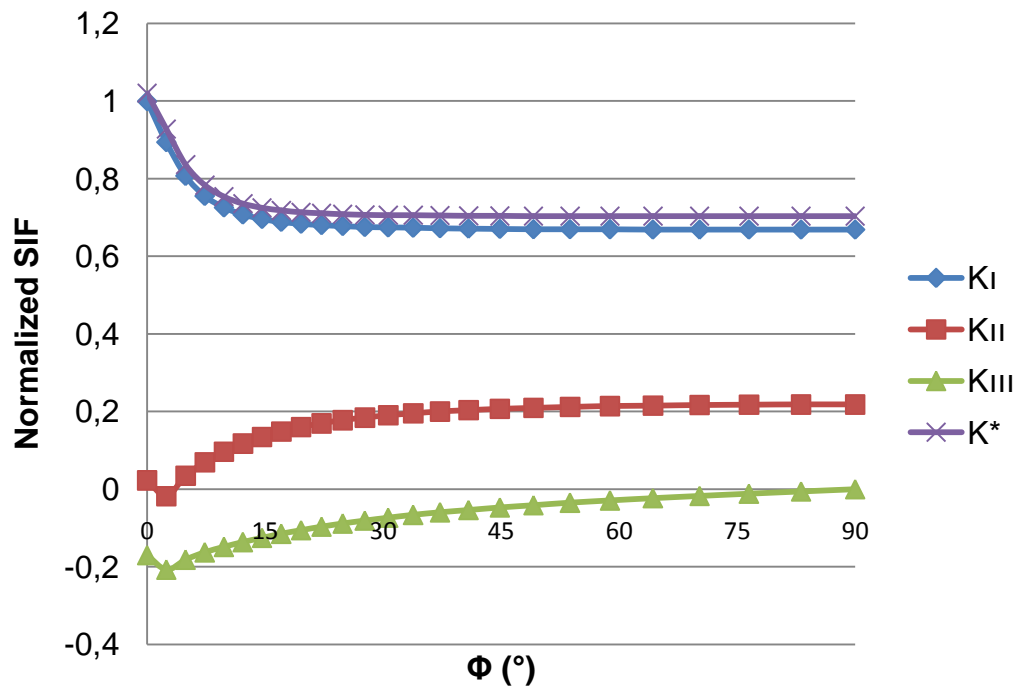


Figure 68. Variation of normalized stress intensity factors for angle phi with $a/c=0.5$

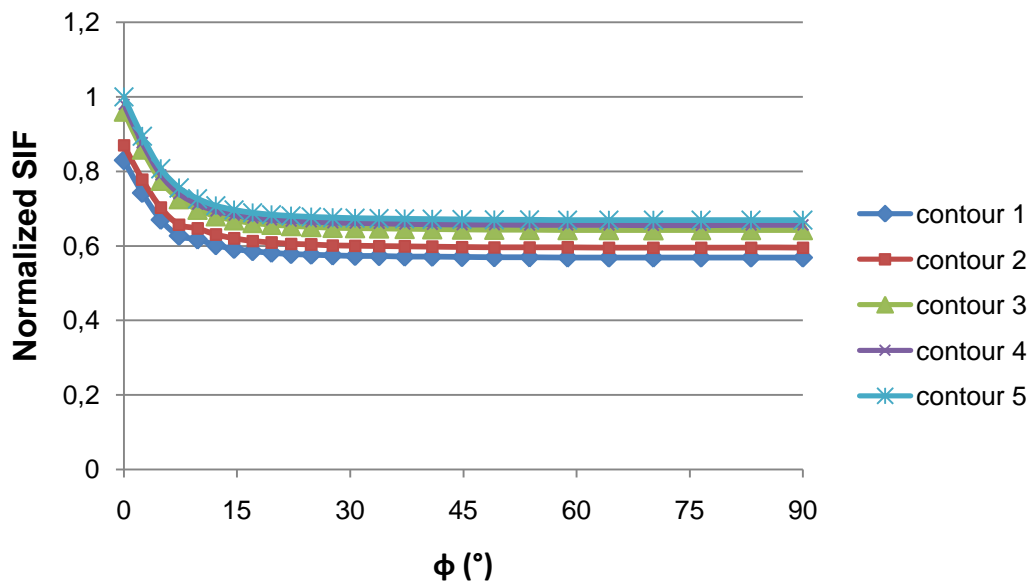


Figure 69. Variation of normalized stress intensity factors for different contours used for J integral

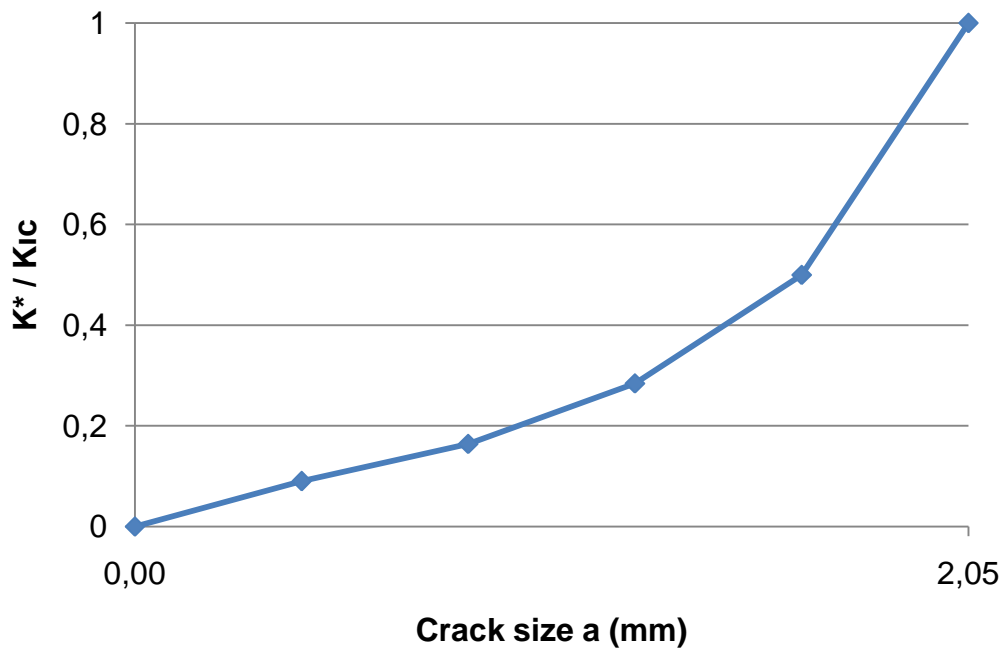


Figure 70. Variation stress intensity factor for crack size with $a/c=0.5$

The effect of a/c is investigated in crack model by changing a parameter while keeping $c=2\text{mm}$. Variations of K^* values are given along crack front in Figure 71. K^* is normalized against maximum value obtained among four configurations. For original crack configuration with $a=1\text{mm}$ and $c=2\text{mm}$, maximum stress intensity factor is obtained at $\varphi=0$ under this combined loading. As a/c ratio gets smaller, stress intensity factor at $\varphi=90$ becomes maximum.

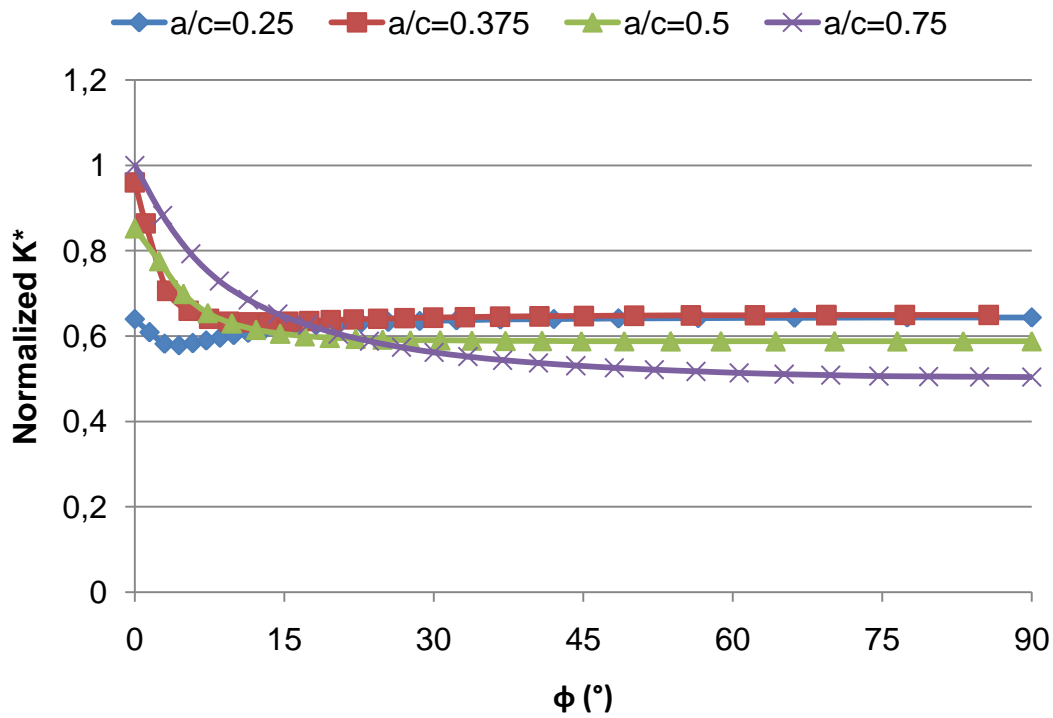


Figure 71. Variation of normalized stress intensity factor for different “a” values

6.3.2 Semi Elliptical Surface Crack at Inner Surface

In this sub model, semi elliptical surface crack is placed at inner surface of closed form member. Solid section of sub model is shown in Figure 72 and crack detail is given in Figure 74. This type of crack is dangerous than the previous one, because the crack remains inside of closed section member. It makes it impossible to detect by eye inspection. Special care must be taken in order to spot this crack. Solutions are obtained by using the same boundary conditions as given in Section 6.3.1. Results are obtained for $a/c=0.5$.

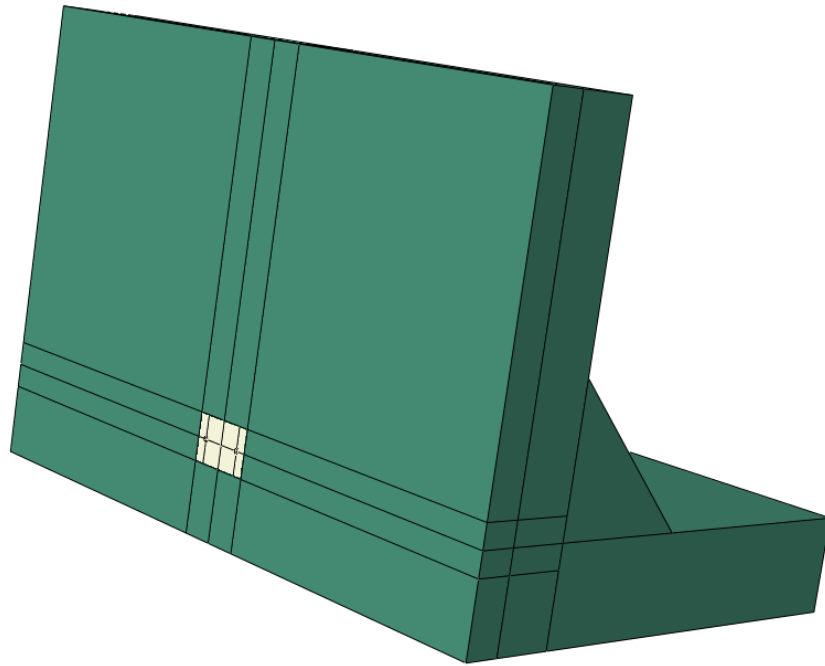


Figure 72. Sub model of semi elliptical surface crack at inside

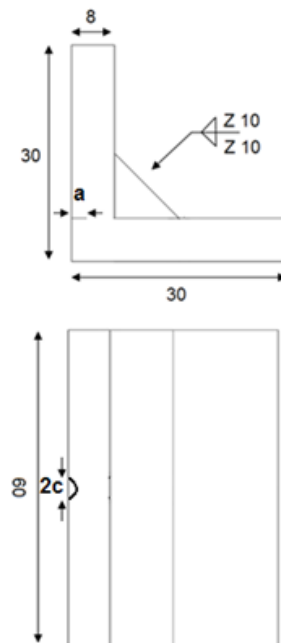


Figure 73. Dimensions of solid section of sub model

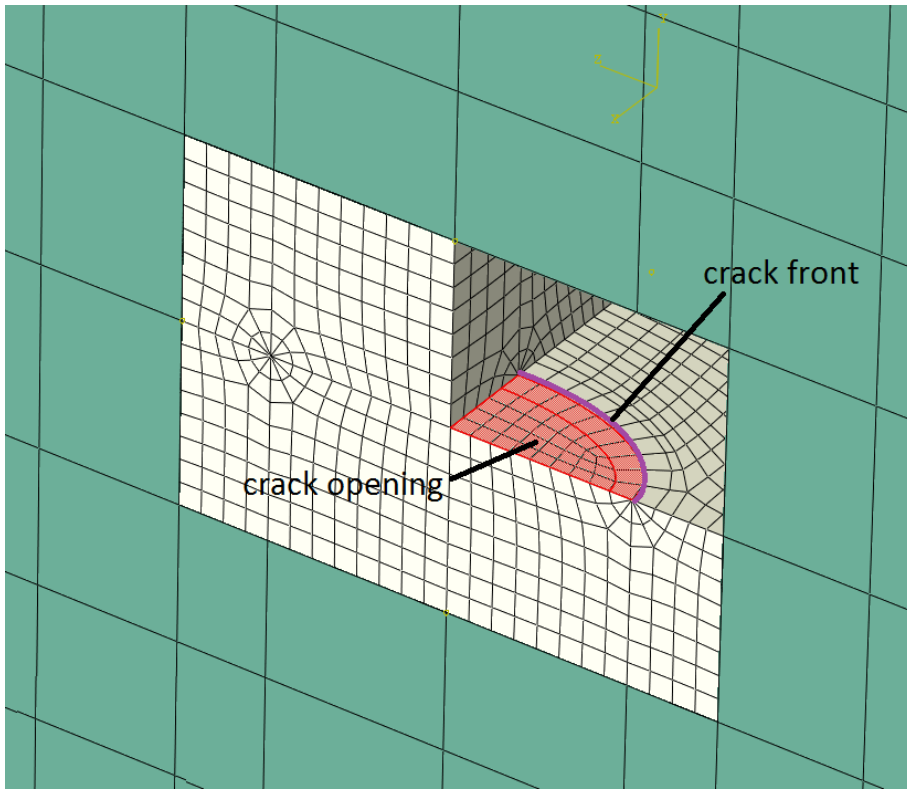


Figure 74. Sub model crack detail

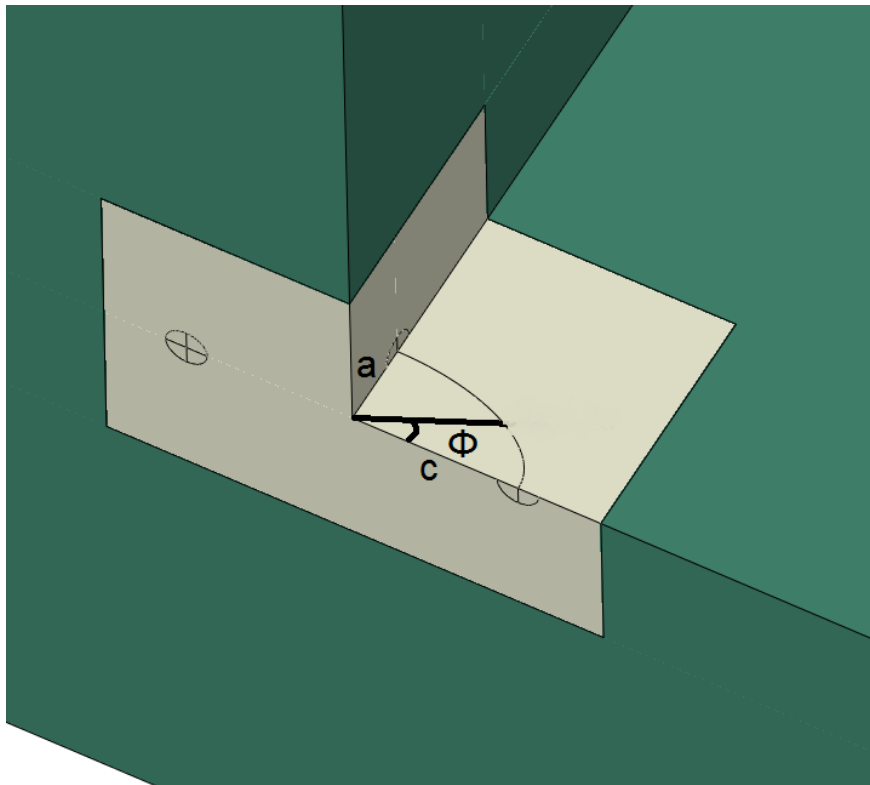


Figure 75. Crack dimensions and angle definition

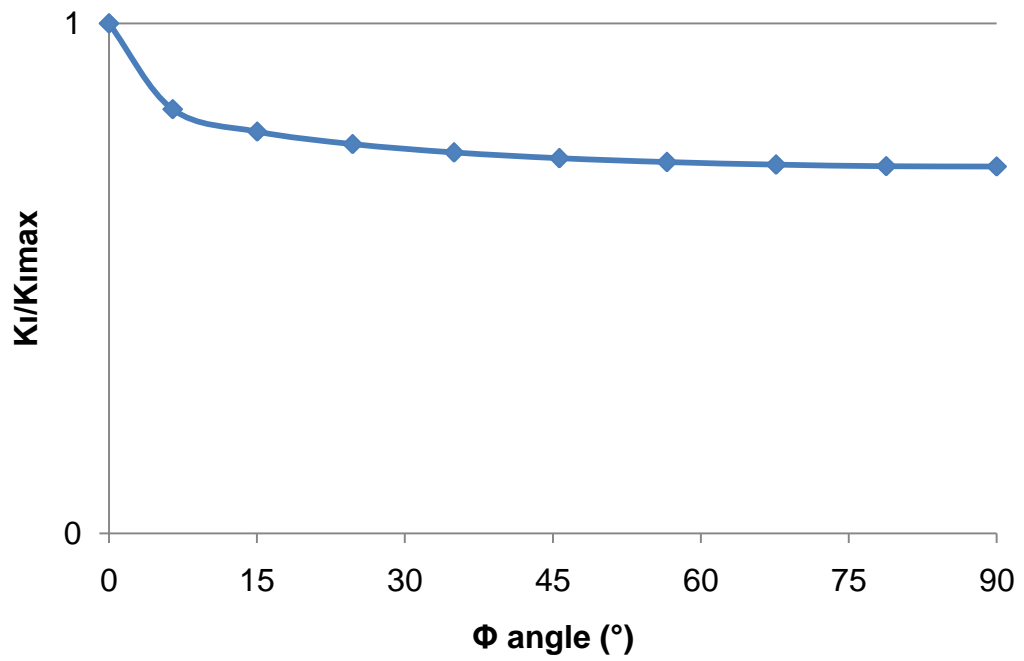


Figure 76. Variation of normalized mode I stress intensity factor for angle phi with a/c=0.5

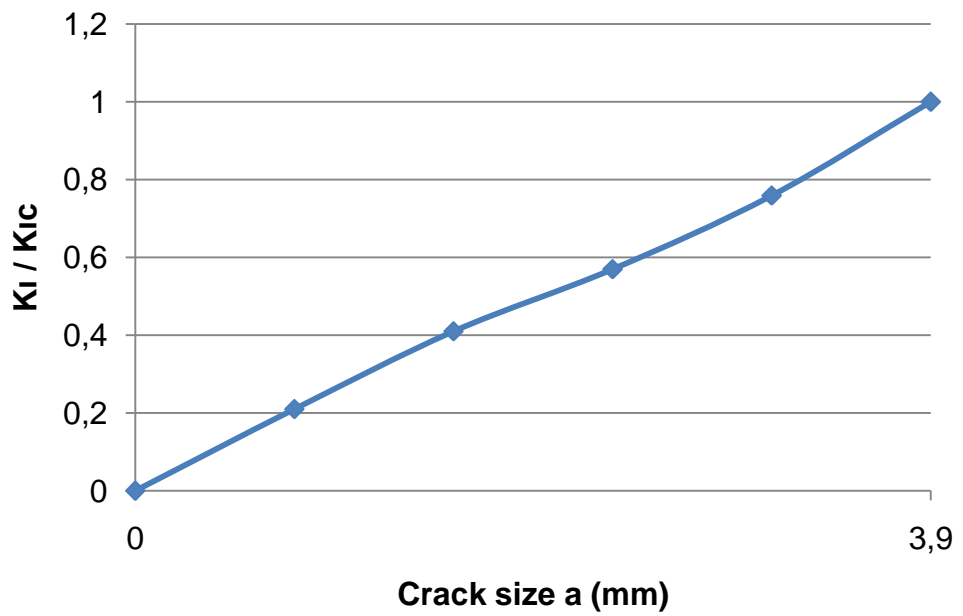


Figure 77. Variation of normalized mode I stress intensity factor for crack size with a/c=0.5

6.3.3 Embedded circular Crack at Weld Inner Surface

In this sub model, embedded circular crack is placed at the inner surface the welded connection. Solid section of sub model is shown in Figure 78 and crack detail is given in Figure 80. This type is also a dangerous one, because crack remains inside of welded connection. Special care by means of an ultrasonic examination must be taken in order to spot this crack. In finite element model, crack is located at mid section of geometry from all dimensions. Solutions are obtained by using the same boundary conditions as given in Section 6.3.1.

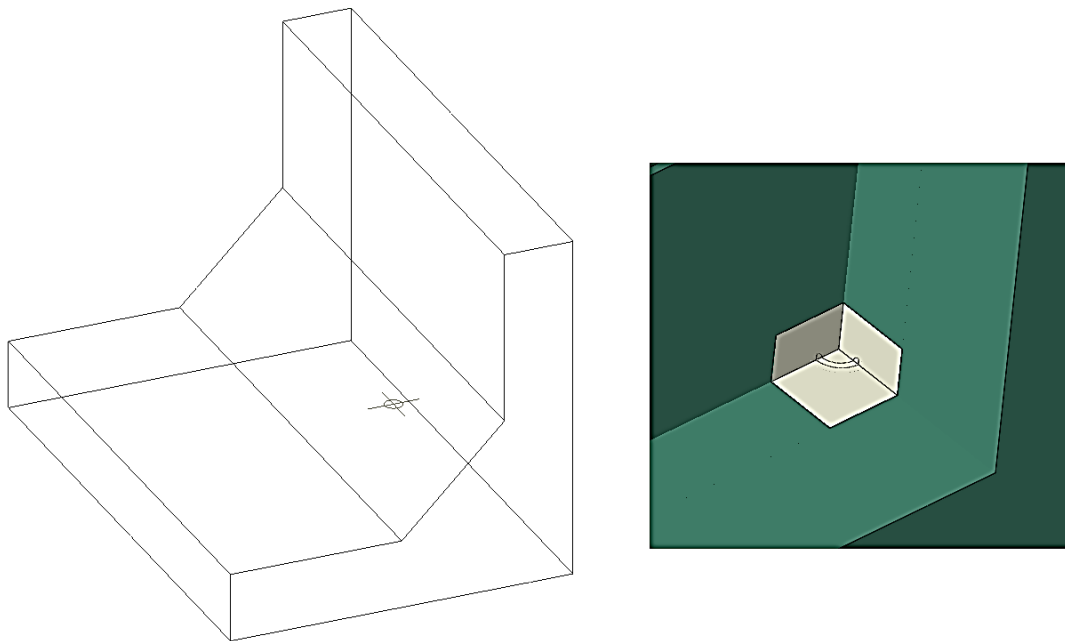


Figure 78. Sub model of embedded circular crack at weld

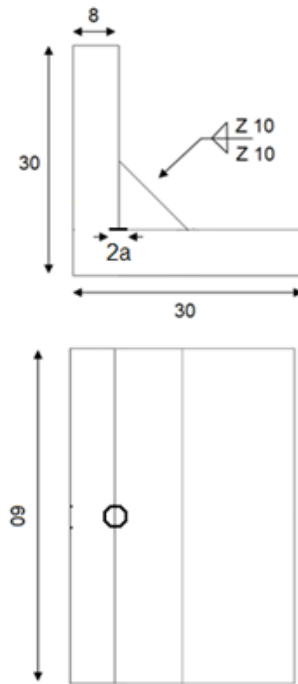


Figure 79. Dimensions of solid section of sub model

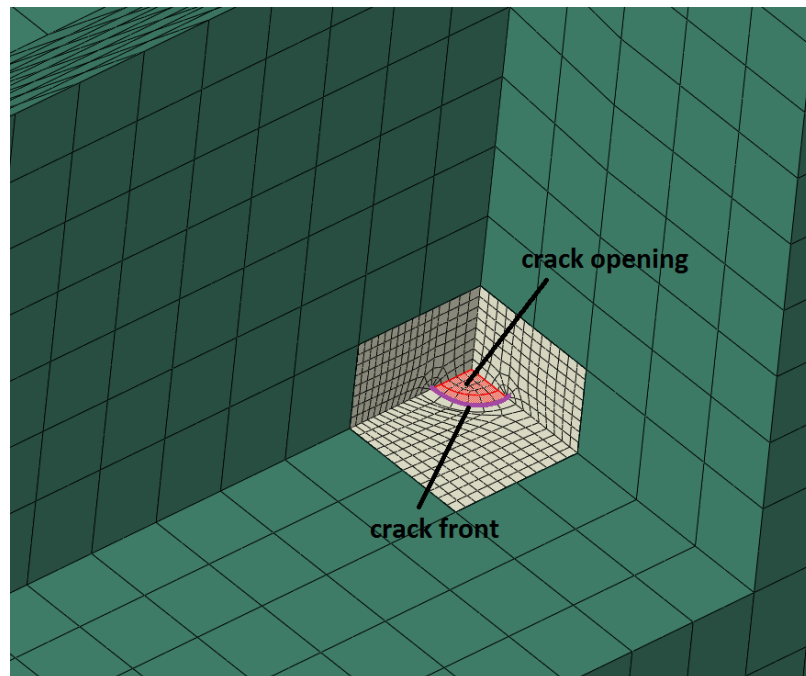


Figure 80. Sub model crack detail

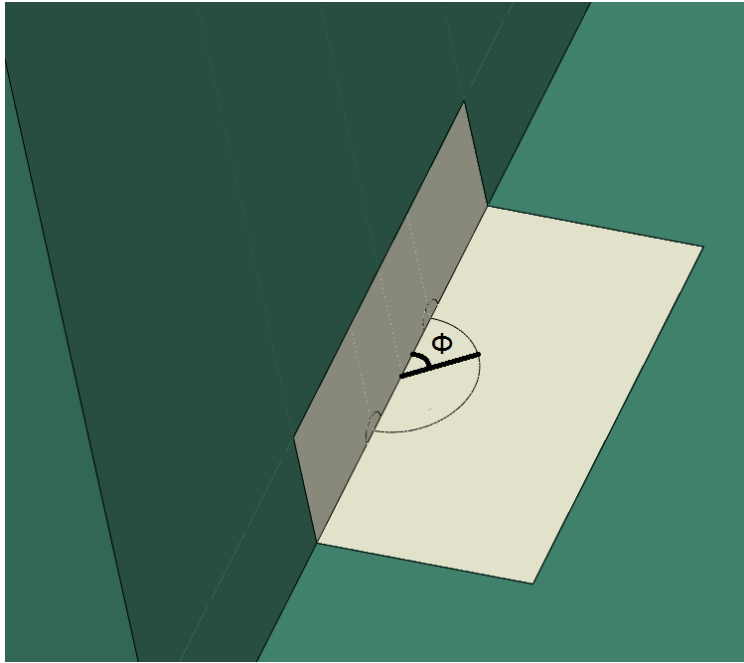


Figure 81. Crack dimensions and angle definition

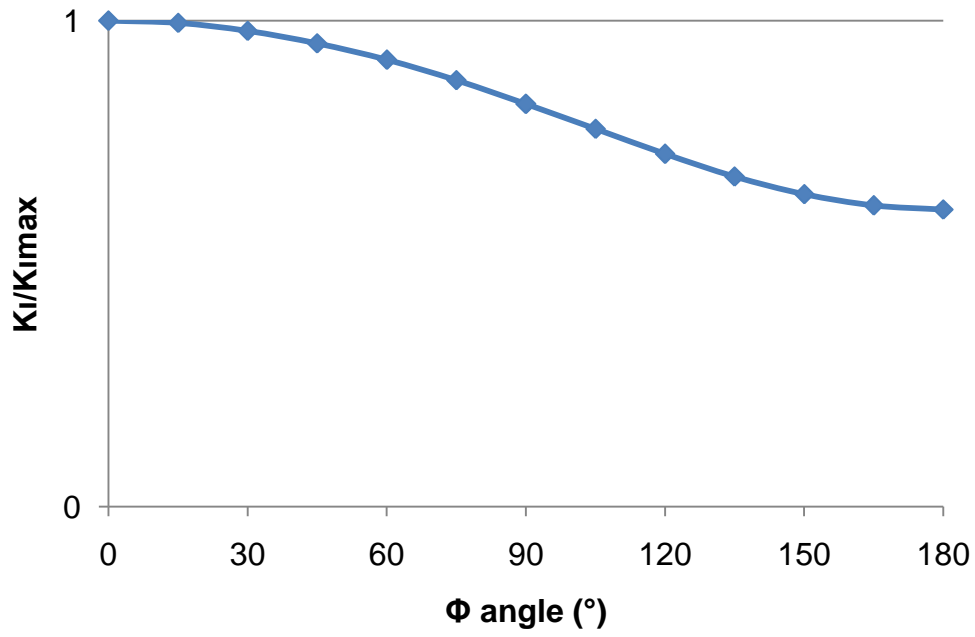


Figure 82. Variation of normalized mode I stress intensity factor for angle phi

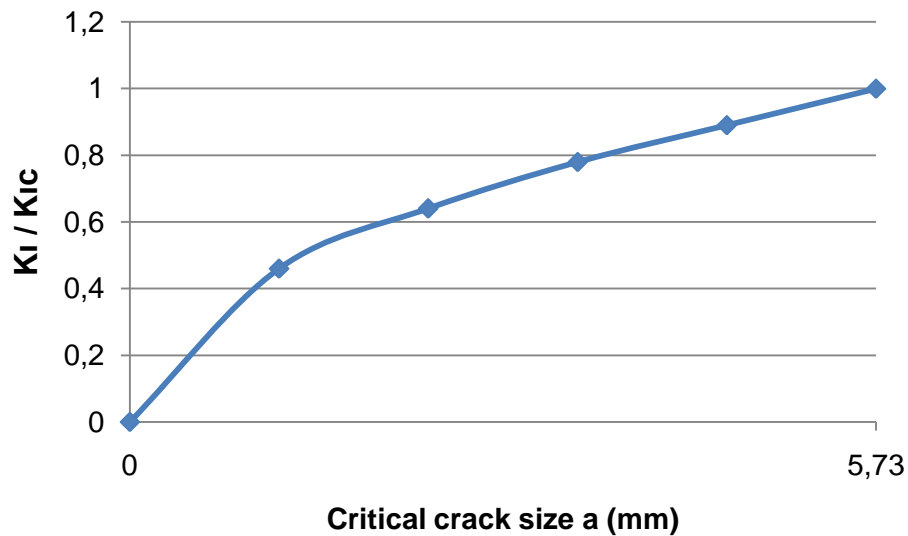


Figure 83. Variation of normalized mode I stress intensity factor for crack size

6.3.4 Conclusion

Stress intensity factor solutions were given for three crack configurations that were determined by previous experiences. Under same load case, semi elliptical surface crack at weld toe, semi elliptical surface crack at inside and embedded circular crack at weld models were studied in this context.

In semi elliptical surface crack at weld toe configuration, mode I, II and III stress intensity factors are plotted and K^* calculated from three stress intensity factors. Effects of different parameters are investigated only for this configuration. This configuration is a commonly seen flaw in practice when such systems are considered. It is noted that K^* is very close to K_I . Therefore it can be concluded that for this loading contribution from K_{II} and K_{III} stress intensity factors can be omitted. Mode I stress intensity factor is determined since it is critical in this load case. Variation of normalized stress intensity factor against phi angle and crack size was given. When results are investigated, maximum stress intensity occurs at surface for this load case and geometry in semi elliptical surface cracks. However when a/c ratio is changed, it is seen that location of maximum stress intensity factor changes to deepest point of crack.

In addition, semi elliptical surface crack at inner surface and embedded circular crack configurations are also studied. However in these cases, only mode I stress intensity factor and constant a/c ratio crack is studied. Stress intensity varies along crack front for circular cracks since loading is not uniformly distributed along section.

For given load case and geometry, for a/c=0.5, stress intensity factor comparison for three different crack configurations are given in Figure 84. Crack size a is normalized against

most critical condition's crack size which belongs to semi elliptical surface crack at weld toe. Among three of them, semi elliptical crack at weld toe gives highest stress intensity factor for this load case and geometry.

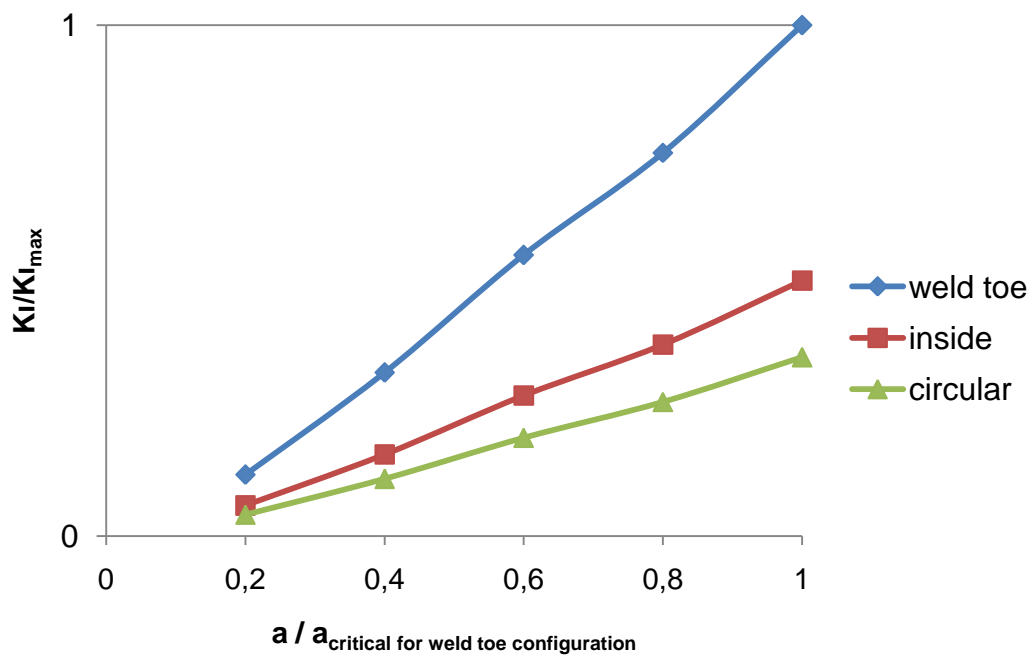


Figure 84. Comparison of three crack configuration

CHAPTER 7

TEST STUDIES

Finite element method allows designers to evaluate their design prior to prototyping. This makes it possible to find deformations on the body or failure status of the structure. In the scope of this thesis work, a structure is evaluated against failure when cracks at welded connections are present. Due to the nature of welding process, it is highly possible for cracks to occur in the vicinity of a welded connection. Since it is impractical to discard all components or structures with flaws, a limit that can structure withstand for its operational life must be determined. Then the structure is controlled against this limit during production and scrap rate is significantly reduced. In addition, cracks may occur during operational life of the structure. High stress locations are determined after finite element analysis and strain measurements are made during tests. Since some parts of the structure work under high stress conditions, cracks are likely to occur under repetitive loading. These cracks should be carefully evaluated in order that the structure could continue its operational life safely.

The launcher prototype is manufactured and equipped with all necessary electronic and mechanical elements. The structure is then tested under real operational conditions. Real firing tests are conducted on the launcher and certain measurements are taken during tests. Some of these measurements are strain measurements at critical locations and displacement measurements. These measurements are used to tune global finite element model of the structure.

During manufacturing of the launcher, all welded connections are inspected for any inherent cracks. They are compared with tolerance values by quality department and decided whether it is acceptable or a repair on the part is necessary. Under operational conditions, certain locations are determined and checked for any flaws occurring near the welds. These flaws are evaluated using finite element models for the launcher to operate safely. A verified and tuned global finite element model is built and its solutions are used to create sub models around critical locations and evaluate cracks near welded connections.

7.1 Firing Test of Multi Barrel Launcher

Firing test of launchers is final step of the design. The structure is tested under real operational loads. During test studies necessary measurements are taken in order to verify finite element models. If necessary, finite element models are tuned up using test results. Verification of models enables designers to use the same model for further design iterations if necessary.

Firing tests are conducted at special fields where all necessary security precautions are taken. Test personnel studies for every possible failure scenario and make sure that everything is covered up. In these tests, real munitions are used; therefore, they are very costly studies. Every possible measurement is taken from a single rocket firing.



Figure 85. Firing of rocket from launcher

In this thesis, strain and displacement measurements from cradle are used for verification purposes. However, there are many other measurements collected that are used by different design groups or for any other purposes. Information about strain and displacement measurement is given in following sections.

7.1.1 Strain Measurement

Strain measurement is a way to determine structure's response to external loading. Strain gages are utilized in strain measurements. These gages can measure the strain relative to a state at measurement location. This means, measured values can be initially zeroed at a given state of system. Metal foil strain gages are very common type of gages and in this test work foil type is used. This type contains thin metal strips placed on a very thin backing material. Strain is measured via resistance change due to length change of these metal strips. Strain gages are placed on the structure using special bonding elements. After successful curing of the bonding element, strain gage becomes a part of the structure beneath it. It allows gage to measure the same strain with metal under it.

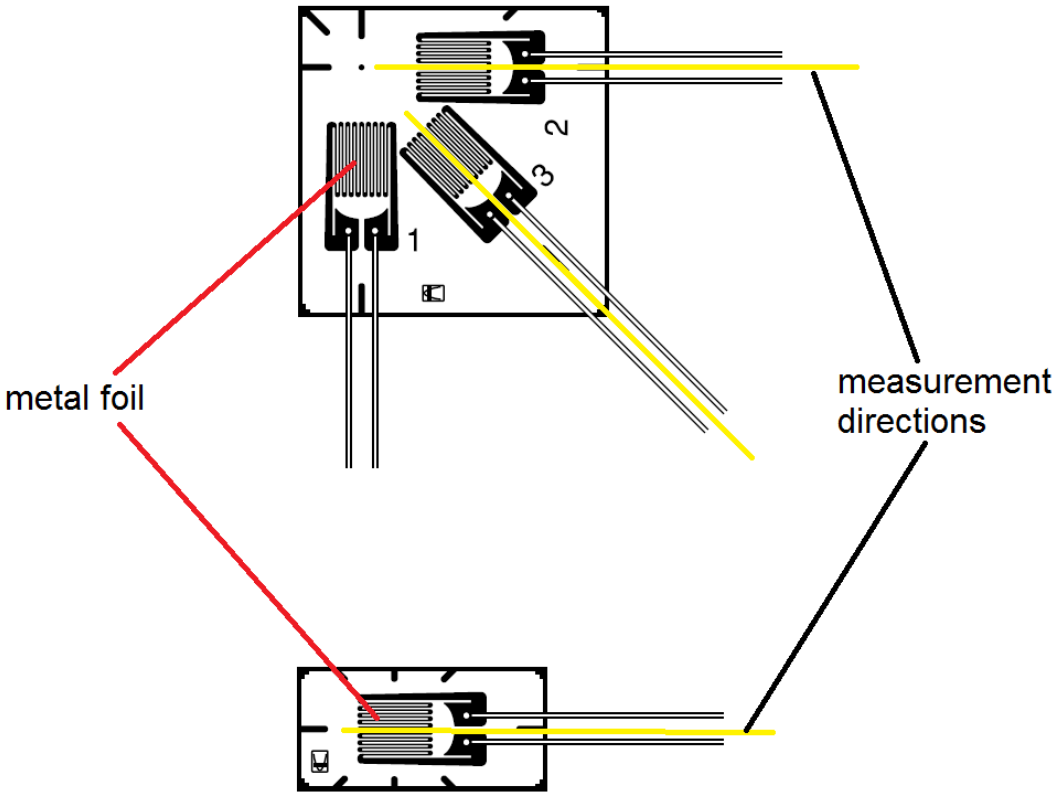


Figure 86. Three axis and single axis metal foil strain gages [37]

Resistance change is measured using Wheatstone bridge configuration. One or more of the elements in the bridge become strain gages. In a quarter bridge strain gage configuration, one of resistors is replaced with a strain gage. Any apparent change in strain gage's resistance is measured by means of voltage change at output ports. This voltage change is calibrated against strain gages property and voltage input [38]. Strain gages are chosen specific to application. Bounding material, environment, loading rate and amplitude are the parameters that affect type of strain gage and adhesive to be used. Strain gages are selected according to material on which it will be used so that thermal expansion coefficients and bounding surfaces match. Environment affects measurement and life of strain gages. For example, high temperature changes at specimen body will add thermal strain component to total measurements. Also a humid and wet environment will cause strain gage to malfunction. Therefore necessary protective materials must be used to ensure correctness and quality measurement. Strain gage's measurement limit and dynamic loading life are major parameters to be chosen carefully for test application. In test studies waterproof metal foil strain gages were utilized due to harsh weather conditions. Also a thermal protective layer was applied on top of strain gage application zone. The working temperature of adhesive was checked for low environment temperature at test site for day and night conditions. Strain gage data was collected by a general purpose data acquisition system.

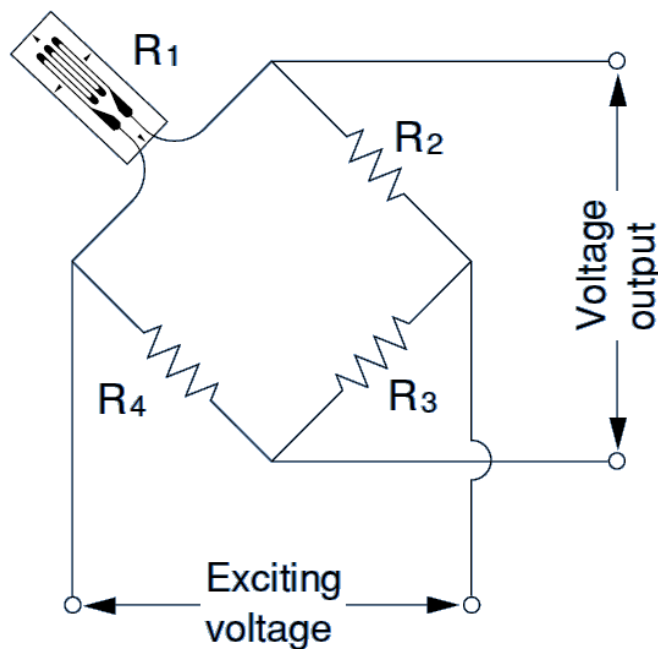


Figure 87. Quarter bridge strain gage circuit[37]

$$\Delta E_o = \left(\frac{\Delta R}{4R} \right) E, \quad (7.1)$$

$$R_1 = R_2 = R_3 = R_4 = R \text{ and } \Delta R \ll R$$

$$\Delta \varepsilon = \left(\frac{\Delta R}{R} \right) \frac{1}{K} \quad (7.2)$$

$$\Delta \varepsilon = 4 \left(\frac{\Delta E_o}{E} \right) K \quad (7.3)$$

Where ΔE_o is voltage output change, E is exciting voltage, ΔR is resistance change, R is resistance, K is gage factor.



Figure 88. Sensor locations

In order to verify global finite element model, strain measurement from the cradle is used. After finite element solutions, strain gage locations are determined. These locations are determined by strain amplitude and distribution at that location. In the test studies, measurement from ten strain gage locations is used for comparison purposes. Comparison of these measurements was given in Section 5.

7.1.2 Displacement Measurement

Displacement measurement is a way to determine structure's dynamic response. Linear potentiometric transducers are utilized in displacement measurements. These sensors can measure linear displacement between two points. Displacement is measured via resistance change due to position change of piston. Displacement sensors are mounted on structure at two ends.

Resistance change is measured using data acquisition systems. This voltage change is calibrated against displacement sensor's property, voltage input and gain factor.

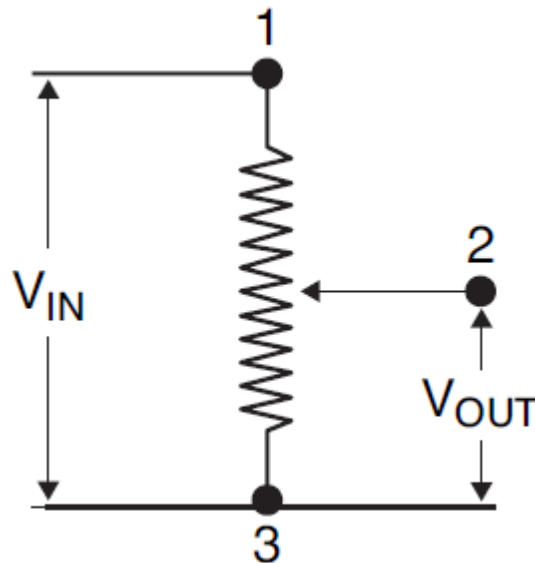


Figure 89. Linear potentiometric transducer circuit [39]

$$\ell = \left(\frac{V_{out}}{V_{in}} \right) K, \tag{7.4}$$

Where

V_{out} is voltage output, V_{in} is voltage input, K is sensor sensitivity, ℓ is measured distance.



Figure 90. Sensor locations

In order to verify global finite element model, displacement measurement from the cradle is used. In the test studies, measurement from two displacement locations is used for comparison purposes. Comparison of these measurements was given in Section 5.

7.2 Fracture Toughness Tests

Material characterization tests were performed in order to determine fracture toughness of structural material. Specimens were prepared from the same material class obeying dimension ratios proposed in the standard. Tests were conducted according to ASTM E399 standard. Test specimens were machined by estimating a fracture toughness value for the material. This estimate was involved in dimension calculations for specimens along with material's young modulus and yield strength. Therefore, there is some possibility of obtaining invalid results. It will not be feasible to machine all test specimens at once due to chance of getting invalid results. Test study should be performed in steps. Initial test specimens may be machined using standard directives and material properties. After these specimens were tested, results are checked for any invalidity. In case of an invalid result, specimen geometry must be revised in order to fit validity requirements. In some cases, results may be valid but very close to validity boundaries. The geometry still may be updated in order to decrease the probability of obtaining invalid results.

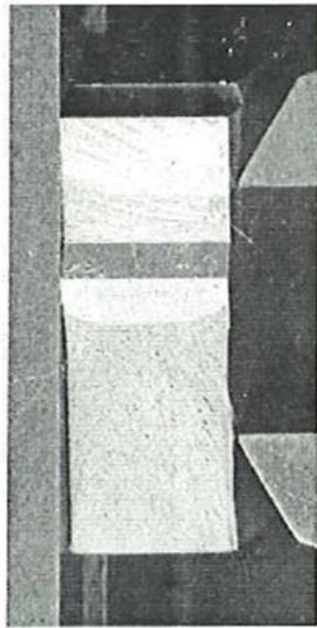


Figure 91. Broken face of a test specimen

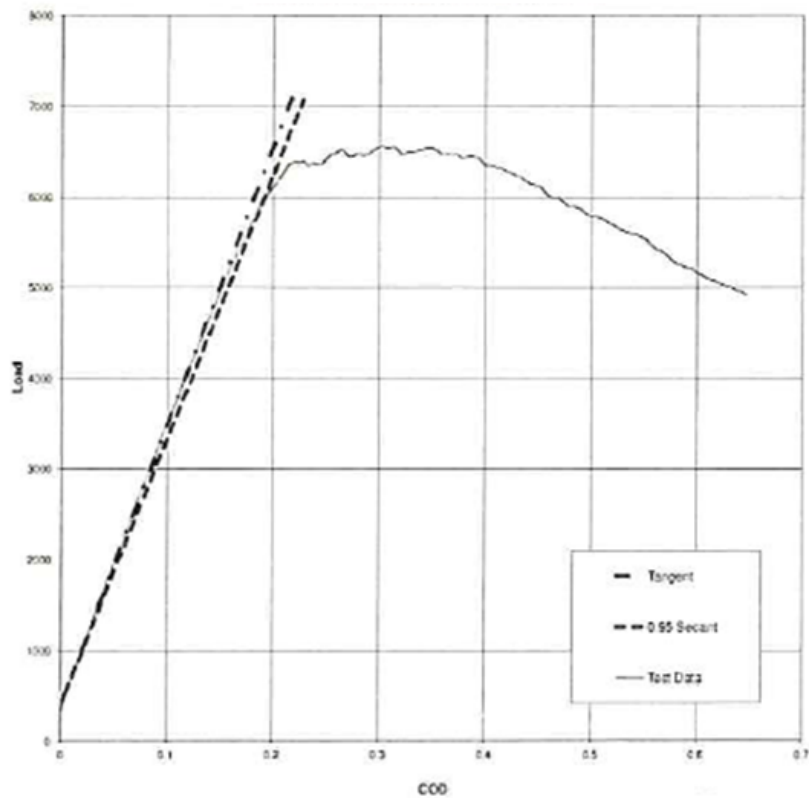


Figure 92. Load versus crack opening displacement curve for a test specimen

In the scope of this thesis work, material's fracture toughness tests were performed for St52 steel by working with a test institute offering fracture toughness tests. Fracture toughness of

St52 can be in the range of 100 and 120 MPam^{0.5}. Mechanical properties common steel materials like St52 are defined over a minimum limiting value. Producers sell these metals by conforming minimum values. However for the most of the time, materials exhibit higher performance than given standard values. Therefore with the knowledge of limits of the material, designs can be more efficient using the material to its limits. Test specimens were prepared according to the standard and necessary updates on the geometry were performed after initial investigations. Information about ASTM E399 standard and details of validity checks were given at Chapter 4.

CHAPTER 8

SUMMARY AND CONCLUSIONS

In this chapter, general summary of the thesis and some conclusion remarks are presented.

8.1 Summary

In this thesis welded connections of a multi barrel rocket launcher is investigated on fracture mechanics basis. A global finite element model of the system was created and solved under firing loads. The global model includes necessary kinematic connections and springs in order to reflect structural and dynamic response of the structure. With measurements taken from firing test of the launcher, global finite element model results were verified. Results showed that global finite element model is quite accurate on capturing system's response to dynamic loading.

General information about launcher systems was given. Operating principles and components of the system were presented. In addition, damage tolerant and safe life design philosophies were briefly mentioned and insight about them was provided.

Some theoretical background information about fracture mechanics was given. Stress intensity concept was presented and derivations were given. Then fracture toughness of materials which gives material's limit for fracture was presented.

Standard test methods for fracture toughness determination for metals and welded metals were presented. Information about specimen preparation criteria and data evaluation methods was presented.

Finite element modeling methodology was presented and crack modeling approach was verified using some case studies. A recent study was selected as well as some analytical results obtained from literature. In these cases, examples for different crack configurations were studied. Reproduced results were compared with original work and good agreement was achieved.

Then sub model was created for a critical section determined from global finite element model results. Boundary conditions were imported from global model to sub model. Cracks at three different configurations were studied in this thesis work. These configurations were

determined from previous design experiences and determined as most likely to occur. Stress intensity factor variations against crack front angle and crack size were given for one load case. Semi elliptical surface crack at weld toe, at inner surface and embedded circular crack inside weld configurations were studied. Semi elliptical surface crack at weld toe configuration gave the highest stress intensity factor for mode I among those.

Information about firing tests of the launcher system was given. Measurements that were used to verify global model were mentioned and operational principles of strain gages and displacement sensors were explained. Also material characterization tests for fracture toughness were performed and information about test procedure, and specimen preparation was given.

8.2 General Conclusions

Critical systems that are subjected to high amplitude dynamic and repeated loading must be subjected to thorough structural evaluations. Design of such systems can not be based on yielding or tensile strength of material. The system will probably have geometric imperfections. These imperfections may be inherent due to manufacturing or occur after some loading. Such a structure with imperfections or flaws must be investigated carefully. Fracture mechanics is used for damage tolerant design of the structure with imperfections.

Limiting value of materials up to which they can be loaded can be much less in case of fracture mechanics. Therefore, a design cycle including fracture mechanics analysis must be implemented. In this thesis, finite element method is used. Modeling methodology was presented here and study of a connection under one load case was given. Fracture mechanics analysis is important in design study for structural integrity assessment, and it must be included in the design process.

Validation of global finite element model is important for accurate evaluation of the structure. Although preparation and verification studies are labor intensive, it affects further analyses based on it and it is crucial for critical structural assessment. Elements to be included or excluded from global finite element model must be determined carefully in order to obtain structure's response. Iteration and modifications may be necessary in this step.

Sub modeling method is an appropriate way of modeling cracks. When global finite element models are large, it is impractical to include details such as crack in the model. Therefore sub modeling is applied. Global finite element model is solved once for one load case and various sub models can be created from the same global model solution. It allows different configurations to be studied at same location.

In this thesis work a methodology for modeling cracks in very big and complicated systems was proposed besides numerical results of investigated cases for critical crack size. Critical flaw size of 2.05mm is found for a semi elliptical surface crack located at weld toe. The

launcher system is checked using non destructive testing methods for critical flaw size around welded connection which is found to be critical location. Damage tolerant and safe life design concepts were introduced briefly. The work presented here is a part of safe life design approach for launcher system design and manufacturing. Critical locations of welds in the system will be checked after repeated loading of firings for crack size.

8.3 Recommendations for Future Work

In this study, cracks are studied for critical crack size. For a future work, crack growth analysis can be performed in order to determine load cycles for failure. This makes it also possible to determine inspection periods for the system. Also elastic plastic fracture mechanics can be implemented in future work regarding cracks in welded connections.

REFERENCES

- [1] Wang C.H., "Introduction to Fracture Mechanics", Department of Defence: Defence Science and Technology Organization, DSTO-GD-0103, 1996
- [2] Anderson T.L., "Fracture Mechanics: Fundamentals and Applications 3rd Edition", Taylor & Francis Group, 2005
- [3] Acar B., "Finite element analysis of fracture mechanics problems", Master's Thesis, 1997
- [4] Gordon A.P., McDowell D.L., "Numerical simulation of time-dependent fracture of graded biomaterial metallic interfaces", International Journal of Fracture, Vol.126, 2004, pp.321-344
- [5] Negre P., Steglich D., Brocks W., "Crack extension at an interface: prediction of fracture toughness and simulation of crack path deviation", International Journal of Fracture, Vol.134, 2005, pp.209-229
- [6] Lie S.T., Lee C.K., Chiew S.P., Yang Z.M., "A consistent crack modeling and analysis of rectangular hollow section joints", Finite Elements in Analysis and Design, Vol.42, 2006, pp.639-649
- [7] Diamantoudis A.Th., Labeas G.N., "Stress intensity factors of semi-elliptical surface cracks in pressure vessels by global-local finite element methodology", Engineering Fracture Mechanics, Vol.72, 2005, pp.1299-1312
- [8] Giglio M., Manes A., "Crack propagation on helicopter panel: Experimental test and analysis", Engineering Fracture Mechanics, Vol.75, 2008, pp.866-879
- [9] Shi Y., Sun S., Murakawa H., Ueda Y., "Finite element analysis on relationship between the J-integral and CTOD for stationary cracks in welded tensile specimens", International Journal of Pressure Vessels and Piping, Vol.75, 1998, pp.197-202
- [10] Meneghetti G., "The use of peak stresses for fatigue strength assessment of welded lap joints and cover plates with toe and root failures", Engineering Fracture Mechanics, Vol.89, 2012, pp.40-51
- [11] Negre P., Steglich D., Brocks W., "Crack extension in aluminium welds: a numerical approach using the Gurson-Tvergaard-Needleman model", Engineering Fracture Mechanics, Vol.71, 2004, pp.2365-2383

- [12] Manjgo M., Medjo B., Milovic L., Rakin M., Burzic Z., “Analysis of welded tensile plates with a surface notch in the weld material and heat affected zone”, *Engineering Fracture Mechanics*, Vol.77, 2010, pp.2958-2970
- [13] Paonelli L.D., Carr G.E., Gubeljak N., Predan J., Chapetti M.D., “Fracture toughness analysis of a ductile steel by means of 3D surface displacements”, *Engineering Fracture Mechanics*, Vol.98, 2013, pp.109-121
- [14] Atzori B., Meneghetti G., Susmel L., “Estimation of the fatigue strength of light allow welds by an equivalent notch stress analysis”, *International Journal of Fatigue*, Vol.24, 2002, pp.591-599
- [15] Kai X., Yong L., Lie S.T., “Analysis of non-loading carrying fillet welds using SGBEM”, *International Journal of Fracture*, Vol.129, 2004, pp.149-159
- [16] Lin G., Meng G., Cornec A., Schwalbe K.H., “The effect of strength mis-match on mechanical performance of weld joints”, *International Journal of Fracture*, Vol.96, 1999, pp.37-54
- [17] Guo Y., W., You W.,Y., Tronskar J.,P., “Development of Fracture Toughness using SENT specimens and Validation Tests on large Strained Pipeline Weldment”, *International Committee of Analysis for Steel and Iron Industry*, 2008
- [18] Lee H.Y., Nikbin K.M., ODowd N.P., “A generic approach for a linear elastic fracture mechanics analysis of components containing residual stress”, *International Journal of Pressure Vessels and Piping*, Vol.82, 2005, pp.797-806
- [19] Liljedahl C.D.M., Tan M.L., Zanellato O., Ganguly S., Fitzpatrick M.E., Edwards L., “Evolution of residual stresses with fatigue loading and subsequent crack growth in a welded aluminium alloy middle tension specimen”, *Engineering Fracture Mechanics*, Vol.75, 2008, pp.3881-3894
- [20] Barsoum Z., Barsoum I, “Residual stress effects on fatigue life of welded structures using LEFM”, *Engineering Failure Analysis*, Vol.16, 2009, pp.449-467
- [21] Bao R., Zhang X., Yahaya N. A., “Evaluating stress intensity factors due to weld residual stresses by the weight function and finite element methods”, *Engineering Fracture Mechanics*, Vol. 77, 2010, pp.2550-2566
- [22] Barsom J.M., Rolfe S.T., “Fracture and Fatigue Control in Structures: Applications of Fracture Mechanics Third Edition”, ASTM MNL41, 1999
- [23] “PES Testing”, Last accessed on January 06, 2013, http://www.productevaluationsystems.com/fracture_mechanics.php
- [24] ASTM E399-09, Standard Test Method for Linear-Elastic Plane-Strain Fracture Toughness K_{Ic} of Metallic Materials

- [25] Bezensek B., Hancock J.W., “The toughness of laser welded joints in the ductile-brittle transition”, Engineering Fracture Mechanics, Vol.74, pp.2395-2419
- [26] BS 7448 Part 2:1997, Fracture mechanics toughness tests: Part 2. Method for determination of K_{Ic} , critical CTOD and critical J values of welds in metallic materials.
- [27] Broek D., “Elementary Engineering Fracture Mechanics”, MartinusNijhoff Publishers, 1984
- [28] Newman Jr. J.C., Raju I.S, “Analyses of Surface Cracks in Finite Plates Under tension or Bending Loads”, NASA Technical Paper 1578, 1979
- [29] Woyak D., Baillargeon B., Marrey R., Grishaber R., “Linear Elastic Fracture Mechanics (LEFM) Analysis of Flaws within Residual Stress Fields”, SIMULIA Customer Conference, 2010
- [30] ABAQUS Documentation v6.12
- [31] Shih C. F., Asaro R. J. , “Elastic-Plastic Analysis of Cracks on Bimaterial Interfaces: Part I—Small Scale Yielding”, Journal of Applied Mechanics, 1988, pp.299–316
- [32] ANSYS Structural Analysis Guide 13.0
- [33] Köşker S., “Three Dimensional Mixed Mode Fracture Analysis of Functionally Graded Materials”, Master’s Thesis, 2007
- [34] TWI Manufacturing, engineering, materials and joining specialists, Last accessed on January 06, 2013, <http://www.twi.co.uk>
- [35] AIS Forensic Engineering, Forensic testing Laboratory , Last accessed on January 06, 2013, <http://www.ais-forensic-engineering.com>
- [36] Sih G.C., Macdonald B., “Fracture mechanics applied to engineering problems-strain energy density fracture criterion”, Engineering Fracture Mechanics, 1974, pp.361-386
- [37] “KYOWA Strain Gages”, Last accessed on June 13, 2013, http://www.kyowa-ei.co.jp/eng/product/strain_gages/gages
- [38] Hoffmann K., “An Introduction to Stress Analysis and Transducer Design using Strain Gauges”, HBM Test and Measurement, 2012
- [39] OMEGA Linear Potentiometers, Manual M2034-0405, 2012
- [40] Private communication with Bülent ACAR